Nonlinear light beam propagation in reorientational nematic liquid crystals

Nina Kravets

University "Roma Tre"

This dissertation is submitted in partial fulfillment of the requirements for the degree of

Doctor of Philosophy in Electronic Engineering

Supervisor:
Prof. Gaetano Assanto

Coordinator:
Prof. Giuseppe Schirripa Spagnolo

March 2015

I dedicate this thesis to my sister.

Acknowledgements

First, I would like to thank Prof. Gaetano Assanto for one the most important in my career possibilities of joining into his research group Nonlinear Optics and OptoElectronics Lab (NooEL). I thank for believing in me and seeing more my skills than I see by myself; for motivating me and raising my autonomy in his unique style. I would like to thank Dr. Armando Piccardi for introduction to area and collaboration on experiments all along my PhD program. A very special thank to Dr. Alessandro Alberucci who provided me with help starting from the help with theoretic part of my research all along my PhD program, till valuable advices on work in general. I would like to thank Dr. Malgosia Kaczmarek and Dr. Oleksandr Buchnev from the School of Physics and Astronomy in Southampton for providing samples of very high quality, essential to carry out all the sophisticated experiments. I thank Dr. Stefania Residori for hosting me in Institut Non Linéaire de Nice for a practice on manufacturing samples. Many thanks to Dr. Yuri Reznikov for opening the world of liquid crystals to me. Many thanks to all the great scientists I have met on conferences and meetings for showing me how versatile and never-ending the research in liquid crystals is. I thank also other people working with me in "Roma Tre" University both for scientific advices and all the time spent together. In alphabetic order: Raouf Barboza, Giosuè Caliano, Lorenzo Colace, Andrea De Iacovo, Barbara Licia Mauti, Saravanan Rajamani, Francesco Santoni, Alessandro Stuart Savoia, Vito Sorianello. A lot of thanks to my friends for making these three years bright and full of moments to remember. And of course thanks to my family for being so close staying so far from me. Thank you all, you are a very important part of this stage of my life.

Abstract

Liquid crystals (LC) are excellent media for the exploration of nonlinear phenomena, particularly due to their high and nonlocal response to electric and magnetic fields. Besides the fundamental interest, the field-induced reorientation of LC molecules is widely used in display applications and is promising for optical signals processing such as attenuators, tunable lens and smart-windows. Recently, a great deal of attention has been dedicated to spatial (2+1)D optical solitons in nematic liquid crystals, the so called nematicons. Nematicons are diffractionless self-confined light beams, that is, guided by their own waveguide in the dielectric. Specifically, diffraction is balanced out by self-focusing through the reorientational nonlinearity. Moreover, owing to the highly nonlocal character of the response, nematicons are stable and robust to external perturbations. Being self-induced graded-index guides for co-polarized signals, nematicons are an avenue to a wide range of all-optical devices and reconfigurable routers. When the electric field and the average alignment of molecules are normal to each other, the reorientational response presents a threshold in power before the material properties get modified by the impinging light. This dissertation deals with the investigation of beam self-trapping near such threshold in nematic liquid crystals, a configuration scarcely explored in the existing literature. The first chapter introduces the main features of liquid crystals and of nematicons in threshold-free geometries, including self-focusing, self-trapping and self-steering. Tthe second chapter discusses how self-focusing in the presence of threshold provides optical bistability and hysteresis in beam width versus power, due to step-like nonlinear response with excitation. This is indeed the first report on bistability with propagating beams and the first experimental demonstration of soliton bistability. The third chapter studies nematicon propagation near the threshold, in bias-free cells allowing the direct observation of beam-walk-off: combining self-steering and the inherent anisotropy of liquid crystals, the system is capable of switching from positive to negative refraction as power changes. This is the first demonstration of such a power controlled transition in refraction, which, besides the other, allows optimizing all-optical routers based on nematicons, as optical self-steering is maximized.

Table of contents

List of figures

Chapter 1

Introduction

1.1 Nonlinear waves

Modern physics successfully describes phenomena in astronomy, acoustics, electromagnetics, hydromechanics, oceanography, condensed matter, etc. In most branches of physics wave phenomena take place. This dissertation deals with wave phenomena in optics. The most studied problems are modeled and solved in the linear limit, when the superposition principle can be used. However, a wealth of interesting phenomena and effects lies in the nonlinear regime, when the wave amplitudes become relatively large.

It is remarkable that similar equations can explain phenomena of different origin, even in the presence of nonlinearity. Watching sea waves one rarely thinks of nonlinear optics, but it turns out that the models describing water waves can sometimes (under some conditions) resemble those for optical beam propagation in nonlinear media [1]. When the nonlinear response balances diffraction or dispersion in a medium, the resulting wavepacket can preserve its shape upon propagation in space or time (or both), and is named a solitary wave or a soliton. Depending on whether the differential equations supporting solitary solutions are integrable or not, these self-confined wavepackets are called solitons or solitary waves [2]. However, in this work the terms will be used interchangeably. Solitons, being nonlinear wavepackets, do not obey the same principles of linear waves. For example, solitons tend to interact like particles rather than waves [3]. The first theoretical description of solitons by the Dutch mathematicians Korteweg and his student de Vries addressed such particle-like behavior [4]. Korteweg and de Vries succeeded to explain the robust solitary wave propagating in a shallow canal with invariant shape over a long distance, observed more than half a century earlier by Sir Russell [5]. The latter report gave a start to the intense study of solitons in various branches of physics. This dissertation specifically deals with the

generation, the propagation and some outstanding properties of optical spatial solitons in nematic liquid crystals.

1.2 Liquid crystals

Liquid crystals (LC) are states of matter exhibiting properties of both crystalline solids and liquids. Namely LC are liquids possessing some degree of long-range order. Depending on the character of the order we can distinguish various LC phases. The simplest is the isotropic phase, when all the molecules have neither positional nor orientational (angular) order. Thus, despite the fact that each LC molecule is anisotropic, macroscopically the medium has equal properties in all directions: it is an isotropic liquid. When the LC molecules are preferentially oriented along a given direction (i.e. the sum of their anisotropies does not vanish when a spatial average is performed), they give rise to a direction-dependent response at the macroscopic scale: the LC is said to be in the nematic phase (see Fig. 1.1). Thus, the

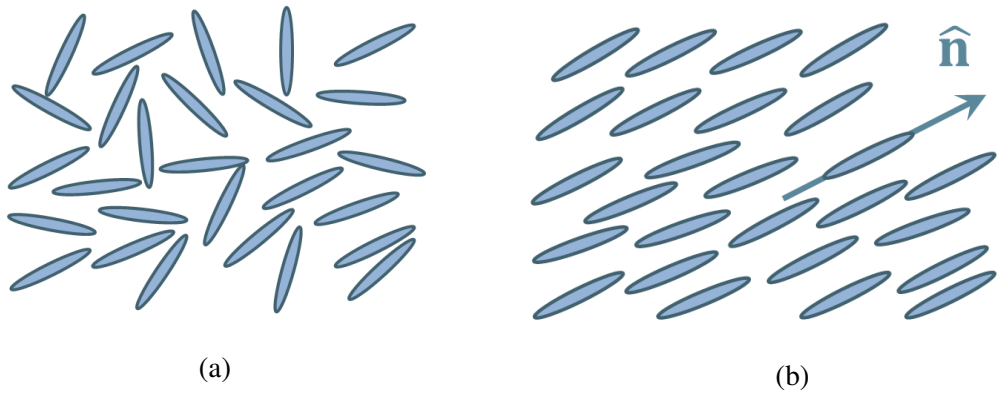

Fig. 1.1 Pictorial sketch of the (a) isotropic and (b) nematic liquid crystal phase

nematic LC (NLC) response to external stimuli can be described with a tensor, the latter possessing three (biaxial symmetry) or two (uniaxial phase) distinct eigenvalues. Typical LC show a uniaxial nematic phase, i.e. a cylindrical symmetry around a specific direction called molecular director [6]. In optics, the director corresponds to the optic axis of such anisotropic uniaxial crystal. Any phase with some orientational order but without positional order can be considered nematic. In the nematic phase the orientational order parameter S characterizes the angular distribution of the molecules around the direction of the director. It is usually expressed by a Legendre polynomial of even (second) order:

$$S = \frac{1}{2}\langle 3cos^2\alpha - 1\rangle \tag{1.1}$$

where brackets stand for the average both in time and space. The order parameter takes values in the range $S \in [0;1]$; it vanishes when the molecules are randomly aligned and the LC turns to be an isotropic liquid. When all the main (long) axes of the molecules are exactly parallel to the director, then the order parameter is equal to 1 and complete NLC orientation (i.e., crystal-like order) takes place. The order parameter and the LC phase depend both on temperature, chemical composition and external excitations. For the most common thermotropic LC the nematic phase occurs in a certain temperature interval, which can vary with chemical composition. Mixing different LC it is possible to widen and shift significantly such temperature region. For example, the E7 LC mixture exists in the nematic phase at room temperature and shows the nematic-isotropic transition at about $+58°C$. The commercial E7 mixture, the one employed in all the experiments shown in this thesis, comprises molecules of a few different LC, namely about 51% (by weight) of CB, 25% of 7CB, 16% of 8OBC and 8% of CT [7].

1.3 Elastic forces in liquid crystals and nonlocal response

Strong mutual interactions of electromagnetic origin are present between the molecules in liquid crystal; these are macroscopically modelled as elastic forces that tend to restore the equilibrium orientation of the elongated molecules as one of the possible distortions (splay, bend or twist) occurs. Frank's elastic constants quantitatively characterize their values and depend on both LC composition and temperature. These elastic forces lead to a nonlocal response to external stimuli. This property is actually used when preparing sample with a given director distribution, as it is enough to treat properly the boundaries of a LC cell to change accordingly the molecular orientation even in the bulk of the sample [8].Director distribution at the equilibrium is determined by the minimization of the system energy, yielding a molecular distribution which is in general inhomogeneous, making the NLC a non-uniform anisotropic crystal. Inhomogeneities in the director distribution can be either smooth or abrupt, in the latter case leading to the formation of disclinations, that is, points/lines where the director cannot be defined [9]. In the case of smooth changes, the transition area depends on the elastic properties and usually extends much further than the external stimulus (e.g. voltage, light perturbation) [10, 11]. Two typical uniform orientation geometries are mostly used in the following: i) the planar orientation, when the molecules are oriented parallel to a bounding surface; it is usually realized by mechanical rubbing or photo-treating the boundaries. ii) the homeotropic orientation, when the molecules are

oriented orthogonally to the bounding surface; in this case a hydrophobic-like polymer layer sets the LC molecules standing on the boundaries [8].

1.4 Linear optics of nermatic liquid crystals

Light propagation in NLC at low powers ($\ll$ 1mW) can be treated as linear propagation in uniaxial crystals. If the director distribution is homogeneous, planar light waves propagating in with a fixed wavevector can be described by a superposition of two independent linearly polarized (eigen)waves, ordinary and extraordinary. The former is polarized in a plane perpendicular to the plane containing the light wavevector and the optic axis (director): it experiences the ordinary refractive index. The latter has the electric field polarized in a plane containing wavevector and director: it experiences a direction-dependent refractive index. The dielectric properties are thus defined by a tensor $\boldsymbol{\varepsilon}$

$$\boldsymbol{\varepsilon} = \begin{pmatrix} \varepsilon_\perp & 0 & 0 \\ 0 & \varepsilon_\perp & 0 \\ 0 & 0 & \varepsilon_\parallel \end{pmatrix}. \tag{1.2}$$

The uniaxial medium is assumed to have positive anisotropy if the dielectric constant along the director $\varepsilon_\parallel$ is higher than across it $\varepsilon_\perp, \Delta\varepsilon = \varepsilon_\parallel - \varepsilon_\perp > 0$. Hereby only LC with positive anisotropy are considered. Ordinary polarized light propagates as in isotropic media with a refractive index $n_o = n_\perp = \sqrt{\varepsilon_\perp}$. Extraordinary polarized light perceives a refractive index dependent on the angle θ between director and wavevector:

$$n_e = \sqrt{\frac{n_\perp^2 n_\parallel^2}{n_\perp^2 \sin^2\theta + n_\parallel^2 \cos^2\theta}}. \tag{1.3}$$

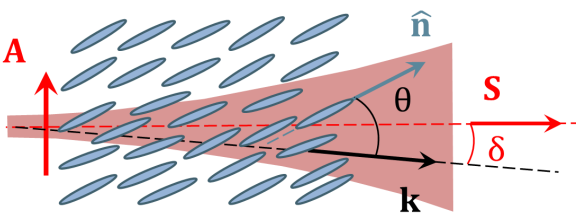

Fig. 1.2 Simple sketch of extraordinary polarized light propagation in positive uniaxial nematic liquid crystal. **A** indicates the optical electric field, **k** the wavevector, **S** the Poynting vector, $\hat{\mathbf{n}}$ the director, θ the angle between wavevector and director and δ he walk-off.

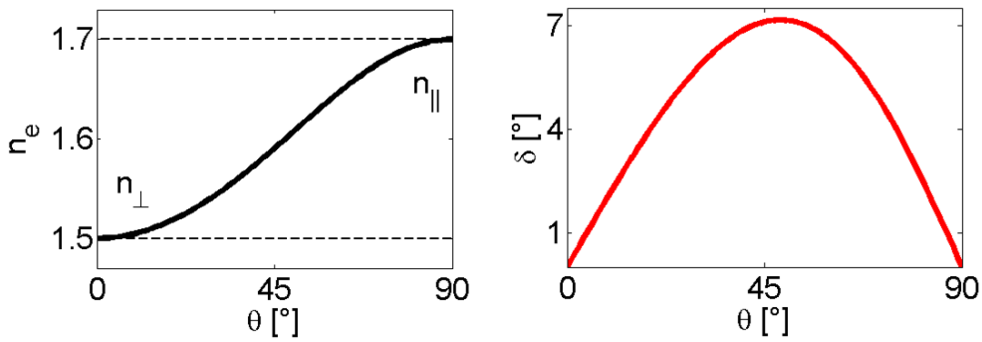

(a) (b)

Fig. 1.3 Extraordinary refractive index (a) and walk-off angle (b) dependence on angle θ between director and wavevector in NLC mixture E7.

Extraordinary refractive index n_e takes its maximum value when molecules (the director) are parallel to the field direction ($\theta = 90°$) (see Fig. 1.3). Moreover, since ε is a tensor, the electric field of light is no longer parallel to the displacement field, and the energy propagates (along the Poynting vector) at the walk-off angle δ from the wavevector

$$\delta = \arctan\left(\frac{\Delta\varepsilon \sin(2\theta)}{\Delta\varepsilon + 2n_\perp^2 + \Delta\varepsilon \sin(2\theta)}\right) \tag{1.4}$$

Basically, once a given LC is chosen, θ determines all the parameters of light propagation and scattering, walk-off, phase and group velocities, Rayleigh distance and so on.

1.5 Reorientational nonlinearity and spatial optical solitons

The electric field, at optical frequency or static, gives its contribution to the free energy

$$F_E = \frac{\Delta\varepsilon}{2}(\hat{n}\cdot\mathbf{E}) \tag{1.5}$$

where $\Delta\varepsilon$ is the anisotropy of the dielectric permittivity or optical anisotropy in the case of static or optical fields, respectively. As the field amplitude becomes bigger, the propagation of light in the extraordinary polarization cannot be considered as linear anymore. As the elongated molecules turn into (induced) dipoles, they tend to align to the external field by rotating, until the latter torque is balanced out by elastic forces. The contribution of elastic forces to the free energy is described by a distortion in the initially homogeneous orientation:

$$F_{elastic} = \frac{K_1}{2}\left(\nabla\cdot\hat{n}\right)^2 + \frac{K_2}{2}\left(\hat{n}\cdot\nabla\times\hat{n}\right)^2 + \frac{K_3}{2}\left|\hat{n}\times\nabla\times\hat{n}\right|^2. \tag{1.6}$$

The Frank elastic constants K_1, K_2 and K_3 quantify the three main distortions: splay, bend and twist, respectively [6]. The molecular orientation at the equilibrium stems from a balance between all the present torques/forces.

Let us consider a liquid crystal sample with a homogeneous initial director distribution at angle θ_0 with respect to the z axis, subject to a homogeneous quasi-static electric field E^{LF} in the plane xz and excited by an extraordinary polarized light wave $A = A_0 \exp\left[\mathrm{i}k_0 n_e(\theta_0)z\right]$ with vacuum wavevector k_0 and slowly varying amplitude A_0. Both fields act along the x axis. Using the Euler equations for the free energy minimization we can find a reorientational equation for a given field profile. Let us stress that, if the polarization of the electric field at optical frequency, the low-frequency electric field and the director lie on the same plane, molecular reorientation occurs only in the plane xz containing the initial director and the field vectors. Basically, in every point in space a single angle θ defines unambiguously the molecular orientation. Together with the nonlinear - Schrödinger - like equation for a light beam propagating in the presence of reorientation, the complete model is then [12]:

$$\begin{aligned}\left(K_1\cos^2\theta + K_3\sin^2\theta\right)\frac{\partial^2\theta}{\partial y^2} + \left(K_1\sin^2\theta + K_3\cos^2\theta\right)\frac{\partial^2\theta}{\partial z^2} + K_2\frac{\partial^2\theta}{\partial x^2} + \\ (K_1-K_2)\left\{\sin 2\theta\left[\left(\frac{\partial\theta}{\partial z}\right)^2 - \left(\frac{\partial\theta}{\partial y}\right)^2 - \left(\frac{\partial^2\theta}{\partial y\partial z}\right)\right] + \cos 2\theta\frac{\partial\theta}{\partial y}\frac{\partial\theta}{\partial z}\right\} + \\ \frac{1}{2}\varepsilon_0\Delta\varepsilon^{LF}\sin(2\theta)\left|E^{LF}\right|^2 + \frac{1}{4}\varepsilon_0\Delta\varepsilon\sin\left[2\left(\theta-\delta\right)\right]|A|^2 = 0\end{aligned} \tag{1.7}$$

$$2\mathbf{i}k\frac{\partial A}{\partial z} + \Delta_\perp^2 A + k_0^2 A\Delta\varepsilon\left(\sin^2\theta - \sin^2\theta_0\right) = 0 \tag{1.8}$$

where $\Delta_\perp = \frac{\partial}{\partial x^2} + \frac{\partial}{\partial y^2}$, $k = k_0 n_o(\theta_0) = \frac{2n(\theta_0)\pi}{\lambda}$ is the wavenumber corresponding to wavelength λ and the initial angle θ_0 between director and wavevector. Basically, the non-homogeneous light field (beam) provides a stronger reorientation close to its peak. The reorientation vanishes towards the beam periphery, giving rise to a bell-shaped orientation profile (see Fig. 1.4). The refractive index follows the angle profile and acts like a lens for the extraordinary polarized light, leading to self-focusing. Due to nonlocality and the reorientational dependence on the angle providing a saturable response a robust spatial optical soliton can then be generated in reorientational liquid crystals. We pinpoint two main regimes for finite-size light beams propagating in NLCs and subject to reorientational nonlinearity. In the perturbative regime the all-optical reorientation is negligible with respect to the director

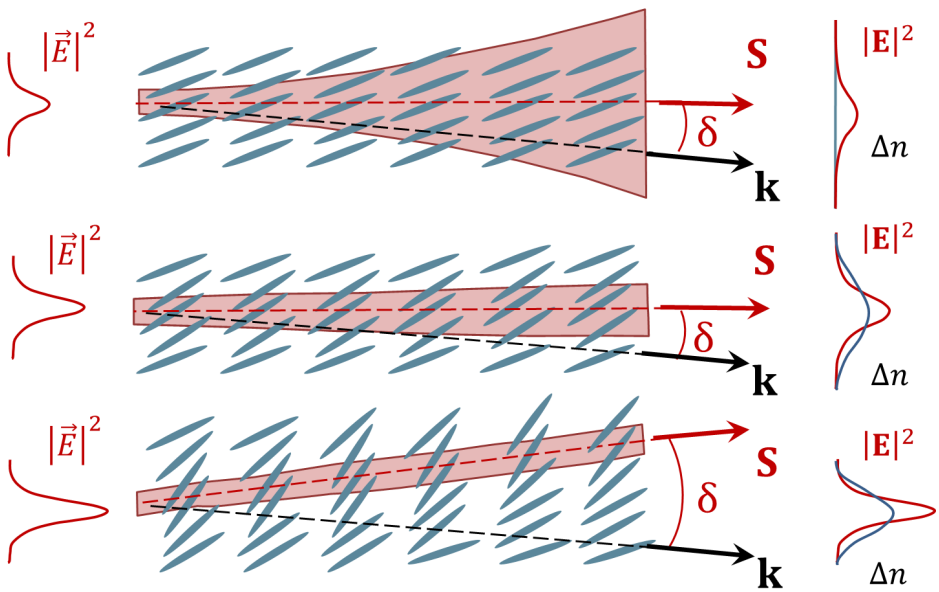

Fig. 1.4 Sketch of (top) linear propagation (middle) self-focusing and (bottom) self-steering of Gaussian beam in nematic liquid crystal

angle in absence of light. In this regime, the walk-off angle δ stays almost unaltered with the input angle, whereas the optical torque creates a nonlinear index well able to modify the transverse shape of the beam, eventually forming a spatial soliton. In the non-perturbative regime, occurring for larger input powers, the optical contribution to θ is large enough to induce an appreciable change in the walk-off, thus on the beam trajectory: a self-steering effect takes place, simultaneously with the self-trapping [13].

1.6 Previous studies of nematicons

Spatial optical solitons in LC are robust self-confined (self-trapped) optical wavepackets that can be created by laser beams at relatively low power (few milliwatts) and can guide copolarized weak signals [14]. That is why their study, after pioneering work on self-focusing in dye-doped LC in cylindrical capillary [15–17], stirred great interest. Along with the reorientational, the thermal contribution to a nonlinear refractive index change [8], in most cases counteracting, and consequent impact on soliton formation [11, 18] was investigated. The optical beam self wave-guided propagation of soliton-like or "breathing" nature in nonlinear medium was explained both numerically and analytically as solutions of nonlinear Schrödinger equation using the Snyder-Mitchell model [19–23]. Later the first observation of stable spatial (2+1)D purely reorientational optical soliton in undoped nematic liquid crystal

in suitable geometry, so called nematicon [24], have led to an investigation of numerous phenomena involving nematicons of both fundamental and applied interest. Among them power-controlled self-steering [25], bias-controlled in-plane self-steering via the birefringent walk-off change [26], short-range interaction of two optical beams in strongly nonlocal NLC [27], spiraling and long-range interaction of two co-propagating [28, 29] or counter-propagating solitons [30]. All the above represents the interest for optoelectronic application as optical dynamic inter-connectors, demultiplexers, other circuit elements. That is why the time required for soliton creation by an optical beam and time dynamics of following manipulations was a topic of interest as well [31]. Along with planar nematic geometry cholesteric or chiral NLC can host the propagation of nematicons [32]. Experimentally the propagation, steering [33] and interaction [34] of nematicons in twisted and chiral NLC was observed recently. Moreover it has been demonstrated that, due to the intrinsic modulation of refractive index in chiral NLC, discrete diffraction [35] of optical beam or splitting in two soliton beams [36] can take part. Among the most counter-intuitive phenomena observed with spatial solitons was negative refraction at the interface between an isotropic medium and a highly anisotropic NLC [37]. The explanation and further exploration of it is provided in section 2.2.3. An excellent review paper on nematicons and related phenomena was published in 2012 by M. Peccianti and G. Assanto [38]. Detailed outline of nematicons phenomena, theoretical explanation and numerical models, experimental observation and possible applications is carefully gathered and accessibly presented in recently published book edited by G. Assanto as well [39].

1.7 The Frèedericksz transition

From the reorientational equation (1.7) it is clear that the field-driven molecular torque changes with the angle between the director and the field vector. No torque is expected when the electric field is perpendicular or parallel to the director. However it is intuitively clear that, in the presence of strong field, the energetically most convenient state is the one with molecules aligned to the field direction. It was shown first for magnetic fields and later for electric fields that a step-like transition takes place at certain critical values of the external excitation when field and director are initially orthogonal. Physically, for high fields the torque is able to amplify the natural fluctuations in the molecular alignment due to the finite temperature of the system [40]. Moreover, due to the equivalence between the head and the tail of the director (i.e., centrosymmetry) reorientation can be positive or negative with an equal probability, i.e., the system is subject to a pitchfork bifurcation [41]. Such transition

was studied by Frèedericksz in the first half of XX century [42]. Experimental and theoretical works have showed that the Frèedericksz transition occurs in LC subject to either magnetic or electric field and - in most cases - it is a second order transition [6]. Device elements based on the Frèedericksz transition, like twisted and double-twisted nematic cells [43], are used nowadays in display applications. It was theoretically predicted that, under certain conditions for the LC parameters, a first-order optical Frèedericksz transition (FO-OFT) and optical bistability can take place [40, 44]. The FO-OFT criterion requires a specific relationship between elastic and dielectric constants, one that is barely possible to satisfy with standard LC. However, achieving two stable states of an optical system with bistability can be crucial for all-optical devices comprising memory effects, so this topic has been further studied by several groups since the eighties.

Chapter 2

Optical bistability close to the Optical Frèedericksz transition

In this Chapter I aim to investigate optical bistability in nematic liquid crystals supporting the nonlinear propagation of a light beam, i.e. two distinct LC director distributions supported by beam profiles corresponding to the same input power. I discuss hereby the feedback required for optical bistability. In order to find stable director distributions in the presence of external excitation I solve the partial differential reorientational equation (1.7) numerically. Finally I show the results of the experimental observation of bistability with finite-size beams in reorientational nematic LC.

2.1 First-order Optical Frèedericksz transition and bistability

First let me consider in more details the optical bistability related to FO OFT. It presumes two distinct states in director orientation supported by the same input excitation. Usually Frèedericksz transition is a second-order transition, i.e. there is unambiguous correspondence between field and director orientation and hysteretic effects are ruled out. However if transition becomes of the first order, director can follow a discontinuous reorientation with the external field, i.e., sudden jumps in the molecular distribution can take place: thus two stable orientations can be supported by same field value, the chosen one depending on the previous history of the system. In other words, a first-order transition is necessary to observe bistabilty.

In classical approach the OFT is caused by a single light beam of linear polarization impinging on a homeotropically oriented pure NLC cell. Several criteria were found for the existence of FO OFT using different assumptions. Each criterion was representing a specific relation between LC parameters: anisotropy and elastic constants. Estimated requirement was difficult to satisfy with existing LCs [40, 44], that explained why the FO OFT in pure LC under single light beam irradiation was not observed yet. Later the criteria were extended to include cell characteristics and anchoring parameters [45, 46].

In order to observe the bistability experimentally some additional feedback was required. FT was shown to become FO in presence of two counteracting fields, when one field induced the transition whilst the other restored the unperturbed molecular orientation. It was demonstrated theoretically that light-induced FT in standard pure NLC can be enhanced or suppressed by presence of an external magnetic field [47, 48]. It can even cause the switching from a first to a second order transition (and vice versa) for certain LC. Reversely, magnetic FT can become FO in presence of illumination [49]. Similar phenomena occurs also for counteracting electric and optical fields [50, 51]. The all-optical bistability related to FO OFT was experimentally achieved using two incoherent counter-propagating laser beams [52]. Few approaches to bistability close to OFT was concerning the optical-electric feedback (see for example [53–55]).

Another approach is based on using doped liquid crystals. In this case it is sufficient a single light field. The feedback is provided by the light-induced nonlinear torque by the dopant counteracting the torque by NLC itself. Standard NLC doped with a photosensitive molecules changing the anisotropy sign to opposite due to $trans - cis$ photo-isomerization underwent the first order reorientational transition under linearly polarized light illumination in presence of biasing voltage and was shown to possess the optical bistability [56, 57]. Recently the FO-OFT and optical bistability accompanied with hysteresis loop was demonstrated in positive NLC doped with a negative dichroic dye [58]. This experiment was the most similar to original idea of FO OFT. Transition was demonstrated being of the second order in pure standard NLC mixture, whereas the addition of a dye in certain concentrations satisfied the criterion from [44], thus leading to the observation of FO OFT.

In all the above mentioned investigations light was taken to propagate across a thin film of NLC (film thickness was about or less than the light beam diameter).

Chasing the bistability, the propagation of non-uniform light beam over distance much longer than beam width in nonlinear medium was studied first experimentally [59] and then described theoretically in early 80-s [60]. In experiments Gaussian cw beam with waist of 80 μm was propagating in a 20 cm long heated cell filled up with Sodium vapour: the

beam was found to diffract at low powers, whereas self-collimated beams were observed for high input intensities. Saturation of nonlinearity prevented catastrophic self-focusing and provided two stable distinct states (diffracting at low intensity and self-confined state at high intensity). Only a second-order OFT however was observed without an external feedback. Later was provided by a semitransparent mirror reflecting a part of radiation, defined by an iris of certain width placed at the output of the sample. Theoretically it was demonstrated later that in general nonlinear medium, possessing specific nonlinearity (namely step-like or cubic-quintic) can support optical solitons (including spatial - self-confined light beams) with different propagation parameters at the same power.

Conceptually such bistability differs from originally predicted close to FO OFT as it requires nonuniform light field and change in the light intensity profile as amount of the nonlinearity changes. In this thesis I refer to this later optical bistability and show that in NLC the step-like reorientational nonlinearity close to OFT supports the light propagation in two distinct regimes (diffracting and self-confined) corresponding to same input Gaussian beam.

2.2 Cell geometry and ruling equation

I consider the planar nematic LC cell bounded only in one direction by two parallel glass plates separated by $L_x = 100\mu m$. The other two dimensions can be assumed infinitely extended, although given that in the lab reality they corresponded to $L_y, L_z >> 100\mu m$. At variance with previous studies of first-order (FO)-OFT, I consider light propagating along the infinite length of a cell with field polarized along the short (x) side. A quasi-static (1kHz) uniform electric field can be applied to the cell by a couple of plane transparent electrodes on each of the bounding glass plates. This additional field is essentially co-aligned with the electric field of the light beam, thus director reorientation is substantially planar (see Chapter 1).

In order to have OFT I take the wavevector direction to be parallel to the unperturbed director (initial moleculal orientation), i.e. both oriented along z. For the sake of simplicity I consider no changes along z (see Fig. 2.1b), i.e, I am assuming translational invariance along the propagation direction of light. Thus director distribution obeys

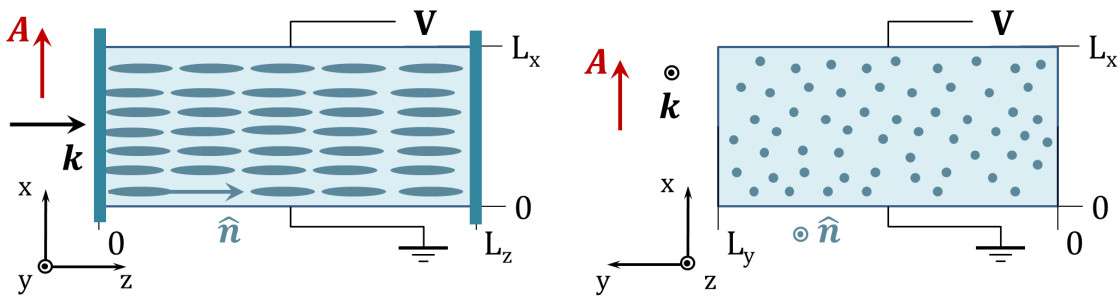

Fig. 2.1 Sketch of the sample in the unperturbed state. (a) Side view of xz plane and (b) cross section in xy at a given propagation distance z. Blue ellipses and dots represent the elongated LC molecules in the nematic pahse with director along the axis z.

$$\left(K_1\cos^2\theta + K_3\sin^2\theta\right)\frac{\partial^2\theta}{\partial y^2} + K_2\frac{\partial^2\theta}{\partial x^2} - (K_1 - K_2)\sin 2\theta\left(\frac{\partial\theta}{\partial y}\right)^2 + \frac{1}{2}\varepsilon_0\Delta\varepsilon\sin(2\theta)\left|E^{LF}\right|^2 + \frac{1}{4}\varepsilon_0\Delta\varepsilon\sin\left[2(\theta-\delta)\right]|A|^2 = 0 \tag{2.1}$$

$$\frac{\partial\theta}{\partial y} = 0\Big|_0^{L_y};\theta = 0\Big|_0^{L_x} \tag{2.2}$$

The reorientational equation simplifies significantly (2.1) comparing to its general form (1.7). The corresponding boundary conditions along y are represented by vanishing first derivatives of the reorientation angle θ. Strong anchoring conditions along x correspond to setting to zero the reorientation (2.2) (see also article no.1 “Bistability with Optical Beams Propagating in a Reorientational Medium” in A).

2.3 Homogeneous field. Electric Frèedericksz transition

In the simplest case molecular reorientation is due to a uniform electric field, i.e. a voltage applied thought the planar electrodes in $x = 0$ and $x = L_x$, in absence of light.

In this case reorientation is homogeneous not only along z but also along y. A one-dimensional model is sufficient to provide reorientation at each bias field, with a reorientation profile which is symmetric with respect to the cell mid-plane, so that a complete description is given by the maximum reorientation θ_{max} positioned for symmetrical reasons in $x = \frac{L_x}{2}$ (see Fig. 2.2a). As the molecules are initially perpendicular to the field, the reorientation

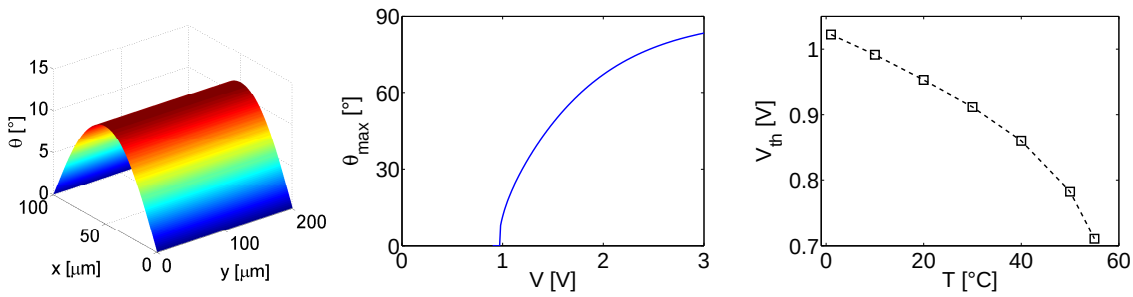

(a) (b) (c)

Fig. 2.2 Numerical solution of the reorientational equation in the standard E7 LC mixture at 18°C: (a) Reorientation profile due to a uniform electric field applied through plane electrodes biased at 1V. (b) Maximum reorientation versus applied voltage. (c) Calculated threshold voltage versus temperature.

takes place only above a threshold (see Fig. 2.2b), when the Frèedericksz transition occurs. Such threshold for uniform electric fields and planar alignment is given by the expression:

$$E_{LF}^{th} = \frac{\pi}{L_x}\sqrt{\frac{K_1}{\varepsilon_0\left(\varepsilon_{\parallel}-\varepsilon_{\perp}\right)}} = \frac{V_{th}}{L_x} \tag{2.3}$$

(given that mainly splay distortions are occurring) [6]. The threshold E_{LF}^{th} depends on sample size, anisotropy and elastic constants at each temperature. Examples of threshold voltage V_{th} at various temperature T for E7 are provided in Fig. 2.2c. As the elastic constant K_1 reduces faster with temperature than the dielectric anisotropy $\Delta\varepsilon = \varepsilon_{\parallel} - \varepsilon_{\perp}$, the threshold field/voltage decrease as temperature increases [7].

2.4 Gaussian beams and optical Frèedericksz transition

Let me consider now reorientation due to non-uniform optical fields, namely TEM_{00} Gaussian beams with axis in the cell mid-plane $L_x/2$. In this case the threshold depends on the field profile of waist ω_0:

$$|A|^2 = |A_0|^2 \exp\left(\frac{-2\left(x^2+y^2\right)}{\omega_0^2}\right) = \frac{2P_{th}}{\pi\omega_0^2\eta}\exp\left(\frac{-2\left(x^2+y^2\right)}{\omega_0^2}\right) \tag{2.4}$$

where η is the characteristic impedance of the medium.

As in the case of uniform fields, reorientation is symmetric with respect to $x = L_x/2$ (see Fig. 2.3a) provided I neglect the reorientational self-effects mentioned in section 1.5. Above

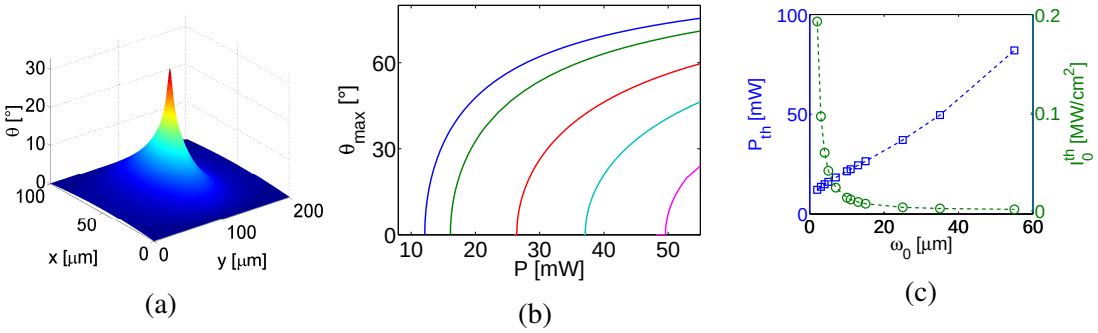

Fig. 2.3 Numerical results for standard E7 mixture at 18°C: (a) Reorientation caused by a $2\mu m$-waist Gaussian-beam carrying a power of 15 mW. (b) Maximum reorientation versus beam power; the colour lines represent Gaussian profiles of different waists ω_0: 2, 5, 15, 25 and 35 μm from left to right (blue, green, red, cyan and magenta) respectively. (c) Calculated threshold power P_{th} and intensity I_0^{th} versus waist.

threshold there is reorientation dependence on light power and waist, assuming that the beam profile remains unchanged even under reorientation. In this approximation I calculate the threshold power values, as plotted in (c). The numerical solutions of the reorientational equation demonstrate the increase of threshold power and, correspondingly, the reduction in threshold peak intensity $I_o^{th} = \frac{|A_0^{th}|^2}{n\eta}$ as the Gaussian waist gets larger, in agreement with previous works [61–64].

2.4.1 Reorientation hysteresis versus input power

Here I consider self-focusing due to reorientation. As mentioned before, when non-uniform reorientation takes place, the refractive index distortion acts like a lens self-written by the light itself. It mediates self-focusing and the creation of spatial solitons. The reorientation dynamics with power of a real (i.e., accounting for diffraction, thus for the evolution along z) Gaussian beams is illustrated in Fig. 2.4. Starting from a homogeneous director distribution (low power, linear case), no reorientation takes place up to a certain threshold power P_{th}^{inc} defined by the beam waist (magenta curve). Then molecular reorientation and soliton formation occur, once the threshold is overcome, and the soliton width determines which of the reorientational curves plotted in Fig. 2.3b is followed by reorientation angle θ with power (blue curve).

Clearly, information about the initial director distribution is lost once a soliton is formed. When the power decreases the reorientation keeps the beam self-confined down to the threshold power P_{th}^{dec} defined by the soliton width above OFT. At lower powers, the system

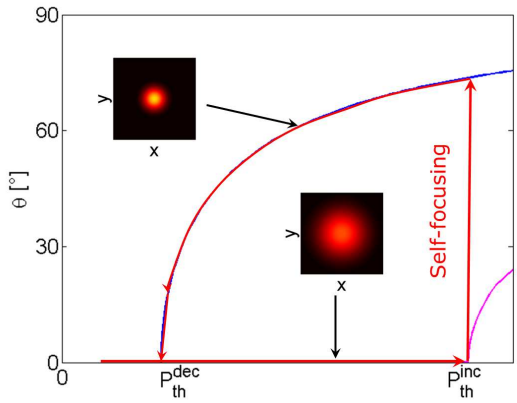

Fig. 2.4 Simplified sketch of reorientation dynamics with power when self-focusing is accounted for. Blue and magenta curves represent reorientation by two field profiles of different waists (see insets). The red line is a guide to the eye along the hysteresis loop.

relaxes back to a uniform director distribution and the cycle is completed. Since threshold powers are defined by the beam waist, by varying the difference between the Gaussian waist in the linear case and the soliton width, the width of the hysteresis cycle can be tuned. When the initial Gaussian profile is wider than the soliton width, according to the model it is $P_{th}^{inc} \geq P_{th}^{dec}$ and reorientation follows a hysteresis loop counterclockwise with increasing/decreasing power: optical bistabily occurs. Two states of the beam/NLC system exist and are stable within the range $\left(P_{th}^{inc}; P_{th}^{dec}\right)$, encompassing a diffracting (linear) and soliton (nonlinear) propagation (see also article no.2 “Beam hysteresis via reorientational self-focusing” in A).

2.4.2 Experimental realization

For the experimental demonstration I used a planar LC cell, containing standard E7 mixture between two glass slabs 1.5×20 mm^2 separated 100μm by Mylar spacers. Two additional glass slabs were attached to seal the entrance and the output of the cell. This is done to prevent meniscus formation due to surface tension [24]. All the four boundary surfaces were treated to ensure planar alignment with the director distribution homogeneous along z axis at rest (see Fig. 2.5). Indium Tin Oxide (ITO) electrodes were deposited on top and bottom interfaces, so that an additional uniform quasi-static (at frequency about 1 kHz) electric field could be applied along the x axis. The beam entering the cell was a TEM_{00} Gaussian of wavelength of 1.064μm, polarized linearly along $\hat{x}$, i.e. exciting a purely ordinary configuration in the absence of reorientation. A half-wave plate before a polarizer allowed the control of the

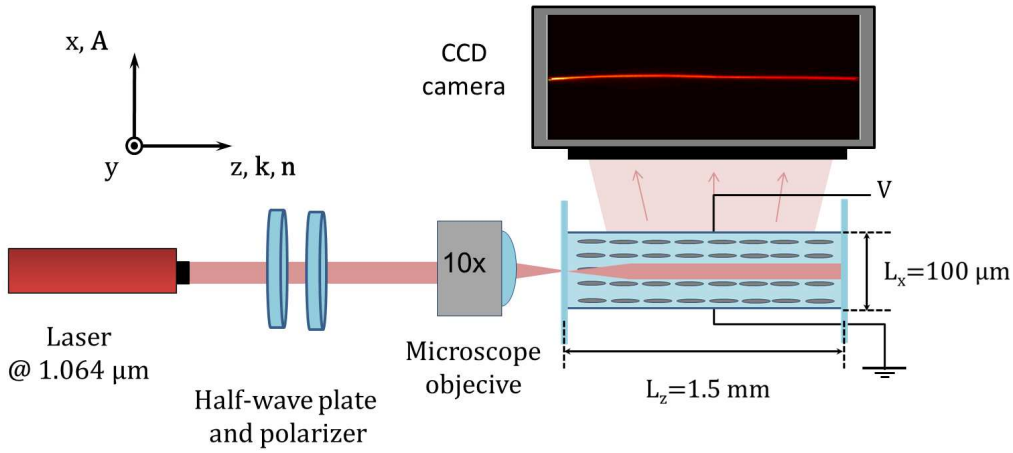

Fig. 2.5 Sketch of the experimental set-up.

light power. The beam was focused using a 10× microscope objective to a waist of about $2\mu m$ at the entrance of the cell. Diffraction spreading allowed to easily distinguish between diffracting and self-confined soliton-like propagation [65]. The beam evolution in the plane *yz* of the sample was monitored by a CCD camera collecting the out-of-plane scattered light. It is worth noticing that nematic LC scatter quite a bit, hence they allow the direct observation of beam propagation. However, the same scattering leads to significant energy losses upon propagation. NIR light was employed to reduce losses and extend soliton-like propagation compared to shorter wavelengths.

2.5 Voltage-assisted first-order optical Frèedericks transition

To avoid beam instabilities (see for beam images the Supplemental Material to article no.1 in A), occurring at high powers, and to support molecular reorientation I applied an external uniform electric field. To preserve the uniform initial director distribution as well as director and optical field orthogonality, however, the external field (from the bias voltage) should not induce reorientation in the absence of light. Due to existence of an electric Frèedericksz threshold as discussed in section 2.3, it is possible to reduce significantly the OFT power threshold by applying a bias lower than V_{th} while keeping the director distribution unperturbed.

2.5.1 Model: impact of external bias and temperature

The application of co-acting optical and quasi-static electric fields does not eliminate the threshold effects due to one of them in the absence of the other. Nevertheless, these two simultaneous fields may help reorientation at amplitudes lower than threshold (i.e. $V < V_{th}, P < P_{th}$). As in the previous cases, the reorientation profile remains symmetric around the maximum reorientation θ_{max} in the cell mid-plane (Fig. 2.6b). As it can be seen in Fig. 2.6b in the presence of $V = 0.92V < V_{th}$, the bias-assisted optical Frèedericksz transition was still step-like nature but at lower power thresholds P_{th} if compared to the unbiased sample. By varying the bias, the transition power could be widely adjusted. Taking into account the temperature dependence of the elastic constants as well as the dielectric and the optical anisotropies, additional tuning of the threshold could be achieved. Fig. 2.6 illustates the dependence of P_{th} for Gaussian beams of different waists in the presence of various bias voltages (2.6c) at room temperature 18°C and of P_{th} with temperature (2.6d).

2.5.2 Experiments: optical bistability, hysteresis and its tuning

I experimentally verified that the voltage of 0.92V caused no reorientation without light. Thus an optical beam was injected spread owing to diffraction in the linear regime for powers up to about 16 mW. A stable spatial soliton was created at powers higher than P_{th}^{inc}=16.5 mW. The acquired beam paths in yz are presented in Fig 2.7: images a,b,d,f correspond to increasing power. As the power was decreased back to 15 mW the beam remained self-confined. A decreasing power eventually led back to the linear behaviour below P_{th}^{dec} = 14.5 mW. To better visualize the beam width versus power, Fig. 2.8a shows the power dependence of the width ω^* (intensity distribution) at z=1 mm (marked with white dashed lines in Fig. 2.7) normalized to ω_0 (input waist). It is apparent that optical bistability took place in the power range between 14 and 17 mW. The system has two stable regimes of a light beam either diffracting or self-trapping. The beam width follows a hysteresis loop as power increases and decreases. Such loop occurred in each z section since the beam width changes nearly-monotonically with propagation (see Fig. 2.8b,c).

In order to compare experimental and simulation results, we modeled the soliton as a self-confined shape-preserving beam, approximated by a z-independent Gaussian function with a waist equal to the soliton width. The diffracting beam (in experiments featuring a $2\mu m$ waist) must be modelled with a z-invariant Gaussian providing the same maximum reorientation angle just above threhshold. We found that the diffracting beam in experiments

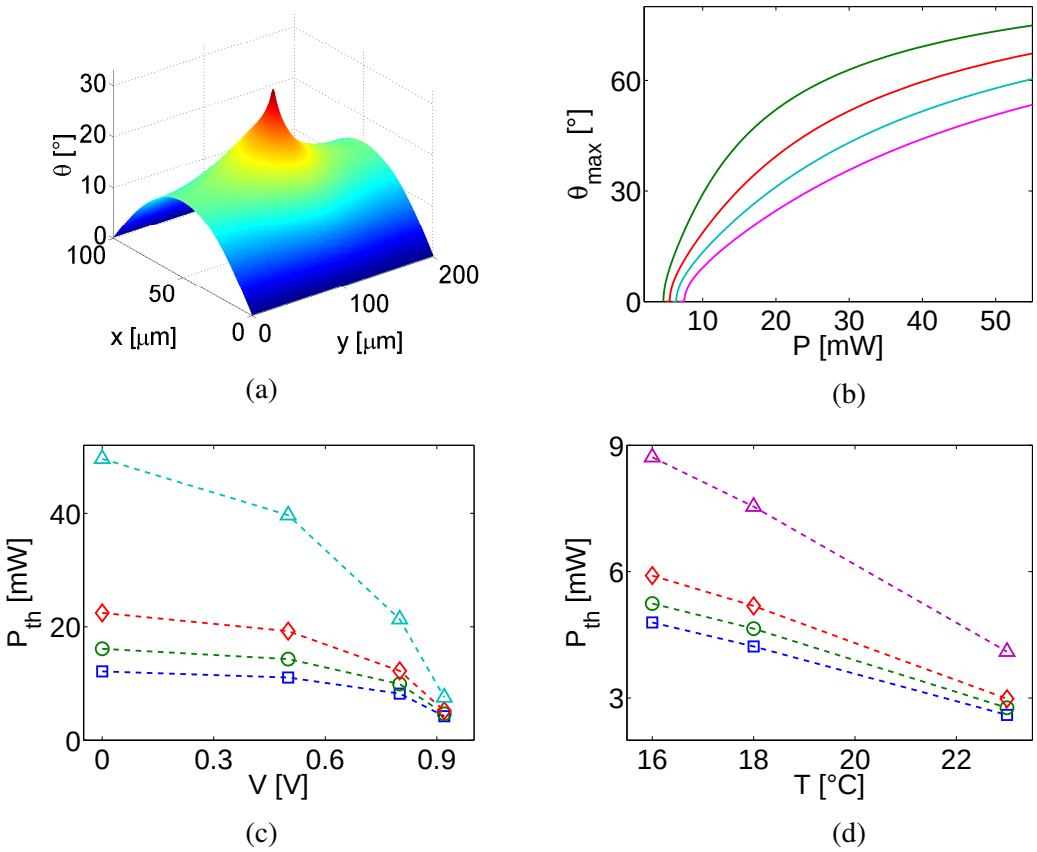

Fig. 2.6 Numerical solutions of the reorientational equation for standard E7 at 18°C: (a) Reorientation caused by a 2μm-waist Gaussian beam at P=6 mW, in the presence of a 1V additional bias. (b) Maximum reorientation dynamics versus power with 1V bias; colours represent Gaussian profiles of different waists ω_0: 5, 15, 25 and 35 μm from left to right (green, red, cyan and magenta) respectively. (c) Calculated power threshold P_{th} (Gaussian beam with waist of $2\mu m$ (blue line with squares), $5\mu m$ (green line with circles), 11μm (red line with diamonds) and 35μm (cyan line with triangles) at 18°C versus bias; (d) calculated P_{th} versus temperature in the presence of a 0.92V bias (d)

.

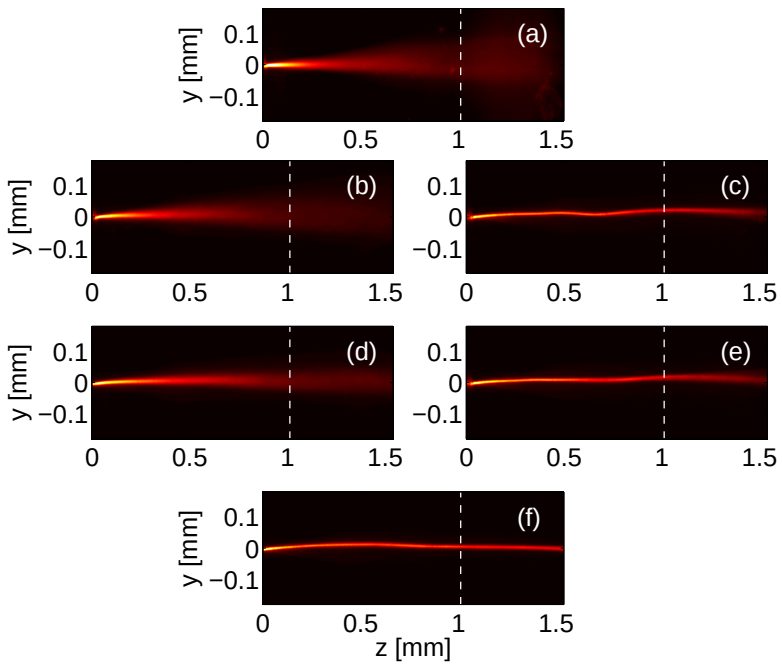

Fig. 2.7 Intensity evolution of a laser beam in the nematic LC cell at power (a) 1mW, (b,c) 15mW, (d,e) 16mW and (f) 20mW. Right panels correspond to increasing excitation, left panels to decreasing excitation.

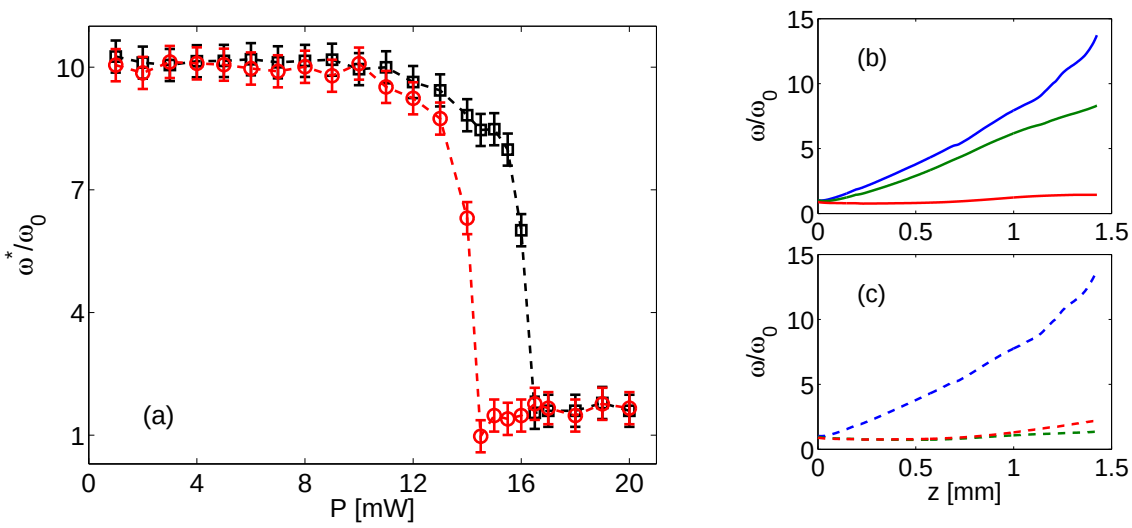

Fig. 2.8 (a) Measured beam width (along y) in $z = 1$mm, normalized to initial waist and plotted versus input power as the latter was ramped-up (black line with squares) and ramped-down (red line with circles). Normalized beam width versus propagation as power (b) increased from 2 (blue) to 15.5 (green) and to 20 mW (red) and (c) decreased back from 20 (red) to 15.5 (green) to 2 mW (blue).

could be modelled by a shape- and amplitude- preserving Gaussian of $\omega_{eff} = 11\mu$m (see Supplemental Material in A).

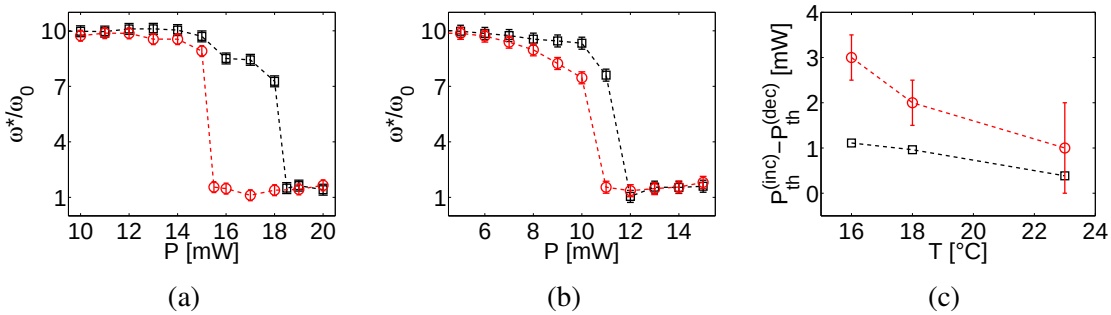

Fig. 2.9 Measured beam width along y at $z = 1$mm, normalized to input waist, versus increasing power (black line with squares) and decreasing power (red line with circles) at (a) 16°C and (b) 23°C. (c) Comparison of numerically predicted (black line with squares) and experimentally evaluated (red line with circles) hysteresis size.

The theoretically predicted power threshold corresponding to a Gaussian beam of waist 11 μm is about 5.2 mW, about three times lower than the experimentally evaluated threshold of 16.5 mW corresponding to a diverging beam. Scattering losses, coupling imperfection and longitudinal effects are among the reasons of such discrepancy. By applying the same scaling (about $\times 3$) to the threshold estimated for self-confined beams, it matches the threshold of 3.5μm predicted for z-invariant beams, in good agreement with the experimentally observed soliton width.

By varying the sample temperature the width of the hysteresis loop could be tuned at a fixed bias. As predicted, the loop was wider at lower temperatures (see Fig. 2.9a) and narrower at 23°C (see Fig. 2.9b), in agreement with the predicted power threshold versus temperature (see Fig. 2.6d). Figure 2.9c shows experimentally evaluated and numerically computed width of the hysteresis loop versus power (see also article no.3 “Nematicons in planar cells subject to the optical Frèedericksz threshold” in A).

2.6 Conclusions

Optical bistability with finite-size beams was predicted and experimentally observed close to the optical Frèericksz transition. The required feedback was provided by self-focusing via the reorientation nonlinearity of nematic LC. It was demonstrated that, in a finite interval of input powers, the beams can propagate as either diffracting or soliton wavepackets, depending on the "history" of the system. Bistability was accompanied by hysteresis in beam width as

power increased and decreased. The size of such loop, i.e. the interval of powers supporting bistability, was tuned by the parameters of the system and the experimental conditions (temperature), as well as by an external voltage bias below the transition threshold.

Chapter 3

Self-induced negative refraction

Chapter 1 showed that an extraordinarily polarized beam can induce an inhomogeneous rotation of the director, in turn leading to self-focusing and eventual formation of spatial solitons and corresponding to a guiding index well for co-polarized signal(s). This occurs because the director is the optic axis of the uniaxial NLC, and determines at the same time the extraordinary index of refraction as well as the walk-off of the extraordinary wave (see Eq. 1.4). Since the mutual orientation of wavevector and director defines the direction of light propagation through walkoff, the net effect is a power-dependent self-deflection of extraordinary polarized beams by way of reorientation [66]). In this chapter I demonstrate that, in geometries close to the OFT, optically induced rotation of the NLC molecular director may lead to a transition from positive to negative refraction across the interface between NLC and an isotropic medium.

Negative refraction takes place when incident and refracted light rays propagate in the same half-plane with respect to the normal at the interface between two different dielectrics. Besides negative refraction, hereby I show that the overall angular span of the light paths set by beam power (i.e. without external fields) is maximized near the OFT. In practice, spatial soliton formation and power-controlled beam self-steering can be used to control the direction of light-induced graded-index waveguides, paving the way to a new family of all-optical devices - routers and spatial demultiplexers - where light itself defines the topology of the network. The results of this thesis allow the significant improvements of all-optical readdressing, with a larger number of output ports as compared to previous configurations.

3.1 Light steering in reorientational NLC

Most NLCs are positive uniaxial media with the optic axis coincident with the molecular director. As in any anisotropic media, the propagation of extraordinary polarized light beams occurs along directions defined by the mutual orientation of wavevector and optic axis. In particular, the Poynting vector in uniaxials always lies between the wavevector and the optic axis, with a walk-off angle

$$\delta = \arctan\left(\frac{\Delta\varepsilon \sin(2\theta)}{\Delta\varepsilon + 2n_{\perp}^{2} + \Delta\varepsilon \sin(2\theta)}\right). \tag{3.1}$$

Clearly, the value of such angular deviation depends on the dielectric constants and θ. The high anisotropy of liquid crystals provides large walk-offs, with values as high as 9° according to wavelength and temperature [67]. Molecular reorientation through the application of magnetic or electric fields can change θ and consequently δ, providing beam steering. In various NLC cell geometries both power- and bias-controlled beam steering has been investigated theoretically and experimentally [26, 30, 68–78].

The simplest scheme for beam steering corresponds to a nematicon generated across the interface between an isotropic medium and a NLC; nematicon bending was studied at dielectric curved surfaces, namely glass spheres and air bubbles [76, 77]

Nonetheless, for signal processing the control of the beam trajectory is desirable. Nematicon steering was initially achieved by applying a low-frequency bias to a planar cell. In the simplest case an external electric field is applied perpendicular to the plane containing the director and the wavevector: The NLC molecules can therefore rotate out of that plane, increasing θ until the director becomes normal to the light field polarization and, in turn, the walk-off δ vanishes [79]. The maximum deflection observable in this case is defined by the alignment θ providing the initial δ.

When an external bias is applied with electrivc field in the principal plane of extraordinary wave propagation, it provides molecular rotation and beam steering through a distortion of the director distribution. When the corresponding cell size is finite, that results in beam oscillation within the finite potential [68]. In other geometries, a considerable bias-controlled beam steering may be observed [26, 69]. An approach to in-plane steering consists in realizing two pairs of interdigitated comb electrodes on top and bottom cell interfacs, with a dominat component of the electric field perpendicular to the comb fingers. The NLC molecules, sandwiched between the electrodes, tend to reorient parallel to this field and to the interfaces, up to an angle dependent on the applied bias. The extraordinary beam can then be

steered by the changes in walk-off up to its maximum value. The latter limit can be doubled by using dual-frequency NLC, where the sign of the dielectric anisotropy changes depending on the frequency of the bias [70]. Beam deflection can be further enhanced by defining non-uniform electric field distributions in distinct NLC zones and exploiting light refraction as the wavepacket travels from one to the next [80–82]. The record in bias-controlled steering of nematicons was recently reported with conductive micro-rods immersed in the NLC [78].

Nematicon deflection was also obtained by using other beams, either collinear (other nematicons) or orthogonal (diffracting beams). One of the first demonstration of the steering of optical spatial solitons was realized with a diffracting beam extraordinary polarized and propagating normal to the plane of steering [83]. Such an external beam, counteracting the torque generating the soliton, gave rise to a nonlinear lens which could alter the soliton trajectory. Controlling beams may also be employed to induce refraction or reflection of the soliton [66]. A soliton may also be steered by other solitons propagating as extraordinary waves, either in planar interactions [30, 71–73] or skew, when they spiral around a common axis by means of mutual attraction and angular momentum [74].

One of the most intriguing features of nematicons is that, under suitable conditions, they can change their path on their own, i.e., by acting on the input power. In finite-size cells, for example, it was demonstrated that, in the presence of strong anchoring, spatial solitons are repelled by the boundaries at a power-dependent rate [75]. As the self-confined beam creates its own index profile, an unequal distance from the two interfaces provides an asymmetric distortion and an effective gradient, with a nonlinear force directed towards the cell mid-plane; the latter results in a quasi-sinusoidal (the effective potential is anharmonic) motion of the nematicon along propagation z with period depending on power. Solitary beams can also exhibit power-controlled self-steering. In this case molecular reorientation chages the walk-off in the principal plane of propagation. An in-plane self-steering as large as 2° was observed experimentally [25].

3.2 Negative refraction

The Snell's law for light refraction stems from Fermat's principle, stating that the motion of optical rays minimizes the optical path between initial and final positions. In the context of Maxwell's equations, Snell's law is simply based on the conservation of the transverse momentum when the dielectric properties of the interface vary solely along the direction normal to it [84]. Accordingly, when light crosses a planar interface between two isotropic media and absorption is negligible, it is subject to an abrupt deflection such that rays propagate

in opposite half-planes with respect to the normal, forming with the latter an angle β which obeys:

$$n_{in} \sin \beta_{in} = n \sin \beta. \tag{3.2}$$

In Eq. 3.2 β_{in} is the incidence angle, n_{in} and n are the refractive indices in the first (incident wave) and second regions (refracted wave), respectively. Thus, after refraction light propagates at an angle β in the medium with refractive index n. These angles define the directions of phase and group velocities of light, which are parallel to each other in isotropic materials. What I just described is positive (standard) refraction. In the last years, however, much attention has been devoted also to negative refraction, revived by the introduction of the so-called metamaterials [85].

The first and most striking effect predicted in metamaterials is the presence of a negative refractive index. This counter-intuitive phenomenon consists of refraction in such a way that the phase velocity is anti-parallel to the energy flow (i.e. the group velocity) and was first predicted by Veselago [86]. He showed that, for media with simultaneously negative dielectric permittivity ε and permeability μ, Maxwell's equations predict that wavevector **k** (along phase propagation) and Poynting vector **S** (along the direction of energy propagation) are opposite to each other. The so called backward waves are expected to propagate in such media leading to reversal of the Vavilov-Cherenkov radiation, of the Doppler effect and of Snell's law. The latter was called negative refraction (NR) at variance with standard (positive) refraction. Negative refraction due to backward waves was also predicted by Schuster within the absorption band of materials more than a century ago [87], but their observation was prevented by the very fast decay of evanescent waves. Later, however, Sir J. Pendry showed that ideal negative-index materials enhance evanescent backward waves: other restrictions come from their physical feasibility, as strong absorption and dispersion in frequency are present [85].

Despite the above type of NR implies that wave vector and Poynting vector are counterpropagating, this condition is not necessary. Negative refraction can also be observed when anomalous refraction occurs in anisotropic materials and photonic crystals: it requires a misalignment between phase and group velocities, a condition less stringent than required in metamaterials [88, 89]. Such type of NR does not require a negative refractive index. In anisotropic media the wavevector is always refracted positively (standard) whereas the group velocity after refraction can lie on the opposite side with respect to the interface normal due to walk-off, so that both incident and refracted Poynting vectore belong to the same half plane. The condition of anti-parallel **k** and **S** is not satisfied, but after refraction **k** and **S** lay on opposite sides of the interface normal.

3.2.1 Linear and nonlinear amphoteric refraction at an interface between anisotropic materials

Let me consider light refraction across an interface between isotropic and uniaxial materials. A plane wave of arbitrary polarization, reaching the input interface with wavevector $\mathbf{k}_{in}$ at some angle β_{in} with respect to the normal, is subject to double refraction. Thus, two components of orthogonal polarizations, ordinary and extraordinary, are excited into the uniaxial, with wavevectors $\mathbf{k}_o$ and $\mathbf{k}_e$, respectively, and energy propagation along $\mathbf{S}_o$ and $\mathbf{S}_e$, respectively. In uniaxials the inverse surface of wave normals for extraordinary waves is ellipsoidal while for ordinary waves it is spherical [84].

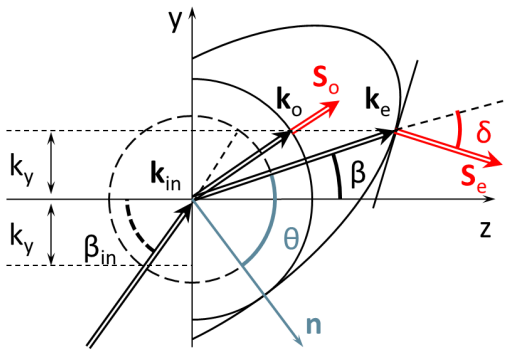

Fig. 3.1 Light negative refraction at isotropic-positive uniaxial interface. The dashed circle is a section of the inverse surface of wave normals in the incidence plane (isotropic medium). The solid circle and ellipse represent sections in a positive uniaxial for light of ordinary and extraordinary polarizations, respectively.

Transverse momentum (proportional to k_y) conservation defines the direction of $\mathbf{k}_o$ and $\mathbf{k}_e$ corresponding to $\mathbf{k}_{in}$ according to Eq. 3.2. $\mathbf{S}_o$ and $\mathbf{S}_e$ are normal to the inverse surface of wave normals in points where $\mathbf{k}_o$ and $\mathbf{k}_e$ touch it. The spherical surface for ordinary waves keeps $\mathbf{S}_o$ and $\mathbf{k}_o$ parallel, but the ellipsoidal surface for extraordinary waves generally implies a non-vanishing walk-off δ between $\mathbf{S}_e$ and $\mathbf{k}_e$ depending on the angle θ between $\mathbf{k}_e$ and $\hat{n}$. In a range of β_{in} defined by material parameters, δ may overcome β and cause $\mathbf{k}_e$ and $\mathbf{S}_e$ to lay on opposite sides of the interface normal, i.e. negative refraction. All anisotropic materials exhibit amphoteric (from the Greek *amphoteroi* meaning "both") refraction involving ordinary and extraordinary polarized light. It is worth to notice that in either positive or negative refraction the phasefronts move forward. Such negative refraction was probably identified in early work on birefringence by Bartholinus in the XVII century, but it was measured in recent experiments. The key parameter to describe NR is the optical anisotropy. Across the

interface between two anisotropic media with distinct orientation of optic axes, the light rays can undergo NR in wider range of β_{in} than in the case of isotropic-anisotropic interface. Light of extraordinary polarization was observed to refract negatively within $\beta \in [-12;0)$ degrees in a twin structure (with optic axis at $\pm 45°$ to the interface normal) of semiconductor with $\Delta n = 0.23$ [90].

NLCs, highly anisotropic material with a large degree of tunability, are ideal candidates for NR investigation. A 12°-wide range of incidence angles was demonstrated to yield NR of extraordinary polarized green light across an interface between air and the standard NLC mixture E7 with director homogeneously oriented at 45° (to the interface normal) in the incidence plane [91]. Using mixtures with different anisotropy and optic axis orientation this range of incidence angles was increased up to 23° [92]. Due to electro-optic reorientation, the optic axis in NLC can be rotated by applying a bias. The related change of walk-off can allow switching refraction from negative to positive and viceversa. Amphoteric refraction takes place at isotropic-NLC interfaces also when nematicons are used as "probe" beams [37]. The refraction of Gaussian beams of mixed polarization has amphoteric character at the interface between an isotropic medium and the E7 NLC mixture: when the optic axis (director) was oriented at 60° to the interface normal in the incidence plane, standard refraction occurred for an ordinary polarized wave, while negative refraction took place for extraordinary waves. The extraordinary component formed a spatial soliton (nematicon) and the ordinary component diffracted, while they propagated on opposite sides of the interface normal [37]. Moreover, the application of external bias rotated the optic axis out of incidence plane and switched the nematicon to a half-plane corresponding to positive refraction.

3.3 Power-controlled switching from positive to negative nonlinear refraction

Let me consider now linear and nonlinear light refraction at the interface of the NLC cell sketched in Fig. 2.1b. In order to avoid spurious effect due to repulsion from the boundaries, I consider the incidence plane and the extraordinary input polarization in yz.

In the absence of molecular reorientation, the optic axis ($\hat{n}$) coincides with the interface normal (see Fig. 3.3a). The refracted wavevector is defined by the Snell's law:

$$n_{in} \sin \beta_{in} = \sqrt{\frac{n_\perp^2 n_\parallel^2}{n_\perp^2 \sin^2 \theta + n_\parallel^2 \cos^2 \theta}} \sin \beta. \tag{3.3}$$

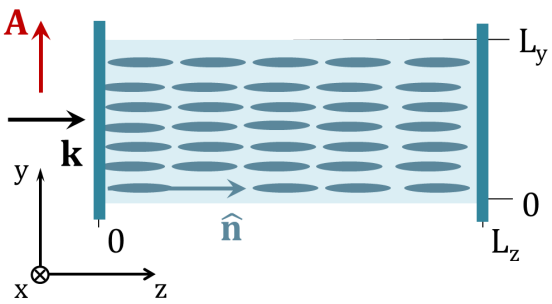

Fig. 3.2 Sketch of the unperturbed NLC cell.

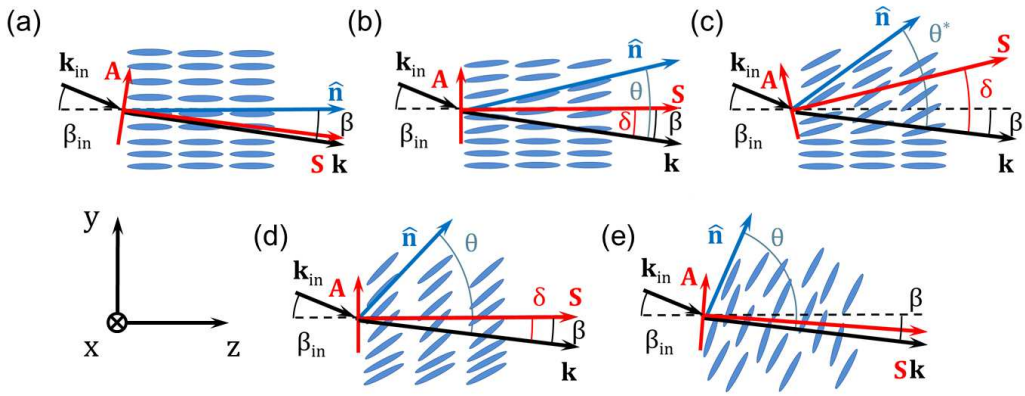

Fig. 3.3 Illustration of negative refraction at an isotropic-uniaxial interface. (a) Positive linear refraction; (b-d) negative refraction and (e) positive nonlinear refraction in the presence of light-induced reorientation.

The beam Poynting vector **S** deviates from **k** to $\delta(\theta)$ and lays between **k** and $\hat{n}$. Only positive refraction occurs for any β_{in} in the weakly nonlinear regime.

In the nonlinear regime, the light beam can impress a non-negligible rotation to the director, thus changing the angle between the wavevector and the optic axis. Owing to the related refractive index change, the wavevector deviates from its initial direction to an angle $\Delta(\theta)$ less then 1° when β_{in} is sufficiently small (see Fig. 3.4a) and remains on the same side with respect to axis z (β and β_{in} keep the same sign). In the highly nonlinear regime the molecules rotate towards the electric field vector, increasing θ and changing δ. At some value of θ, defined by the beam power P, δ compensates β (see Fig. 3.3b) if the latter is smaller than the maximum walk-off δ_{max}. Further increases in $\theta(P)$ provide NR until δ reaches δ_{max} at certain θ^* (Fig. 3.3c) and then reduces to $\delta = \beta$ (Fig. 3.3d). Then refraction changes back to positive (Fig. 3.3e). The Poynting vector, defined by the angle $\gamma = \beta - \delta$ (the angle between $\hat{z}$ and **S**), switches from one side of the normal to the other and back if β_{in}

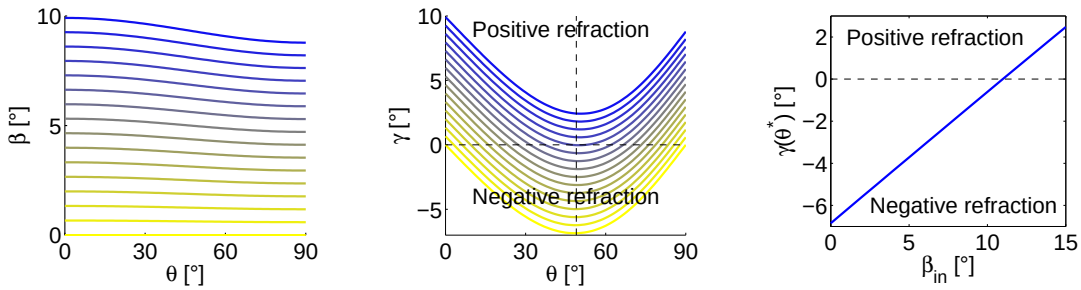

(a) (b) (c)

Fig. 3.4 Changes in refraction and propagation angles with molecular reorientation for a range of incidence angles (from air) from 0° (yellow lines) to 15° (blue lines). The wavevector is defined by angle β and changes its direction only slightly for any reorientation θ in a given range of β_{in}. The Poynting vector defined by angle γ undergoes significant changes with reorientation (b). (c) represents γ when the reorientation to $\theta = \theta^*$ maximizes the walk-off (dashed line in (b)).

is sufficiently small (see Fig. 3.4b), changing sign of the group velocity along y. The angular span of walk-off is limited by the optical anisotropy and β, as θ can take all values from β to $\frac{\pi}{2}$. Thus, in a given geometry, power-controlled beam self-steering is maximized when β is small. The span of β_{in} for which NR occurs at each power is limited by the maximum walk-off and the maximum change in refraction angle: $\delta_{max} + \Delta(\theta^*)$. For the air/standard NLC mixture E7 interface it can be estimated around 12° (see Fig. 3.4c).

3.3.1 Experimental demonstration

For the experimental observation of NR, minor adjustments to the set-up in Fig. 2.5 were needed. The wavevector deflection was provided by displacing the beam axis from the symmetry axis of the microscope objective. To this extent I mounted the mirror before the microscope objective on a micrometric translation stage (Fig. 3.5). Using a couple of convex lenses to form a telescope the beam waist was adjusted in order to optimize the nonlinear interaction. Gaussian beams of shorter Rayleigh lengths maximize the optical torque near the input interface, but the light-matter coupling decays quickly along z due to strong diffractive spreading. On the other hand, beams with long Rayleigh distances produce a weak optical torque due to the lower intensities for a given power (analogously to increasing of threshold power with larger waist in the case of OFT, see Fig. 2.3c). Numerically, a good trade-off was found around $\omega_0 \simeq 8\mu$m. The beam waist at focus was located at some distance from the input interface inside the cell, in order to maximize the effectiveness of the nonlinear response and the soliton propagation distance in the presence of scattering losses.

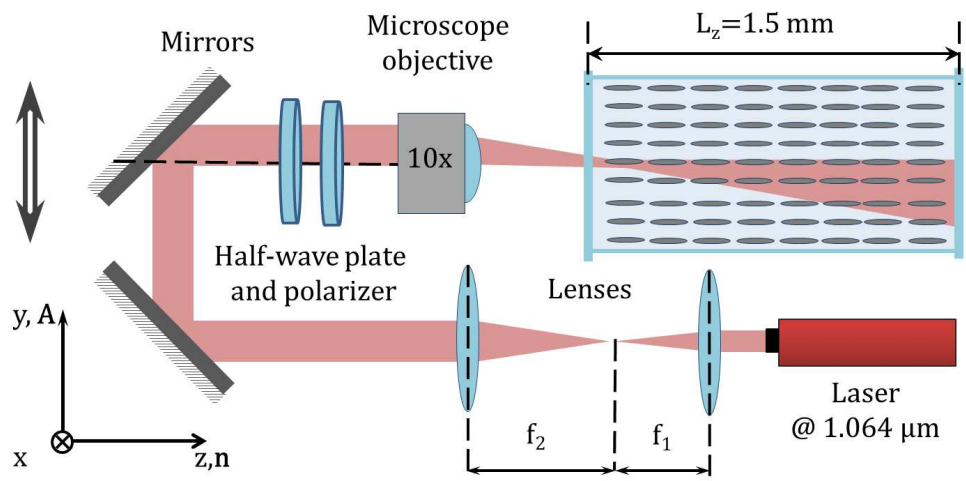

Fig. 3.5 Experimental set-up modified for the observation of NR. A translation of the mirror in front of the microscope objective offset the laser beam from the axis of the objective and provided incidence with a slight tilt. A couple of convex lenses of focal lengths f_1 and f_2 placed at distance $f_1 + f_2$ was used for beam waist adjustments.

Typical examples of beam evolution in the extraordinary polarization and in the linear regime are shown in Fig. 3.6a. The white dashed line represents the normal to the interface, the arrows indicate the orientation of the optic axis $\hat{n}$, the wavevector **k** and the Poynting vector **S**, respectively. The direction of the interface normal was evaluated experimentally by comparing the beam trajectories in extraordinary and ordinary polarizations for the same β_{in} (see Fig. 3.6b). The **S** directions were directly evaluated from images of extraordinary and ordinary beams. These two directions deviate from each other due to walk-off and refraction angle change $\delta(\theta) + \Delta(\theta)$. In the linear case $\theta = \beta$ as $\hat{n}$ is parallel to the interface normal. Using Eq. 3.3 β_{in} was calculated. The plot on Fig. 3.6 shows the estimated β_{in} corresponding to measured $\gamma = \beta - \delta$, the latter being the angle between **S** and the interface normal.

For a fixed $\beta_{in} \simeq -4.9°$ (see Fig. 3.6a) the evolution of an extraordinary polarized beam versus power is shown in Fig. 3.7. From the images it is clearly visible that the beam switches from one half-plane with respect to the interface normal to the other as the beam power grows: to the best of my knowledge, this is the first demonstration of self-induced beam switching from positive to negative refraction. As discussed later, the best trade-off between nonlinearity and required walk-off for NR is close to a β_{in} of about 5°. Let me address in detail the dynamics with power and the corresponding features of beam propagation. As the input power increased, reorientation occurred with consequent changes in beam profile and trajectory. Because of the unavoidable scattering losses and diffraction, the beam intensity diminished in propagation providing a z-varying reorientation. Since self-focusing and **S**

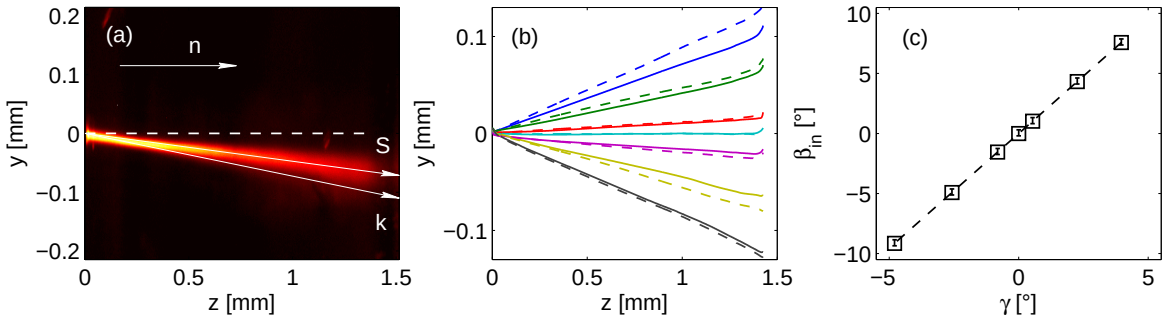

Fig. 3.6 Linear refraction at the interface glass-E7. (a) Intensity evolution of an extraordinary polarized beam and relevant directions. The incidence angle is about −4.9°. (b) Estimated beam trajectories for extraordinary (solid lines) and ordinary (dashed lines) polarizations. Solid and dashed lines of the same colour correspond to the same β_{in} (7.6°, 4.3°, 1°, -1.6°, -4.9°, -9.2° from blue to black). (c) Iincidence angle β_{in} evaluated from measured angles γ between beam Poynting vector and interface normal.

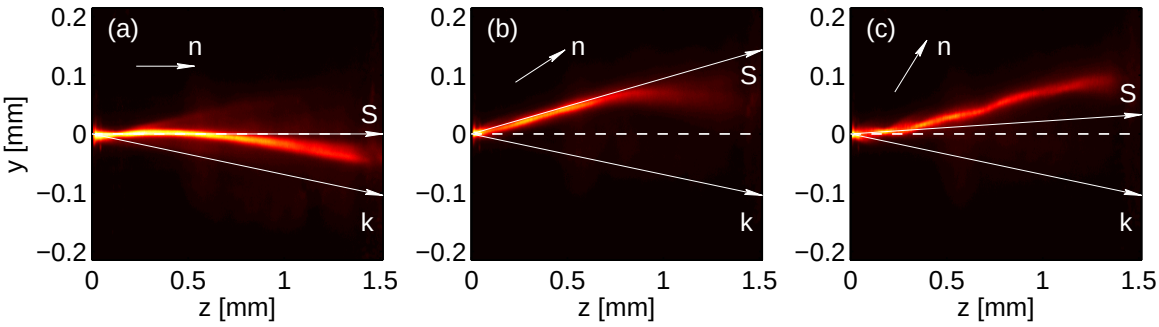

Fig. 3.7 Power-dependent refraction across the interface between isotropic and NLC media:(a) positive refraction at P=20 mW; (b) and (c) negative refraction at 40 mW and 100 mW, respectively. The iIncidence angle was about −4.9°.

direction are defined by θ, they varied in propagation, as well. This resulted in curved trajectories for the light beams.

For a power of 20 mW the beam trajectory became parallel to z in the first portion of its propagation (see beam trajectory in Fig. 3.8a and its profile in z=0.5 mm (green line) in Fig. 3.8b); in the last portion of its propagation, where the intensity was significantly lower, the beam remained in the initial half-plane (see profile in z=1.1 mm (green) in Fig. 3.8c).

At higher powers nonlinear reorientation was strong enough to provide the required walk-off for NR all along the propagation distance, so that the beam propagated in the opposite half-plane (see image and trajectory of a 40 mW beam in Fig. 3.7b Fig. 3.8a (cyan line), respectively and corresponding profiles in cyan in Fig. 3.8b,c). Eventually, at powers higher than 40 mW, θ overcame 45° in the first portion of the propagation and δ decreased

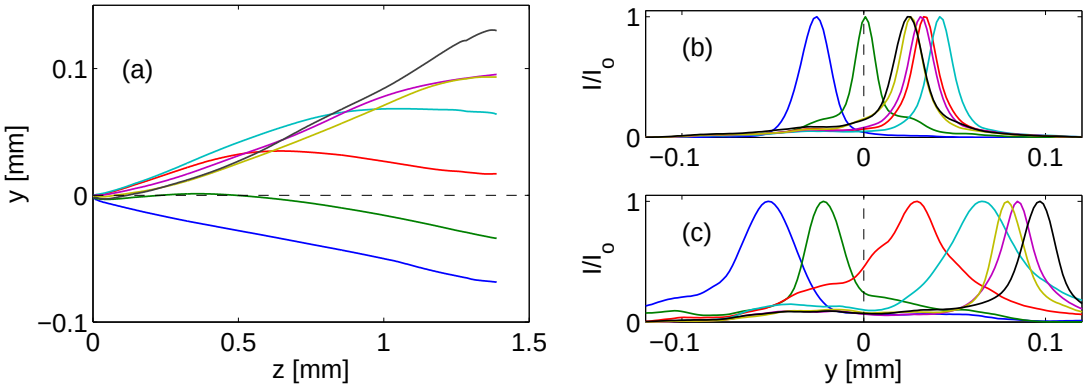

Fig. 3.8 Beam trajectories along z. Blue, green, red, cyan, magenta, yellow and black lines correspond to input powers of 2, 20, 30, 40, 70, 100 and 150 mW, respectively. Beam profiles along y in (b) z=0.5 mm and (c) z=1.1 mm.

as the power was further increased (see image and trajectory of a 100 mW beam in Fig. 3.7c and Fig. 3.8a (yellow line) and corresponding profile in yellow in Fig. 3.8b). Reorientation at 150 mW in the last portion of the propagation reached about 45°, providing maximum walk-off (about 7°) and a lateral beam displacement of about 0.15 mm (see profiles in blue and black in Fig. 3.8c corresponding to beam powers of 2 and 150 mW, respectively). Such angular deflection and transverse displacement due to power-controlled self-steering in pure NLC is a few times larger than reported in [25] and is the largest observed to date.

3.4 Discussion

Light-induced reorientation close to the OFT may lead to changes in refraction from positive to negative across the interface between an isotropic medium and NLC, in a certain interval of incidence angles. In order to estimate the incidence angles providing favourable conditions (lower powers) for the observation of self-induced NR, I acquired the output profiles of light beams at the output of the NLC cell using another 10× microscope objective and a CCD camera (Fig. 3.9). The input power changes from top to bottom images, assuming values of 2, 20, 30, 40, 70 and 100 mW, respectively. The incidence angle changes from leftmost to rightmost images taking values $-9.2°, -4.9°, -1.6°, 1°, 4.3°$ and $7.6°$, respectively. Light-induced NR occurs when the beam crosses the interface normal (white dashed line). For small (absolute value) incidence angles the beam lies close to the interface normal in the linear regime and requires less walk-off to cross it. Thus small incidence angles favour NR.

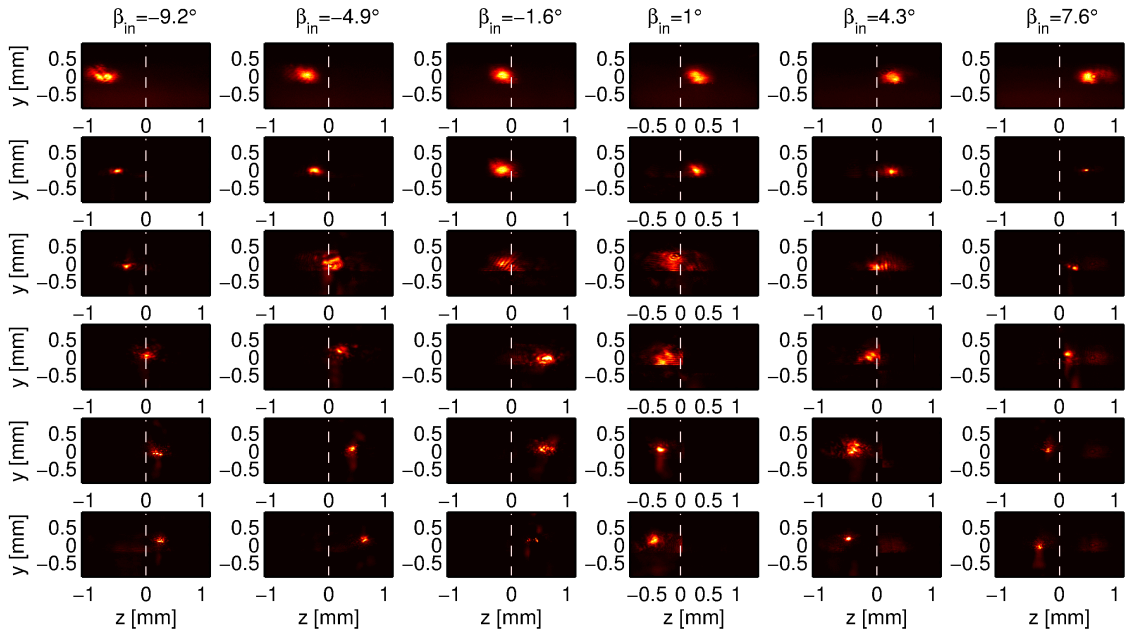

Fig. 3.9 Beam output profiles for different β_{in}. Rows correspond to input powers of 2, 20, 30, 40, 70, 100 mW from top to bottom, respectively. Columns correspond to various incidence angles, as marked.

However, as it can be seen at 20 mW (second row), the beam self-focuses less at smaller angles at the same power, due to smaller reorientation. This is because the nonlinearity reduces as the angle between wavevector and director approaches 0° and normal incidence ($\beta_{in} = 0°$). Therefore, there is a trade-off between nonlinearity and required walk-off for observing beam-induced NR. In agreement with the experimental results, small angles favour NR as they require less walk-off, but yield less nonlinearity; larger angles increase the nonlinearity but also require bigger walk-offs. Light-induced NR may be observed at low powers in an intermediate range of absolute incidence angles. At high powers all β_{in} in $[12°;0°) \cup (0°;12°]$ support light-induced NR (see also article no.4 "Power-controlled transition from standard to negative refraction in reorientational soft matter" in A). The measured output profiles clearly show several resolvable output pots at different powers, demonstrating that such mechanism can be directly employed for power-controlled spatial demultiplexing and signal routing.

Chapter 4

Conclusions

The highly nonlinear and nonlocal responses of liquid crystals to external stimuli make them one of the most fascinating media for the investigation of nonlinear optical phenomena, involving both fundamental issues and potential applications, such as all-optical devices for signal processing. In this context, self-trapped light beams in nematic liquid crystals - nematicons - are one of the most intriguing phenomena. In fact, nematicons are optical waveguides defined by light itself, paving the way to the realization of new generations of light-controlled networks, i.e., systems which can be reconfigured by the optical signals themselves. In this thesis I studied nonlinear light propagation involving nematicons in reorientational nematic liquid crystal near the Frèedericksz transition. Several new phenomena were predicted and have been observed for the first time in such a configuration. Above all, due to threshold-like reorientational nonlinearity, hysteretic effects enable the realization of all-optical memories based on nematicons.

The first topic of this thesis work was optical bistability with two states for light beams of the same power, differing in spatial size. Although predicted theoretically for solitons in media possessing a sharp nonlinear response with intensity, this effect had not yet been observed. In nematic liquid crystals an abrupt increase in nonlinearity occurs at the optical Frèedericksz transition: when the electric field of the beam and the mean alignment of the LC molecules are normal to one another, reorientation takes place only beyond a certain power, the latter value depending on material parameter as well as on geometry (cell size and beam shape). Using Gaussian beams, I showed the existence of two stable states: diffracting beam at low powers (relatively wide) and self-confined (nematicon, narrow) at high powers. I demonstrated experimentally and numerically, that the wavepacket, for a given set of input conditions including the input power, could propagate in either diffracting or solitary regimes, depending on the system "history". Memory effects in this geometry are related to the

dependence of the threshold power on the size of the input beam propagating in the sample: narrower beams induce stronger molecular torques, thus a lower threshold occurs when light undergoes self-confinement. I found a good agreement between observed and predicted hysteresis versus input power.

The second topic of investigation was self-induced nonlinear negative refraction at the interface between an isotropic medium and a nematic liquid crystal. In a certain range of incidence angles and powers, light is observed to undergo nonlinear negative refraction, i.e., its transverse component of Poynting vector changes sign when crossing the interface. Moreover, I demonstrated that the nature of refraction varies from positive to negative as power is increased. This behavior is due to angular steering of beams through the walk-off dependence on input power. I also demonstrated that the overall angular deflection of intense beams is maximized in geometries close to the optical Frèedericksz transition: the observed overall angular steering, a few times larger than in previous studies, is the current record for power-dependent beam self-steering in undoped nematic liquid crystals.

I stress that both phenomena, thanks to the highly nonlinear response of liquid crystals, occur at relatively low (milliwatts) powers and stem from the reorientational response, with negligible thermal effects. Nevertheless, besides reorientational nematic liquid crystals, optical bistability involving spatial solitons is expected to occur also in other media encompassing a sharp change of nonlinear response; likewise, self-induced negative refraction is expected to occur in anisotropic soft matter with power-dependent orientation of the optic axis. Thus the results of this thesis bear interest in various fields of optical physics and engineering, including all-optical memory elements with nematicons, power-controlled self-steering and power-dependent waveguides or spatial demultiplexers.

References

[1] Eryk Infeld and George Rowlands. *Nonlinear Waves, Solitons and Chaos*. Cambridge University Press, second edition, 2000. Cambridge Books Online.

[2] S. Trillo and W. E. Torruellas. *Spatial Solitons*. Springer-Verlag, Berlin, 2001.

[3] George I. Stegeman and Mordechai Segev. Optical Spatial Solitons and Their Interactions: Universality and Diversity. *Science*, 286(5444):1518–1523, 1999.

[4] D. J. Korteweg and F. De Vries. On the change of form of long waves advancing in a rectangular canal, and on a new type of long stationary waves. *Philosophical Magazine*, 39:422–443, 1895.

[5] J. S. Russell. Report on waves. In *Report of the fourteenth meeting of the British Association for the Advancement of Science*, pages 311–390, York, 1844.

[6] P. G. DeGennes and J. Prost. *The Physics of Liquid Crystals*. Oxford Science, New York, 1993.

[7] E. P. Raynes, R. J. A. Tough, and K. A. Davies. Voltage dependence of the capacitance of a twisted nematic liquid crystal layer. *Mol. Cryst. Liq. Cryst.*, 56:63–68, 1979.

[8] F. Simoni. *Nonlinear Optical Properties of Liquid Crystals*. World Scientific, Singapore, 1997.

[9] S. Chandrasekhar. *Liquid Crystals*. Cambridge University Press, second edition, 1992. Cambridge Books Online.

[10] C. Conti, M. Peccianti, and G. Assanto. Route to nonlocality and observation of accessible solitons. *Phys. Rev. Lett.*, 91:073901, 2003.

[11] M. Warenghem, J. F. Henninot, and G. Abbate. Non linearly induced self waveguiding structure in dye doped nematic liquid crystals confined in capillaries. *Opt. Express*, 2:483–490, 1998.

[12] G. Assanto and M. Peccianti. Spatial solitons in nematic liquid crystals. *IEEE J. Quantum Electron.*, 39:13–21, 2003.

[13] Armando Piccardi, Alessandro Alberucci, Nina Kravets, Oleksandr Buchnev, and Gaetano Assanto. Power-controlled transition from standard to negative refraction in reorientational soft matter. *Nat. Commun.*, 5, Nov 2014.

[14] Gaetano Assanto, Marco Peccianti, and Claudio Conti. Nematicons: Optical spatial solitons in nematic liquid crystals. *Opt. Photon. News*, 14(2):44–48, 2003.

[15] Erez Braun, Luc P. Faucheux, and Albert Libchaber. Strong self-focusing in nematic liquid crystals. *Phys. Rev. A*, 48(1):611–622, Jul 1993.

[16] David W. McLaughlin, David J. Muraki, Michael J. Shelley, and Xiao Wang. A paraxial model for optical self-focussing in a nematic liquid crystal. *Physica D*, 88(1):55 – 81, 1995.

[17] David W. McLaughlin, David J. Muraki, and Michael J. Shelley. Self-focussed optical structures in a nematic liquid crystal. *Physica D: Nonlinear Phenomena*, 97(4):471 – 497, 1996.

[18] M. Warenghem, J.F. Blach, and J. F. Henninot. Thermo-nematicon: an unnatural coexistence of solitons in liquid crystals? *J. Opt. Soc. Am. B*, 25:1882–1887, 2008.

[19] A. W. Snyder and D. J. Mitchell. Accessible solitons. *Science*, 276:1538, 1997.

[20] Shigen Ouyang, Qi Guo, and Wei Hu. Perturbative analysis of generally nonlocal spatial optical solitons. *Phys. Rev. E*, 74(3):036622, 2006.

[21] Qi Guo, Boren Luo, and Sien Chi. Optical beams in sub-strongly non-local nonlinear media: A variational solution. *Optics Communications*, 259(1):336 – 341, 2006.

[22] Dongmei Deng and Qi Guo. Propagation of laguerre–gaussian beams in nonlocal nonlinear media. *Journal of Optics A: Pure and Applied Optics*, 10(3):035101, 2008.

[23] W. Krolikowski and O. Bang. Solitons in nonlocal nonlinear media: exact solutions. *Phys. Rev. E*, 63:016610, 2000.

[24] M. Peccianti, A. De Rossi, G. Assanto, A. De Luca, C. Umeton, and I. C. Khoo. Electrically assisted self-confinement and waveguiding in planar nematic liquid crystal cells. *Appl. Phys. Lett.*, 77(1):7–9, 2000.

[25] Armando Piccardi, Alessandro Alberucci, and Gaetano Assanto. Soliton self-deflection via power-dependent walk-off. *Appl. Phys. Lett.*, 96:061105, 2010.

[26] Armando Piccardi, Marco Peccianti, Gaetano Assanto, Andriy Dyadyusha, and Malgosia Kaczmarek. Voltage-driven in-plane steering of nematicons. *Appl. Phys. Lett.*, 94(9):091106, 2009.

[27] Shigen Ouyang, Wei Hu, and Qi Guo. Light steering in a strongly nonlocal nonlinear medium. *Phys. Rev. A*, 76:053832, Nov 2007.

[28] M. Peccianti, K. Brzadkiewicz, and G. Assanto. Nonlocal spatial soliton interactions in nematic liquid crystals. *Opt. Lett.*, 27:1460, 2002.

[29] Wei Hu, Tao Zhang, Qi Guo, Li Xuan, and Sheng Lan. Nonlocality-controlled interaction of spatial solitons in nematic liquid crystals. *Appl. Phys. Lett.*, 89(7):071111, 2006.

[30] Yana V. Izdebskaya, Vlad G. Shvedov, Anton S. Desyatnikov, Wieslaw Z. Krolikowski, Milivoj Belic, Gaetano Assanto, and Yuri S. Kivshar. Counterpropagating nematicons in bias-free liquid crystals. *Opt. Express*, 18(4):3258–3263, 2010.

[31] Jeroen Beeckman, Kristiaan Neyts, Xavier Hutsebaut, Cyril Cambournac, and Marc Haelterman. Time dependence of soliton formation in planar cells of nematic liquid crystals. *IEEE J. Quantum Electron.*, 41:735–740, 2005.

[32] Urszula A. Laudyn, Michal Kwasny, and Miroslaw A. Karpierz. Nematicons in chiral nematic liquid crystals. *Applied Physics Letters*, 94(9):–, 2009.

[33] Urszula A. Laudyn, Michal Kwasny, and Miroslaw A. Karpierz. Electric-field-induced steering in soliton direction of propagation in chiral nematic liquid crystals. *Optics Communications*, 283(7):1463 – 1466, 2010.

[34] Urszula A. Laudyn, Michal Kwasny, and Miroslaw A. Karpierz. Nematicons interaction in chiral nematic liquid crystals. *Molecular Crystals and Liquid Crystals*, 527(1):92/[248]–97/[253], 2010.

[35] Kwaśny Michał, Urszula A. Laudyn, Paweł Jung, and Mirosław A. Karpierz. Possibility of discrete beam propagation in chiral nematic liquid crystals. *Photon. Lett. Poland: Photonics Letters of Poland*, 1:160, 2009.

[36] Abbas Madani, Jeroen Beeckmanc, and Kristiaan Neytsc. An experimental observation of a spatial optical soliton beam and self splitting of beam into two soliton beams in chiral nematic liquid crystal. *Optics Communications*, 298–299(0):222 – 226, 2013.

[37] Marco Peccianti and Gaetano Assanto. Nematicons across interfaces: anomalous refraction and reflection of solitons in liquid crystals. *Opt. Express*, 15(13):8021–8028, Jun 2007.

[38] Marco Peccianti and Gaetano Assanto. Nematicons. *Phys. Rep.*, 516:147 – 208, 2012.

[39] G. Assanto. *Nematicons: Spatial Optical Solitons in Nematic Liquid Crystals*. Wiley Series in Pure and Applied Optics. Wiley, 2012.

[40] S. D. Durbin, S. M. Arakelian, and Y. R. Shen. Optical-field-induced birefringence and freedericksz transition in a nematic liquid crystal. *Phys. Rev. Lett.*, 47:1411–1414, 1981.

[41] Jeroen Beeckman, Kristiaan Neyts, Wout De Cort, and Abbas Madani. Non-linear light propagation and bistability in nematic liquid crystals, 2009.

[42] V. Freedericksz and V. Zolina. Forces causing the orientation of an anisotropic liquid. *Trans. Faraday Soc.*, 29:919–930, 1933.

[43] George W. Gray and Stephen M. Kelly. Liquid crystals for twisted nematic display devices. *J. Mater. Chem.*, 9:2037–2050, 1999.

[44] Hiap Liew Ong. Optically induced freedericksz transition and bistability in a nematic liquid crystal. *Phys. Rev. A*, 28:2393–2407, 1983.

[45] Jianru Shi and Hong Yue. Surface- and optical-field-induced fréedericksz transitions and hysteresis in a nematic cell. *Phys. Rev. E*, 62:689–698, Jul 2000.

[46] Yang Guochen and Zhang Suhua. The first order freedericksz transition at saturation point for weak anchoring nlc cells. *Liquid Crystals*, 29(5):641–646, 2002.

[47] Hiap Liew Ong. Magnetic-field-enhanced and -suppressed intrinsic optical bistability in nematic liquid crystals. *Phys. Rev. A*, 31:3450–3453, May 1985.

[48] A. J. Karn, S. M. Arakelian, Y. R. Shen, and H. L. Ong. Observation of magnetic-field—induced first-order optical fréedericksz transition in a nematic film. *Phys. Rev. Lett.*, 57:448–451, Jul 1986.

[49] Hiap Liew Ong. Optical-field-enhanced and static-field-induced first-order fréedericksz transitions in a planar parallel nematic liquid crystal. *Phys. Rev. A*, 33:3550–3553, May 1986.

[50] J. J. Wu, G.-S. Ong, and S.-H. Chen. Observation of optical field induced first-order electric Freedericksz transition and electric bistability in a parallel aligned nematic liquid-crystal film. *Applied Physics Letters*, 53:1999–2001, November 1988.

[51] S.-H. Chen and J. J. Wu. Observation of first-order Freedericksz transition in a nematic film induced by electric and optical fields. *Applied Physics Letters*, 52:1998–2000, June 1988.

[52] E. Santamato, G. Abbate, R. Calaselice, P. Maddalena, and A. Sasso. All-optical-field-induced first-order fréedericksz transitions and hysteresis in a nematic film. *Phys. Rev. A*, 37:1375–1377, 1988.

[53] I. C. Khoo. Optical bistability in nematic films utilizing self-focusing of light. *Appl. Phys. Lett.*, 41(10):909–911, 1982.

[54] Peng ye Wang, Hong jun Zhang, and Jian hua Dai. Feedback-induced first-order freedericksz transition in a nematic film. *Opt. Lett.*, 12(9):654–656, 1987.

[55] M.G. Clerc, T. Nagaya, A. Petrossian, S. Residori, and C.S. Riera. First-order fréedericksz transition and front propagation in a liquid crystal light valve with feedback. *The European Physical Journal D - Atomic, Molecular, Optical and Plasma Physics*, 28(3):435–445, 2004.

[56] M. Becchi, I. Janossy, D. S. Shankar Rao, and D. Statman. Anomalous intensity dependence of optical reorientation in azo-dye-doped nematic liquid crystals. *Phys. Rev. E*, 69:051707, May 2004.

[57] I. A. Budagovsky, D. S. Pavlov, S. A. Shvetsov, M. P. Smayev, A. S. Zolot'ko, N. I. Boiko, and M. I. Barnik. First-order light-induced orientation transition in nematic liquid crystal in the presence of low-frequency electric field. *Appl. Phys. Lett.*, 101(2):021112, 2012.

[58] F. Simoni, D. E. Lucchetta, L. Lucchetti, H. L. Ong, S. V. Serak, and N. Tabiryan. First-order optical freedericksz transition in a dye-doped nematic liquid crystal. *Opt. Lett.*, 38(6):878–880, 2013.

[59] J. E. Bjorkholm, A. E. Kaplan, P. W. Smith, and W. J. Tomlinson. Optical bistability based on self-focusing. *Opt. Lett.*, 6(7):345–347, Jul 1981.

[60] A. E. Kaplan. Bistable solitons. *Phys. Rev. Lett.*, 55:1291–1294, 1985.

[61] P L Rubin. Threshold of orientational self-focusing of a gaussian optical beam in nematic liquid crystals. *Soviet Journal of Quantum Electronics*, 15(11):1546, 1985.

[62] F. Marquis, P. Meystre, E. M. Wright, and A. E. Kaplan. Dynamics of the optical freedericksz transition. *Phys. Rev. A*, 36:875–887, Jul 1987.

[63] Ru-Pin Pan, H. Hsiung, and Y. R. Shen. Laser-induced freedericksz transition in nematic-liquid-crystal films with an air interface: Study of orientational anchoring and damping. *Phys. Rev. A*, 36:5505–5508, Dec 1987.

[64] I.C. Khoo, T.H. Liu, and P.Y. Yan. Nonlocal radial dependence of laser-induced molecular reorientation in a nematic liquid crystal: theory and experiment. In István Jánossy, editor, *Opticals Effects in Liquid Crystals*, volume 5 of *Perspectives in Condensed Matter Physics*, pages 136–141. Springer Netherlands, 1991.

[65] I. C. Khoo. *Liquid Crystals: Physical Properties and Nonlinear Optical Phenomena*. Wiley, New York, 1995.

[66] A. Piccardi, G. Assanto, L. Lucchetti, and F. Simoni. All-optical steering of soliton waveguides in dye-doped liquid crystals. *Appl. Phys. Lett.*, 93:171104, 2008.

[67] Jun Li, C.-H. Wen, S. Gauza, R. Lu, and S.-T. Wu. Refractive indices of liquid crystals for display applications. *J. Display Technol.*, 1:51–61, 2005.

[68] M. Peccianti, A. Fratalocchi, and G. Assanto. Transverse dynamics of nematicons. *Opt. Express*, 12:6524, 2004.

[69] Armando Piccardi, Alessandro Alberucci, Oleksandr Buchnev, Malgosia Kaczmarek, Iam-Choon Khoo, and Gaetano Assanto. Frequency-controlled routing of self-confined beams in nematic liquid crystals. *Molecular Crystals and Liquid Crystals*, 573(1):26–33, 2013.

[70] Armando Piccardi, Alessandro Alberucci, Oleksandr Buchnev, Malgosia Kaczmarek, Iam Choon Khoo, and Gaetano Assanto. Frequency-controlled deflection of spatial solitons in nematic liquid crystals. *Applied Physics Letters*, 101(8):–, 2012.

[71] M. Peccianti, C. Conti, G. Assanto, A. DeLuca, and C. Umeton. All optical switching and logic gating with spatial solitons in liquid crystals. *Appl. Phys. Lett.*, 81:3335, 2002.

[72] J F Henninot, J F Blach, and M Warenghem. Experimental study of the nonlocality of spatial optical solitons excited in nematic liquid crystal. *Journal of Optics A: Pure and Applied Optics*, 9(1):20, 2007.

[73] Ya. V. Izdebskaya, J. Rebling, A. S. Desyatnikov, G. Assanto, and Yu. S. Kivshar. All-optical switching of a signal by a pair of interacting nematicons. *Opt. Express*, 20(22):24701–24707, Oct 2012.

[74] Andrea Fratalocchi, Armando Piccardi, Marco Peccianti, and Gaetano Assanto. Nonlinear management of the angular momentum of soliton clusters: Theory and experiment. *Phys. Rev. A*, 75(6):063835, 2007.

[75] Alessandro Alberucci, Marco Peccianti, and Gaetano Assanto. Nonlinear bouncing of nonlocal spatial solitons at the boundaries. *Opt. Lett.*, 32(19):2795–2797, 2007.

[76] Yana V. Izdebskaya, Vladlen G. Shvedov, Anton S. Desyatnikov, Wieslaw Krolikowski, and Yuri S. Kivshar. Soliton bending and routing induced by interaction with curved surfaces in nematic liquid crystals. *Opt. Lett.*, 35(10):1692–1694, 2010.

[77] Yana V. Izdebskaya, Anton S. Desyatnikov, Gaetano Assanto, and Yuri S. Kivshar. Deflection of nematicons through interaction with dielectric particles. *J. Opt. Soc. Am. B*, 30(6):1432–1437, Jun 2013.

[78] Yana V. Izdebskaya. Routing of spatial solitons by interaction with rod microelectrodes. *Opt. Lett.*, 39(6):1681–1684, Mar 2014.

[79] M. Peccianti, C. Conti, G. Assanto, A. DeLuca, and C. Umeton. Routing of anisotropic spatial solitons and modulational instability in nematic liquid crystals. *Nature*, 432:733, 2004.

[80] Marco Peccianti, Andriy Dyadyusha, Malgosia Kaczmarek, and Gaetano Assanto. Tunable refraction and reflection of self-confined light beams. *Nat. Phys.*, 2:737–742, 2006.

[81] Raouf Barboza, Alessandro Alberucci, and Gaetano Assanto. Large electro-optic beam steering with nematicons. *Opt. Lett.*, 36(14):2725–2727, 2011.

[82] Armando Piccardi, Alessandro Alberucci, Raouf Barboza, Oleksandr Buchnev, Malgosia Kaczmarek, and Gaetano Assanto. In-plane steering of nematicon waveguides across an electrically adjusted interface. *Appl. Phys. Lett.*, 100:251107, 2012.

[83] A. Pasquazi, A. Alberucci, M. Peccianti, and G. Assanto. Signal processing by opto-optical interactions between self-localized and free propagating beams in liquid crystals. *Appl. Phys. Lett.*, 87:261104, 2005.

[84] M. Born and E. Wolf. *Principles of Optics*. Pergamon Press, New York, 1975.

[85] J. B. Pendry. Negative refraction makes a perfect lens. *Phys. Rev. Lett.*, 85:3966–3969, Oct 2000.

[86] V. G. Veselago. The Electrodynamics of Substances with Simultaneously Negative Values of ε and μ. *Soviet Physics Uspekhi*, 10:509, January 1968.

[87] A. Schuster. *An introduction to the theory of optics*. Edward Arnold, London, 1904.

[88] Ricardo A. Depine and Akhlesh Lakhtakia. A new condition to identify isotropic dielectric-magnetic materials displaying negative phase velocity. *Microwave and Optical Technology Letters*, 41(4):315–316, 2004.

[89] Chiyan Luo, Steven G. Johnson, J. D. Joannopoulos, and J. B. Pendry. All-angle negative refraction without negative effective index. *Phys. Rev. B*, 65:201104, May 2002.

[90] Yong Zhang, B. Fluegel, and A. Mascarenhas. Total negative refraction in real crystals for ballistic electrons and light. *Phys. Rev. Lett.*, 91:157404, Oct 2003.

[91] Oleg P. Pishnyak and Oleg D. Lavrentovich. Electrically controlled negative refraction in a nematic liquid crystal. *Appl. Phys. Lett.*, 89(25):251103, 2006.

[92] Dan Jia, Chengliang Yang, Zenghui Peng, Xiaoping Li, Yonggang Liu, Lishuang Yao, Zhaoliang Cao, Quanquan Mu, Lifa Hu, Xinghai Lu, and Li Xuan. Wide-angle switchable negative refraction in high birefringence nematic liquid crystals. *Liquid Crystals*, 40(5):599–604, 2013.

Appendix A

Journal and conference publications

Nina Kravets, Armando Piccardi, Alessandro Alberucci, Oleksandr Buchnev, Malgosia Kaczmarek, and Gaetano Assanto. Bistability with optical beams propagating in a reorientational medium. *Phys. Rev. Lett.*, **113**:023901, Jul 2014.
Alessandro Alberucci, Armando Piccardi, Nina Kravets, and Gaetano Assanto. Beam hysteresis via reorientational self-focusing. *Opt. Lett.*, **39(20)**:5830–5833, (2014).

Alessandro Alberucci, Nina Kravets, Armando Piccardi, Oleksandr Buchnev, Malgosia Kaczmarek, and Gaetano Assanto. Nematicons in planar cells subject to the optical Frèedericksz threshold. *Opt. Express*, **22(25)**:30663–30668, (2014).

Armando Piccardi, Alessandro Alberucci, Nina Kravets, Oleksandr Buchnev, and Gaetano Assanto. Power-controlled transition from standard to negative refraction in reorientational soft matter. *Nat. Commun.*, **5**, (2014).

Armando Piccardi, Alessandro Alberucci, Nina Kravets, Gaetano Assanto, Oleksandr Buchnev, and Malgosia Kaczmarek. Light beam hysteresis in liquid crystals. In *Photonics Technologies, 2014 Fotonica AEIT Italian Conference on*, (2014).

Armando Piccardi, Alessandro Alberucci, Nina Kravets, Oleksander Buchnev, Malgosia Kaczmarek, and Gaetano Assanto. Bistable optical propagation in nematic liquid crystals. In *Advanced Photonics*, page NW3A.2. Optical Society of America, (2014).

Nina Kravets, Armando Piccardi, Alessandro Alberucci, Oleksander Buchnev, and Gaetano Assanto. Observation of beam self-induced transition from positive to negative optical

refraction in nematic liquid crystals. Accepted to a publication in *MCLC*, Proceedings of 5th Int. Workshop on Liquid Crystals for Photonics, (2014).

Gaetano Assanto, Alessandro Alberucci, Armando Piccardi, Nina Kravets, Malgosia Kaczmarek, and Oleksandr Buchnev. Bifurcation and bistability with light beams in nematics. 5th Int. Workshop Liquid Crystals for Photonics [Invited], (2014).

Armando Piccardi, Alessandro Alberucci, Nina Kravets, Oleksandr Buchnev, Malgosia Kaczmarek and Gaetano Assanto. Beam bistability in nematic soft matter. Contribution submitted to the PIERS 2015, Prague, (2015).

Armando Piccardi, Alessandro Alberucci, Nina Kravets, Oleksandr Buchnev, Malgosia Kaczmarek and Gaetao Assanto, Nonlinear negative refraction in anisotropic dielectrics. Contribution submitted to the Northern Optics and Photonics 2015, (2015).

Armando Piccardi, Alessandro Alberucci, Nina Kravets, Oleksandr Buchnev, and Gaetano Assanto. Self-induced negative refraction in nematic liquid crystals. Contribution submitted to the European Conference on Lasers and Electro-Optics and the European Quantum Electronics Conference 2015, (2015).

Bistability with Optical Beams Propagating in a Reorientational Medium

Nina Kravets,[1] Armando Piccardi,[1] Alessandro Alberucci,[1] Oleksandr Buchnev,[2] Malgosia Kaczmarek,[2] and Gaetano Assanto[1,*]
[1]*NooEL–Nonlinear Optics and OptoElectronics Lab, University "Roma Tre", 00146 Rome, Italy*
[2]*Zepler Institute, University of Southampton, Southampton SO17 1BJ, United Kingdom*
(Received 17 February 2014; published 7 July 2014)

We investigated bistability with light beams in reorientational nematic liquid crystals. For a range of input powers, beams can propagate as either diffracting or self-trapped, the latter corresponding to spatial solitons. The first-order transition in samples exhibiting abrupt self-focusing with a threshold is in agreement with a simple model.

DOI: 10.1103/PhysRevLett.113.023901 PACS numbers: 42.65.Pc, 05.45.Yv, 42.65.Tg, 78.15.+e

Bistability is a fascinating phenomenon in physics and optics. It also plays a pivotal role in electronics, as systems with internal states that depend on their past evolution are the basis of memories and latch elements. In optics, several approaches have been undertaken to achieve optical bistability, i.e., the copresence of two stable states for a given excitation, in which two main ingredients, nonlinear response and feedback [1], were exploited. These approaches include cavities with saturable absorbers [2] or materials with an intensity-dependent refractive index [3], distributed feedback structures [4,5], self-focusing and reflection in Kerr-like media [6,7], increasing absorption versus power [8], linear or nonlinear interfaces [9], and distributed coupling to nonlocal waveguides [10]. Optical bistability was also investigated in plasmonic nanostructures [11], disordered cavities [12], and photonic crystals [13], leading to all-optical memories in InP [14] and Si-compatible devices [15]. Hysteresis was recently reported in QED cavities [16]. Bistable solitons were predicted in media with a nonlinear dependence of the refractive index on light intensity [17,18], but were never observed.

In this Letter, at variance with previous theoretical predictions on bistable solitons [17,18], we discuss and demonstrate bistability with optical beams propagating in reorientational nonlinear media, nematic liquid crystals (NLCs), as either diffracting or self-confined wave packets. Most NLCs are positive uniaxial fluids with long-range orientational order and optic axis set by the alignment of the elongated molecules, as described by the director $\hat{n}(x, y, z)$ [19,20]. The two extremal values of the refractive index are $n_{\parallel}$ and $n_{\perp}$ for electric fields along and normal to $\hat{n}$, respectively. Spatial optical solitons in NLCs (or "nematicons" [21]) have been widely investigated because of potential applications and unique medium characteristics, including high nonlocality and nonlinearity, high damage threshold and extended spectral transparency, and external tunability of both linear and nonlinear dielectric properties [19,20]. The physics of nonlinear reorientation is relatively straightforward: The extraordinarily polarized electric field of the beam induces dipoles in the anisotropic NLC molecules, which undergo a torque and rotate towards the field vector to minimize the overall energy; the resulting orientation is then determined by the balance between torque and intermolecular interactions. Because of the rotation of the optic axis, the extraordinary refractive index increases with optical excitation, and its distribution forms a waveguide for light itself [21].

The reorientational response differs from the standard Kerr type. Its highly nonlocal character supports stable solitons even in $(2+1)$D geometries [22]. The light-driven refractive index change depends on the sine of the angle between electric field $\mathbf{E}$ and director $\hat{n}$ [20], so that the nonlinear strength can be adjusted with the initial director alignment [23,24]. When the vectors $\mathbf{E}$ and $\hat{n}$ are initially orthogonal (see Fig. 1), reorientation can only take place

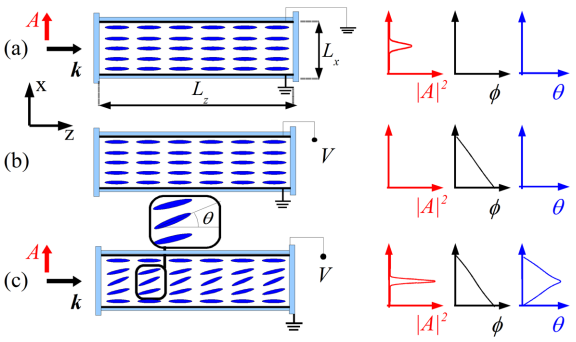

FIG. 1 (color online). Left: Side view of a NLC planar glass cell with thin film electrodes for voltage bias and director $\hat{n}$ anchored parallel to $\hat{z}$ at the boundaries. $\boldsymbol{A}$ and $\boldsymbol{k}$ indicate the beam electric field vector and wave vector, respectively. Right: Sketches of electric potential ϕ, beam intensity at the cell output $[|A|^2(z = L_z)]$, and director orientation θ versus NLC thickness x. (a) In an unbiased cell, no reorientation occurs for input powers below OFT. (b) Without light and for bias below the (electric) Fréedericksz threshold, θ remains zero. (c) The simultaneous presence of a light beam and voltage allows for the overcoming of the Fréedericksz transition; the director reorients in the bulk.

beyond a threshold associated with the optical Fréedericksz transition (OFT) [25] (the electric Fréedericksz transition is driven by voltage). While OFT usually is a second-order transition [19], specific configurations were studied to obtain first-order transitions and hysteresis [7,26–35].

Geometries exhibiting a threshold have a steplike nonlinear response and should support soliton bistability [17]; hence, reorientational NLCs subject to OFT can be expected to exhibit bistability between states corresponding to self-trapped (solitary) and diffracting (linear) beams. Intuitively, for a finite beam (e.g., Gaussian), the threshold power depends on the waist [see Fig. 2(a)] and diffraction. When the input power is increased, once the OFT threshold is overcome and reorientation occurs, self-focusing reduces the beam size and generates a self-confined wave packet; from the latter state, when the power is decreased, the dynamics of the narrower solitary beam no longer obeys the previous reorientational curve. The OFT threshold (from nonlinear to linear regimes) becomes lower, and thus leads to bistability (and hysteresis) between the two threshold values. Analogous to mirrorless optical bistability [6,8], the first-order transition stems from light self-action: Above the threshold, the beam changes the refractive index, yielding self-focusing and modifying its intensity distribution (hence the threshold). In turn, the latter determines the beam whereabouts as the input power decreases back to low (linear) values.

In this Letter, we refer to a planar NLC cell as in Fig. 1, which contains the standard mixture E7. The rubbing of the confining glass slides ensures strong anchoring (planar on top and bottom interfaces and homeotropic on input and output facets) [19], so the director is uniformly parallel to $\hat{z}$; i.e., $\theta = 0$ everywhere at rest, with θ the angle of $\hat{n}$ with the propagation axis z. The NLC sample has a thickness $L_x = 100\ \mu$m along x and extends for $L_z = 1.5$ mm

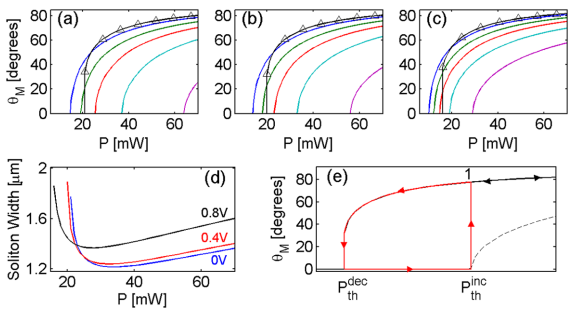

FIG. 2 (color online). Maximum reorientation θ_M versus power for V equal to (a) 0.0, (b) 0.4, and (c) 0.8 V, respectively. Solid lines in color correspond to $w_{\rm in} = 2$, 5, 10, 20, and 40 μm from left to right (blue to magenta), whereas black lines with triangles show θ_M once a soliton is formed. (d) Soliton size versus power. (e) Sketch of hysteresis for $w_{\rm in} = 40\ \mu$m and $V = 0.4$ V; the dashed line refers to reorientation without self-focusing. Here $K = 12 \times 10^{-12}$ N (as in E7), $\lambda = 1064$ nm, and $L_x = 100\ \mu$m.

longitudinally; it can be assumed to be infinitely wide versus y. Thin films of indium tin oxide deposited on the inner interfaces permit the application of a low-frequency voltage V across L_x, with a nearly uniform electric field $E_{\rm LF} \approx V/L_x$. Because reorientation is nonresonant, both low- and optical-frequency fields can contribute to changing the director distribution.

The optical excitation (at $\lambda = 1.064\ \mu$m) is a continuous-wave single-humped (fundamental Gaussian) beam polarized along x, launched in $z = x = 0$ with wave vector $\boldsymbol{k} \| \hat{z}$. The beam electric field is $Ae^{ik_0 n_\perp z}$ ($k_0 = 2\pi/\lambda$, the vacuum wave number), with A the slowly varying envelope. We assume all of the elastic constants to be K [19,20], and we define the optical and low-frequency dielectric anisotropies $\epsilon_a = \epsilon_\parallel - \epsilon_\perp = n_\parallel^2 - n_\perp^2$ and $\Delta\epsilon_{\rm LF}$, respectively [19]. Neglecting birefringent walk-off, the time-independent evolution of an extraordinary polarized beam is described by

$$2ik_0 n_\perp \frac{\partial A}{\partial z} + D_x \frac{\partial^2 A}{\partial x^2} + \frac{\partial^2 A}{\partial y^2} + k_0^2 \Delta n_e^2(\theta) A = 0, \quad (1)$$

$$\nabla^2 \theta + \frac{\epsilon_0}{2K}\left(\frac{\epsilon_a |A|^2}{2} + \Delta\epsilon_{\rm LF} E_{\rm LF}^2\right)\sin(2\theta) = 0, \quad (2)$$

with $D_x = n_e^2(\theta)/\epsilon_{zz}$ as the diffraction coefficient in xz [$\epsilon_{jk}(\theta) = \epsilon_\perp \delta_{jk} + \epsilon_a n_j n_k$ $(j, k = x, y, z)$, with $n_{j/k}$ the Cartesian components of $\hat{n}$] [36]. The photonic potential $\Delta n_e^2(\theta) = n_e^2(\theta) - n_\perp^2$ depends on both bias V and field A according to Eq. (2), thus accounting for nonlinearity [23]. Equation (1) governs light propagation in NLCs, according to the potential Δn_e^2; the distribution of n_e is determined by the balance between the external (optic and electric) torque and the restoring elastic forces [Eq. (2)]. Models similar to Eqs. (1)–(2) apply to solitons in other systems (without OFT), e.g., quadratic and thermo-optic media [37].

For a simple insight into the optics of the phenomenon, we first discuss the solution of Eq. (2) in the (propagation-invariant) limit $\partial_z = 0$, for a Gaussian profile and various input waists $w_{\rm in}$, adding a small perturbation on the initial θ to break the system symmetry. Figures 2(a)–2(c) show the maximum reorientation θ_M for three biases. As expected, molecular reorientation undergoes a second-order transition due to the size of ϵ_a [19,26]. In this geometry both light- and voltage-driven torques tend to rotate the director in the same direction; thus, the bias works against first-order optical transitions [29]. For a given voltage, the narrower the beam, the lower the OFT power threshold [20]; higher $E_{\rm LF}$ [from panels (a) to (c) in Fig. 2] reduces the threshold and the power required for each θ_M.

Next, we look for solitary waves obeying Eqs. (1)–(2) in NLCs encompassing a z-invariant director distribution; the latter assumption implies the lack of elastic forces exerted by input and output interfaces on the director (weak anchoring) and no propagation losses [24]. Substituting the soliton ansatz $A = u_s(x, y)e^{ik_0 n_s z}$ and $\theta = \theta_s(x, y)$ leads to a nonlinear eigenvalue problem; its solutions are plotted in

Fig. 2(d) and as black lines with triangles in Figs. 2(a)–2(c) (see Supplemental Material, Section 1 [38]). Owing to OFT, solitons never exist at powers below $P_{\rm th}^{\rm dec}$, and $P_{\rm th}^{\rm dec}$ decreases as the applied voltage increases [various lines in Fig. 2(d)]. Assuming an initial Gaussian intensity profile of waist $w_{\rm in}$, a nematicon forms only above $P_{\rm th}^{\rm inc}$, the latter depending on $w_{\rm in}$, consistently with the reorientation trend for a given beam profile. Conversely, once reorientation has occurred, the self-confined beam no longer depends on $w_{\rm in}$, i.e., the memory of the previous (linear) state is lost.

To illustrate optical bistability, let us simply consider a beam of waist $w_{\rm in}$ launched in the cell, with $w_{\rm in}$ and V chosen to yield OFT at powers $> P_{\rm th}^{\rm dec}$. Until the power reaches $P_{\rm th}^{\rm inc}$ [lower branch in Fig. 2(e)], θ_M remains zero, as nonlinear effects do not take place. Above $P_{\rm th}^{\rm inc}$ the director rotates and a nematicon forms [point 1 in Fig. 2(e)], with θ_M following the reorientation curve in the presence of self-trapping. The beam size is now set by the soliton existence curve in Fig. 2(d). When the power decreases [from point 1, upper branch in Fig. 2(e)], this narrower (solitary) beam evolves along the black line with triangles in Figs. 2(a)–2(c), experiencing a lower power threshold $P_{\rm th}^{\rm dec}$, independently from $w_{\rm in}$. Between $P_{\rm th}^{\rm dec}$ and $P_{\rm th}^{\rm inc}(w_{\rm in})$, two stable states exist, owing to the light's ability to modify the index distribution n_e. In this model, bistability does not occur for small waists, and wider hysteresis cycles correspond to larger $w_{\rm in}$; moreover, such bistable behavior is not restricted to NLCs with specific anisotropy or elastic response [26,29].

In experiments, the propagation dynamics cannot be ignored, as losses and longitudinal nonlocal effects are present, as, e.g., in nonlinear distributed couplers [39,40]. Below OFT, the (linear) beam profile changes with z, making the threshold power depend on the diffractive properties, such as Rayleigh length and waist location. Even after the nematicon is generated, the sample is not z invariant, due to boundary conditions $\theta = 0$ on the input and output facets. Finally, nematicons change width and power because of both unavoidable scattering and their breathing character [21,41]. In short, the inherent beam dynamics, even in the solitary regime, is expected to produce quantitative discrepancies between the experimental results and the theoretical predictions of Fig. 2.

We carried out the experiments by varying the input beam power stepwise and ensuring that the system reached a steady state (e.g., waiting from tens of seconds up to several minutes near the transitions) before each measurement. In unbiased cells [i.e., $E_{\rm LF} = 0$ V/m in Eq. (2)], OFT could only be achieved at powers high enough (≈50 mW) to cause temporal instabilities [42] (see Supplemental Material, Section 2 [38]); hence, we biased the sample across x to lower the threshold. Our calculations indicated that a bias of $V = 0.92$ V, which is below the electric Fréedericksz threshold, could considerably reduce the OFT threshold (see trend in Fig. 2) and help the observation of bistability. The calculations also showed that the hysteresis cycle could be widened at lower temperatures (Supplemental Material, Section 3 [38]), e.g., by cooling the sample with a Peltier cell. The experimental results confirmed that a voltage $V = 0.92$ V was low enough to not induce reorientation without light (see Supplemental Material, Section 4 [38]), but was adequate to minimize the input power required for OFT. In a sample at 18 °C, a Gaussian beam of waist $w_{\rm in} \approx 2$ μm diffracted at low powers, whereas from 16 to about 20 mW it overcame OFT, self-focused (without spurious effects), and formed a nematicon.

Figure 3 displays the beam evolution in the yz plane when power was first ramped up from 1 to 20 mW, and then down from 20 to 1 mW; (b,c) illustrate the beam evolution in the lower branch of the hysteresis while (b*,c*) that in the upper branch. Figure 4 graphs the acquired beam size ($w = 2\sqrt{\int y^2|A|^2dy/\int |A|^2dy}$) versus z, normalized to the measured initial w_0 for various powers around the cycle. In Fig. 3(a), $P = 1$ mW corresponds to the linear diffraction, i.e., the initial and final states of the bistable cycle that is sought (below $P_{\rm th}^{\rm dec}$). For $P \approx 15$ mW [Figs. 3(b)–3(c)], higher than the power necessary to excite nematicons in threshold-free geometries [21], modest self-focusing occurred with the beam size monotonically increasing along z due to the prevailing diffraction [green line with empty circle and red line with diamond in Fig. 4(a)]. For $P = 20$ mW [Fig. 3(d)] a stable nematicon was excited [violet line with triangle in Figs. 4(a)–4(b)]. Then, from this (20 mW) self-confined state, the input power was

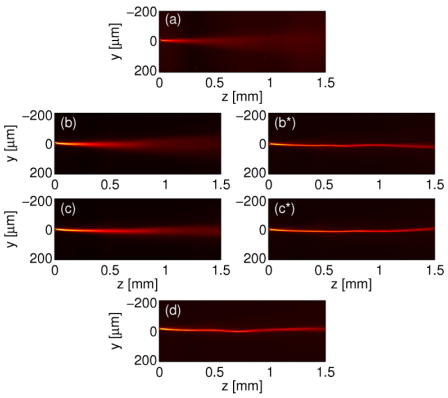

FIG. 3 (color online). Acquired images of a $w_{\rm in} \approx 2$ μm beam evolving in the plane yz for $V = 0.92$ V as power is ramped up and down. (a) Initial as well as final state without self-trapping ($P = 1$ mW); (d) soliton-state at the maximum power ($P = 20$ mW) used in the cycle. The paired panels (b,b*) and (c,c*) show the beam evolution for inputs of 14.5 and 15.5 mW, respectively, as power is raised (diffraction, left) or reduced (self-confinement, right). The initial waist appears to be $w_0 \approx 9$ μm $>$ $w_{\rm in}$ owing to scattering-induced image blurring [41].

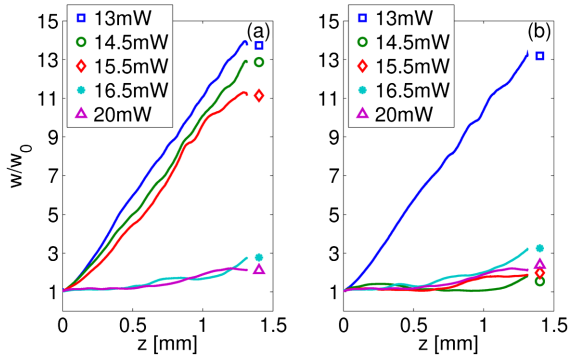

FIG. 4 (color online). Experimental results: normalized beam size w/w_0 (measured across y) versus z as the input power is ramped (a) up and (b) down from 13 to 20 mW and vice versa, respectively. Input powers are specified in the legends.

progressively reduced to the initial value of 1 mW. Figures 3(b*)–3(c*) and Fig. 4(b) (green line with empty circle and red line with diamond) show that beams propagated self-localized even at those powers for which diffraction was observed during ramp-up [Figs. 3(b)–3(c) and Fig. 4(a)]. The beam evolution exhibited "memory" of the previously determined director distribution, making the system bistable through self-action of the wave packet.

Figure 5 plots the beam mean size $\bar{w} = (1/L_z)\int_0^{L_z} w dz$ (measured from scattered light and averaged over L_z to reduce spurious effects due to longitudinal dynamics) normalized to the initial (measured) waist w_0 versus input power for both increasing (black squares) and decreasing (red circles) excitations. OFT prevents the formation of a soliton up to $P_{\rm th}^{\rm inc} = 16.5$ mW, with a beam much wider than the input. For $P > P_{\rm th}^{\rm inc}$ the beam self-confines,

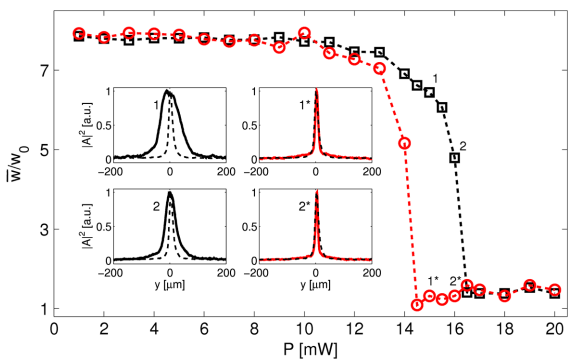

FIG. 5 (color online). Beam size $\bar{w}$ measured versus input power, averaged over L_z and normalized to the initial waist w_0. Black dashed line with squares and red dashed line with circles correspond to raising and falling powers, respectively. Insets: intensity profiles (solid lines) acquired at the cell output and compared with the measured input (dashed lines). The numerical labels refer to the corresponding points in the main plot $\bar{w}/w_0$.

with an average size comparable to w_0. When power is ramped down, self-localization is sustained as long as $P \geq P_{\rm th}^{\rm dec} = 14.5$ mW. For $P < P_{\rm th}^{\rm dec}$, the intermolecular forces restore the homogeneous distribution of θ and the linear propagation regime.

Optical bistability was observed between diffracting and self-trapping beam states in the range $P_{\rm th}^{\rm dec} < P < P_{\rm th}^{\rm inc}$. To compare experimental data and the 2D model, we calculated the director reorientation in the limit $\partial_z\theta = 0$ (as in Fig. 2), using the full tensor for the elastic constants and correcting for the actual temperature dependence (Supplemental Material, Section 3 [38]). The results, graphed in Fig. 6, show that the OFT threshold, computed for a diffracting beam with $w_{in} = 2$ μm, was comparable with that of a shape- and size-preserving Gaussian of waist ≈ 11 μm (see Supplemental Material, Section 5 [38]), with a predicted $P_{\rm th}^{\rm inc} = 5.2$ mW, nearly three times lower than measured. Such a nonunitary scaling factor between theory and experiments is expected and accounts for losses, longitudinal effects, and boundary conditions resulting in a lack of beam invariance. Applying such scaling (assumed waist independent) to the measured $P_{\rm th}^{\rm dec}$, we obtained $P_{\rm th}^{\rm dec} = 4.5$ mW, which, through the soliton reorientation curve, corresponds to a self-trapped beam of waist ≈ 3.5 μm. The latter value compares well with the observed soliton size, further confirming that system bistability stems from distinct beam widths upon self-action.

In conclusion, we investigated bistability with finite-size light beams in reorientational nematic liquid crystals encompassing self-focusing with a threshold. We observed optical bistability encompassing diffracting and self-trapped states, stemming from beam self-action in the medium. The good agreement between theoretical predictions and experiments confirms the origin of the phenomenon. These findings are expected to introduce significant novelties in optical memories as well as on latch-type switches and all-optical routers. The propagation of wave packets with multiple states in thresholded nonlinear

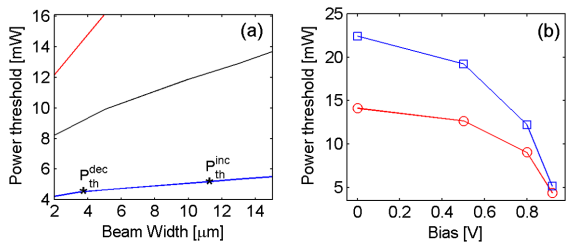

FIG. 6 (color online). (a) Calculated power threshold versus w for $V = 0$ (upper red line), $V = 0.8$ (black middle line), and $V = 0.92$ V (lower blue line); stars indicate the extrema of the observed bistable loop. (b) OFT power threshold versus bias V for $w = 3.5$ μm (nematicon size found from fitting, red line with circles) and $w = 11$ μm (linear diffracting beam, blue line with squares).

systems without external feedback, however, is a general result expected to have a radical impact on nonlinear wave dynamics in various branches of physics.

We thank Professor M. Karpierz and Professor A. A. Minzoni for helpful discussions.

*assanto@uniroma3.it; http://optow.ele.uniroma3.it

[1] H. Gibbs, *Optical Bistability: Controlling Light With Light* (Academic Press, San Diego, 1985).
[2] A. Szoke, V. Daneu, J. Goldhar, and N. A. Kurnit, Appl. Phys. Lett. **15**, 376 (1969).
[3] F. S. Felber and J. H. Marburger, Appl. Phys. Lett. **28**, 731 (1976).
[4] H. G. Winful, J. H. Marburger, and E. Garmire, Appl. Phys. Lett. **35**, 379 (1979).
[5] G. Assanto and G. I. Stegeman, Appl. Phys. Lett. **56**, 2285 (1990).
[6] J. E. Bjorkholm, A. E. Kaplan, P. W. Smith, and W. J. Tomlinson, Opt. Lett. **6**, 345 (1981).
[7] I. C. Khoo, Appl. Phys. Lett. **41**, 909 (1982).
[8] D. A. B. Miller, A. C. Gossard, and W. Wiegmann, Opt. Lett. **9**, 162 (1984).
[9] P. W. Smith, J.-P. Hermann, W. J. Tomlinson, and P. J. Maloney, Appl. Phys. Lett. **35**, 846 (1979).
[10] G. Assanto, B. Svensson, D. Kuchibhatla, U. J. Gibson, C. T. Seaton, and G. I. Stegeman, Opt. Lett. **11**, 644 (1986).
[11] G. A. Wurtz, R. Pollard, and A. V. Zayats, Phys. Rev. Lett. **97**, 057402 (2006).
[12] I. V. Shadrivov, K. Y. Bliokh, Y. P. Bliokh, V. Freilikher, and Y. S. Kivshar, Phys. Rev. Lett. **104**, 123902 (2010).
[13] M. Soljačić, M. Ibanescu, S. G. Johnson, Y. Fink, and J. D. Joannopoulos, Phys. Rev. E **66**, 055601 (2002).
[14] K. Nozaki, A. Shinya, S. Matsuo, Y. S. T. Segawa, T. Sato, Y. Kawaguchi, R. Takahashi, and M. Notomi, Nat. Photonics **6**, 248 (2012).
[15] L. Liu, R. Kumar, K. Huybrechts, T. Spuesens, G. Roelkens, E.-J. Geluk, T. de Vries, P. Regreny, D. V. Thourhout, R. Baets *et al.*, Nat. Photonics **4**, 182 (2010).
[16] Y.-D. Kwon, M. A. Armen, and H. Mabuchi, Phys. Rev. Lett. **111**, 203002 (2013).
[17] A. E. Kaplan, Phys. Rev. Lett. **55**, 1291 (1985).
[18] M. Matuszewski, W. Krolikowski, and Y. S. Kivshar, Opt. Express **16**, 1371 (2008).
[19] P. G. DeGennes and J. Prost, *The Physics of Liquid Crystals* (Oxford Science, New York, 1993).
[20] I. C. Khoo, *Liquid Crystals: Physical Properties and Nonlinear Optical Phenomena* (Wiley, New York, 1995).
[21] M. Peccianti and G. Assanto, Phys. Rep. **516**, 147 (2012).
[22] A. Snyder and D. Mitchell, Science **276**, 1538 (1997).
[23] A. Alberucci, A. Piccardi, M. Peccianti, M. Kaczmarek, and G. Assanto, Phys. Rev. A **82**, 023806 (2010).
[24] A. Alberucci and G. Assanto, Opt. Lett. **35**, 2520 (2010).
[25] S. D. Durbin, S. M. Arakelian, and Y. R. Shen, Phys. Rev. Lett. **47**, 1411 (1981).
[26] H. L. Ong, Phys. Rev. A **28**, 2393 (1983).
[27] P. Wang, H. Zhang, and J. Dai, Opt. Lett. **12**, 654 (1987).
[28] A. J. Karn, S. M. Arakelian, Y. R. Shen, and H. L. Ong, Phys. Rev. Lett. **57**, 448 (1986).
[29] S.-H. Chen and J. J. Wu, Appl. Phys. Lett. **52**, 1998 (1988).
[30] E. Santamato, G. Abbate, R. Calaselice, P. Maddalena, and A. Sasso, Phys. Rev. A **37**, 1375 (1988).
[31] E. Santamato, G. Abbate, P. Maddalena, L. Marrucci, and Y. R. Shen, Phys. Rev. Lett. **64**, 1377 (1990).
[32] M. A. Karpierz, *Soliton-Driven Photonics* (Springer, New York, 2001).
[33] E. A. Babayan, I. A. Budagovsky, S. A. Shvetsov, M. P. Smayev, A. S. Zolot'ko, N. I. Boiko, and M. I. Barnik, Phys. Rev. E **82**, 061705 (2010).
[34] I. A. Budagovsky, D. S. Pavlov, S. A. Shvetsov, M. P. Smayev, A. S. Zolot'ko, N. I. Boiko, and M. I. Barnik, Appl. Phys. Lett. **101**, 021112 (2012).
[35] F. Simoni, D. E. Lucchetta, L. Lucchetti, H. L. Ong, S. V. Serak, and N. Tabiryan, Opt. Lett. **38**, 878 (2013).
[36] A. Piccardi, M. Trotta, M. Kwasny, A. Alberucci, R. Asquini, M. Karpierz, A. d'Alessandro, and G. Assanto, Appl. Phys. B **104**, 805 (2011).
[37] E. A. Kuznetsov, A. Rubenchik, and V. Zakharov, Phys. Rep. **142**, 103 (1986).
[38] See Supplemental Material at http://link.aps.org/supplemental/10.1103/PhysRevLett.113.023901 for detailed calculations and a description of the procedures.
[39] G. I. Stegeman, G. Assanto, R. Zanoni, C. T. Seaton, E. Garmire, A. A. Maradudin, R. Reinisch, and G. Vitrant, Appl. Phys. Lett. **52**, 869 (1988).
[40] G. Vitrant, R. Reinisch, J. C. Paumier, G. Assanto, and G. I. Stegeman, Opt. Lett. **14**, 898 (1989).
[41] C. Conti, M. Peccianti, and G. Assanto, Phys. Rev. Lett. **92**, 113902 (2004).
[42] E. Braun, L. P. Faucheux, and A. Libchaber, Phys. Rev. A **48**, 611 (1993).

Supplemental Material

(Dated: February 18, 2014)

1. CALCULATION OF THE NEMATICON PROFILE

The profile of a reorientational spatial soliton in nematic liquid crystals can be calculated from the nonlinear eigenvalue problem (see Eqs. (1-2) in the article)

$$n_s u_s = \frac{1}{2n_\perp k_0^2}\frac{\partial^2 u_s}{\partial y^2} + \frac{D_x}{2n_\perp k_0^2}\frac{\partial^2 u_s}{\partial x^2} + \frac{1}{2n_\perp}\Delta n_e^2(\theta) u_s, \tag{1}$$

$$\frac{\partial^2 \theta_s}{\partial x^2} + \frac{\partial^2 \theta_s}{\partial y^2} + \frac{\epsilon_0}{2K}\left(\frac{\epsilon_a |u_s|^2}{2} + \Delta\epsilon_{\rm LF} E_{\rm LF}^2\right)\sin(2\theta_s) = 0. \tag{2}$$

We are interested in single-hump solutions (i.e., lowest order solitary waves) versus input beam power, for various applied quasi-static electric fields $E_{\rm LF}$. In the single elastic constant approximation (employed here), the nematicon existence curve depends on the normalized power P/K. The numerical algorithm is based on an iterative standard scheme, with Eq. (1) solved by direct discretization of the differential operator, whereas Eq. (2) is solved via a standard over-relaxed Gauss-Seidel algorithm. The material parameters correspond to the NLC mixture E7 at room temperature and a wavelength of 1064nm, consistently with the experiments. We used a rectangular grid of size $L_x = 100\mu$m across x (as in the actual sample) and $L_y = 400\mu$m along y, the latter large enough not to affect the soliton profile. For the boundary conditions, we assumed the director perturbation θ_s to be zero at the edges of the numerical grid.

The numerical solutions of the system (1-2) strongly depend on the initial guess for the distributions θ_s and u_s, due to thresholding response of Eq. (2). We initially injected a Gaussian beam of waist 2μm and power P_1 high enough to produce reorientation, centered in the midpoint of the grid ($x = 0, y = 0$) as we were looking for symmetric solutions unaffected by the cell boundaries [1]. After computing the soliton profile for P_1, we either increased or decreased the input power: as power grows, a soliton is always found (we limited our study to powers -typically 100mW- which did not saturate the nonlinear reorientation); conversely, as power goes down, nematicons exist only above a threshold, in agreement with OFT.

In the simplest bias-free case $E_{\rm LF} = 0$ V/m, typical profiles of θ_s and u_s in xy are plotted in Fig. 1. In all simulations we took $K = 12 \times 10^{-12}$N and $\Delta\epsilon_{\rm LF} = 14.5$. The nonlinear perturbation θ_s is circularly symmetric by the soliton axis, but it becomes asymmetric further away due to the asymmetric boundary conditions; a similar trend was previously pointed

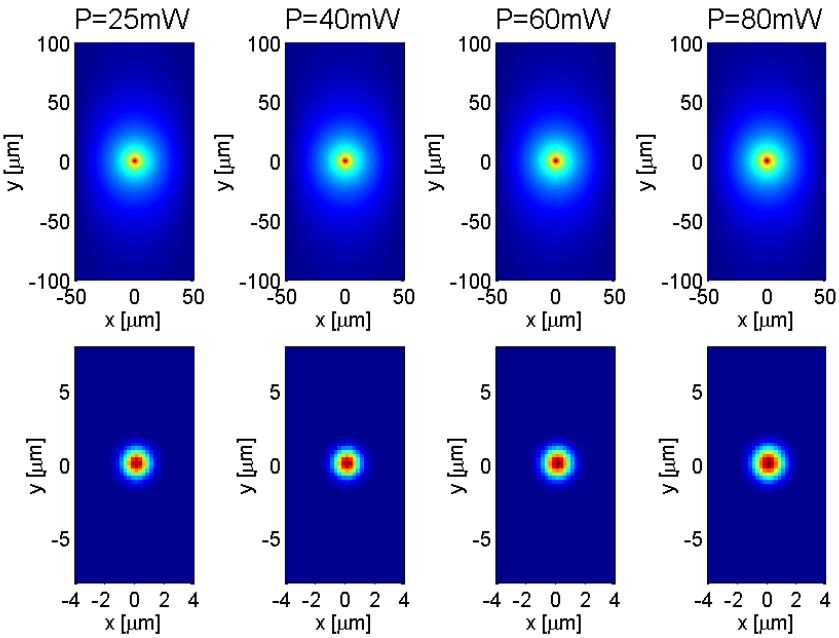

FIG. 1: Reorientation θ_s (top) and beam profile $|u_s|^2$ (bottom) in the plane xy for an unbiased cell excited by Gaussian beams of the indicated powers.

out in geometries withouth OFT [1, 2]. Cross-sections of θ_s and u_s along x and y, and corresponding to the peaks in Fig. 1 are graphed in Fig. 2: the soliton profile is nearly Gaussian due to the highly nonlocal response; θ_s is almost the same as in geometries free from OFT (that is, with nonzero initial θ). The nonlinear disturbance strictly follows the Green function of the Poisson equation, even if the system is highly nonlinear and cannot be linearized in the limit of small θ perturbations.

The calculated soliton width versus power is graphed in Fig. 3, with nematicons existing only above a threshold due to OFT. The solitons, when they exist, are quite narrow (less than 2μm) due to the strong nonlinear effect, with a slight astigmatism (less than 10% difference in widths) ascribable to the unequal diffraction coefficients ($D_x \neq 1$ in general) along x and y, respectively [3]. Moreover, the width has a local minimum versus power, analogously to the thresholdless case. We stress that, since θ_M monotonically increases with excitation (as reported in the main text), the nonlinear eigenvalue n_s evolves monotonically, as well, thus ensuring soliton stability according to the Vakhitov-Kolokolov criterion [4]. The solitons also depend on the applied low-frequency field $E_{\rm LF}$. The light power threshold

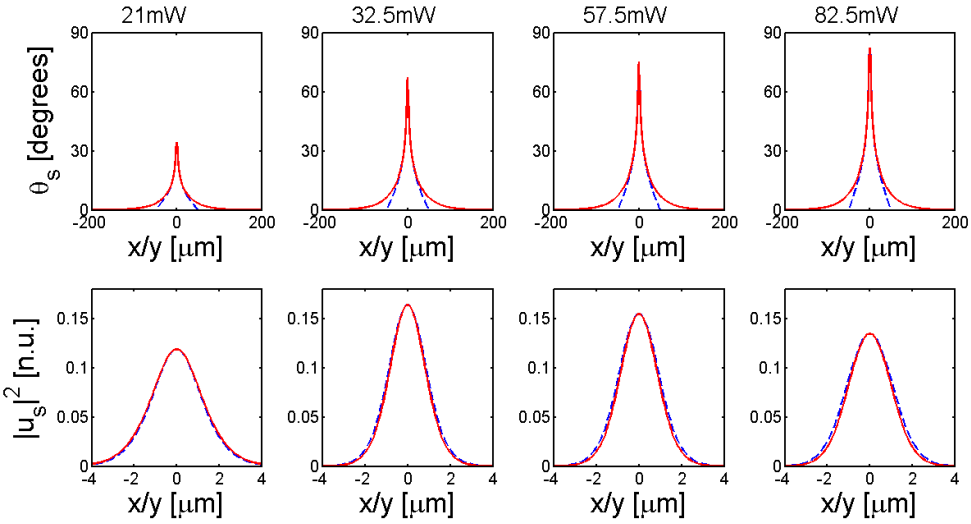

FIG. 2: Cross sections of θ_s (top) and $|u_s|^2$ (bottom) versus x in $y = 0$ (blue dashed lines) and versus y in $x = 0$ (red solid lines), for a bias-free cell as power varies (as marked). The soliton profile is normalized to a unity norm. Please note the different horizontal scales in top and bottom graphs.

for soliton existence shifts towards lower values as the bias increases, owing to the additional torque acting on the induced molecular dipoles; at the same time, the minimum achievable width increases at higher biases owing to the smaller refractive index change induced by light itself.

Finally, once OFT is overcome, the calculated soliton profile does not depend on the previous state of the director distribution. In agreement with Ref. [5] where the plane wave case was dealt with, for a fixed intensity profile the optical anisotropy of E7 cannot modulate the light-matter coupling to the extent required for optical bistability.

2. BEAM INSTABILITY IN BIAS-FREE CELLS

As we discussed in the main text, despite the substantial absence of material absorption, the high optical excitations required to overcome the OFT threshold in unbiased samples could not be employed in actual measurements due to the occurrence of unstable dynamics in time. Fig. 4 shows the acquired beam evolution in the absence of applied voltage. Up

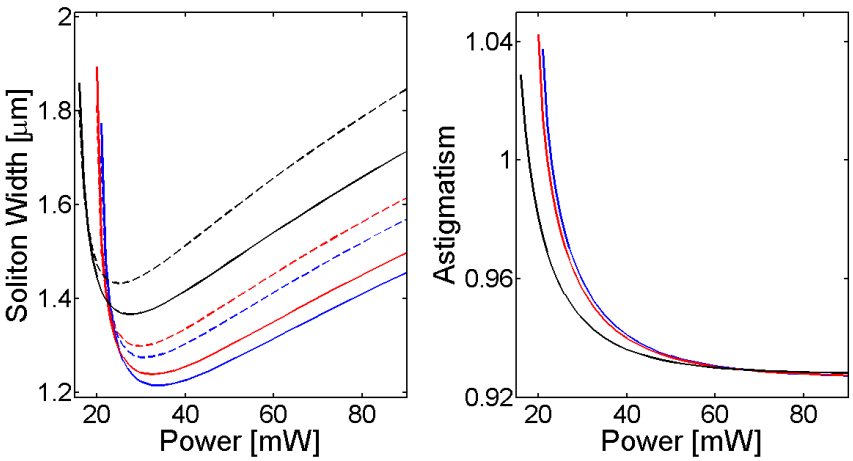

FIG. 3: Left: soliton width versus input power for various applied voltages: 0V (blue lines), 0.4V (red lines) and 0.8V (black lines); dashed and solid lines plot the width computed along x and along y, respectively. Right: soliton astigmatism, i.e. ratio of the widths across y and across x, versus power.

to 40mW, the light-induced torque is not large enough to reorient the NLC and the beam diffracts linearly. When power reaches 50mW, the Freedericksz threshold is overcome and the beam undergoes strong self-focusing near the cell entrance; after this initial stage, the beam does not reach a stationary configuration but gives rise to multiple temporally-varying filaments, as reported in Ref. [6] in a cylindrical geometry.

3. ACCURATE CALCULATION OF THE REORIENTATIONAL CURVE

In the reorientation equation, the single elastic constant is a (convenient) approximation often employed in the study of nematicons, without bearing on the overall features of self-confinement. However, the exact computation of the reorientational response is required when carrying out a quantitative comparison with the experimental results. Being interested in z-invariant solitary solutions, we could neglect the z-derivative of θ, assume a Gaussian profile of the (extraordinary polarized) electric field A with a varying waist w and take the quasi-static electric field $E_{\rm LF}$ to be homogeneous inside the sample [7]. Under these approximations, the director angle θ is the solution of [8]

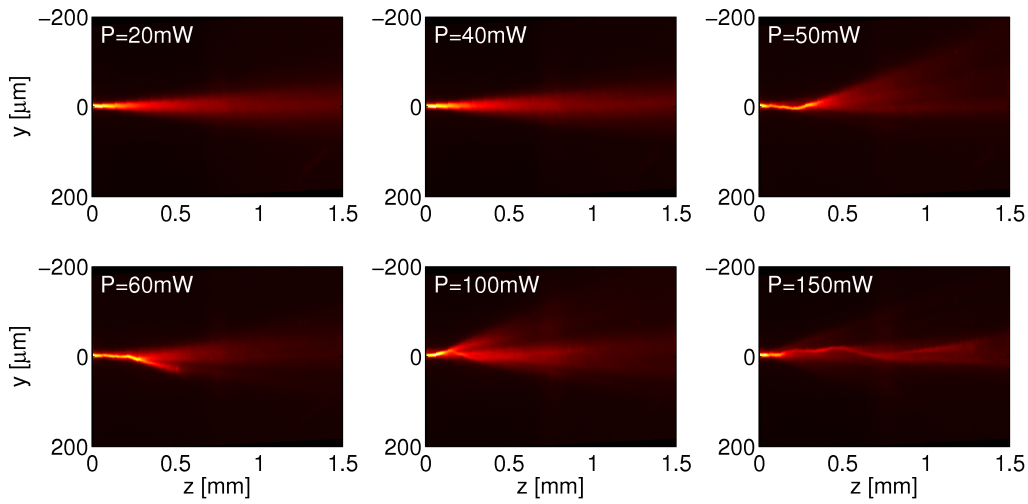

FIG. 4: Acquired beam evolution in the plane yz of an unbiased cell and various input powers.

$$\left(K_1\cos^2\theta + K_3\sin^2\theta\right)\frac{\partial^2\theta}{\partial x^2} + K_2\frac{\partial^2\theta}{\partial y^2} + \frac{K_3-K_1}{2}\sin(2\theta)\left(\frac{\partial\theta}{\partial y}\right)^2 + \frac{\epsilon_0}{2}\left(\frac{\epsilon_a|A|^2}{2} + \Delta\epsilon_{\rm LF}E_{\rm LF}^2\right)\sin(2\theta) = 0. \quad (3)$$

Equation (3) can only be solved numerically. We assume θ to be zero at the glass/NLC interfaces (i.e., $x = \pm - L_x/2$) and $\partial\theta/\partial y = 0$ for $|y| \to \infty$ (in the code we took a grid size $L_y = 2L_x$=200μm, large enough not to significantly affect the maximum reorientation θ_M). We solved Eq. (3) for various beam powers P and widths w, applied electric field $E_{\rm LF} = V/L_x$ and sample temperatures. All the material parameters (i.e., three elastic constants for splay, bend and twist, refractive indices for polarizations parallel and orthogonal to the optic axis, dielectric and optical anisotropies $\Delta\epsilon_{\rm LF}$ and ϵ_a, respectively) corresponded to the mixture E7 employed in the experiments and were taken from Refs. [9]-[10]. Fig. 5 shows how the maximum reorientation θ_M versus beam power P depends on input waist and applied bias. As in the limit of a single elastic constant discussed with reference to Fig. 2 in the main text, the reorientation is stronger for narrower beams; the external voltage allows decreasing significantly the excitation required for optical induced reorientation, thus helping to prevent the insurgence of time-dependent instabilities in beam dynamics (see Section 2 above). At the same time, for biases approaching the electric Freedericksz threshold, the OFT threshold powers corresponding to different beam waists get closer and closer: in this

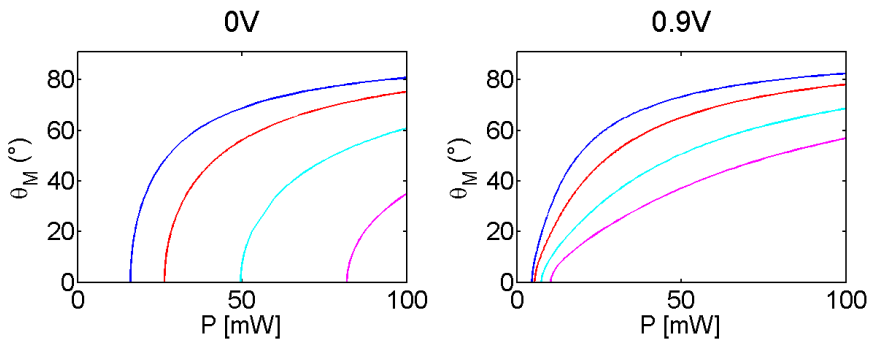

FIG. 5: Maximum reorientation θ_M versus beam power for (left graph) no bias and (right graph) a bias of 0.9 V. The input beam waists are 5, 15, 35 and 55μm from leftmost (blu) to rightmost (magenta) lines, respectively.

limit, the hysteresis cycles become narrower, as in the case of a single elastic constant. We pinpoint that the threshold power depends on a linear superposition of K_1 and K_2.

The numerical results on hysteresis size versus applied bias from Eq. (3) are presented in the main text (Fig. 6). To investigate the temperature dependence of the threshold power, we set the applied bias to 0.92V as in the measurements and considered two input waists, 2 and 11μm, respectively, which correspond to the diffracting and self-trapping cases (main text). Fig. 6(a) graphs the calculated θ_M versus power at two temperatures, Fig. 6(b) the threshold power dependence from sample temperature. Finally, Fig. 6(c) plots the hysteresis cycle width versus temperature: clearly the hysteresis loop gets wider as temperature decreases.

The model does not account for the soliton dynamics as temperature varies. For a given bias, the lower is the temperature the larger is the OFT power, eventually leading to spurious time-dependent instabilities of the soliton trajectory (section 2 above). The temperature 18°C was a convenient trade-off.

4. BISTABILITY VERSUS APPLIED VOLTAGE

Figure 7 plots the measured beam waist (normalized to the input value and averaged over the propagation length) of a 2mW beam versus applied voltage, showing the electrical Freedericksz transition in the presence of light. It is apparent that a convenient choice of

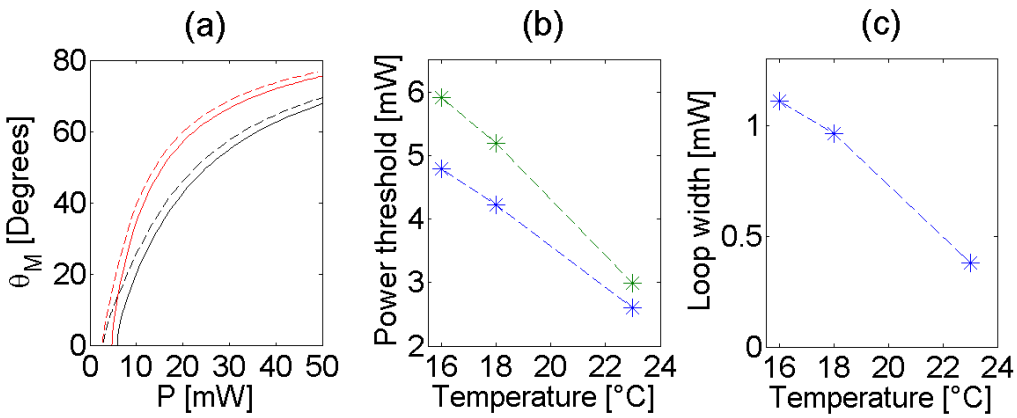

FIG. 6: (a) Maximum reorientation angle θ_M versus input beam power P for a sample temperature of 16 (dashed lines) and 23°C (solid lines), respectively; the beam waists are 2 (red) and 11 μm (black), respectively. (b) Threshold power versus temperature for beam waists of 2 (blue dashed line) and 11μm (green dashed line), respectively. (c) Width of the hysteresis cycle in mW from (b). Here the applied voltage is 0.92V.

bias $V \approx 1$V considerably facilitates the OFT without overruling it.

Figure 8 plots the beam width (averaged over L_z) versus input power P for a bias of 1V, for increasing (black squares) and decreasing (red squares) excitation, respectively. The observed hysteresis is rather marginal as compared to standard experimental errors.

Fig. 9 shows acquired images of beam evolution in the plane yz for various biases V and an input power of 2mW (upper panels) and the corresponding output profiles in xy (lower panels). For $V = 0.9$V, the beam diffracts, as it does for lower biases without any appreciable differences. As the voltage is increased up to 1 V, the beam undergoes small changes owing to the weak director orientation.When the bias reaches 1.05V, reorientation suffices to yield a 1D confining index well across x, with a slight x-shift of the beam due to the modified walkoff [11]. Finally, for $V = 1.5$V reorientation yields nonlinear confinement and the beam self-traps in both x and y due to combined nonlinear (light) and electro-optic (bias) responses.

From these results we estimated that a voltage slighly below $V = 0.95$V would allow us observing optical bistability while lowering the OFT requirements on input beam power. We actually used $V = 0.92$V in the experimental measurements reported in the main text.

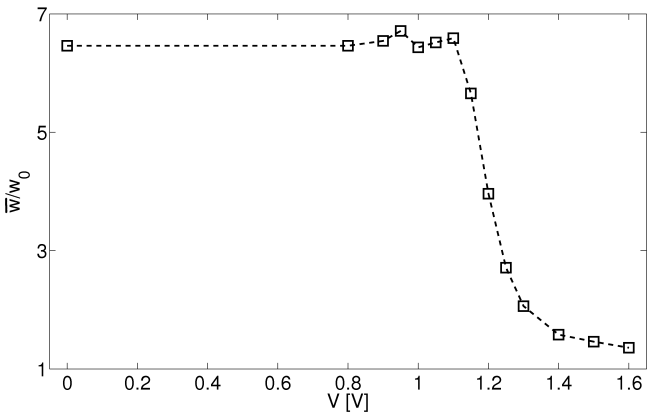

FIG. 7: Beam width versus applied voltage, as measured from scattered light out of the plane yz and averaged over the propagation length L_z. Here the input beam power is 2mW and the waist 2μm. The dashed line is a guide to the eye.

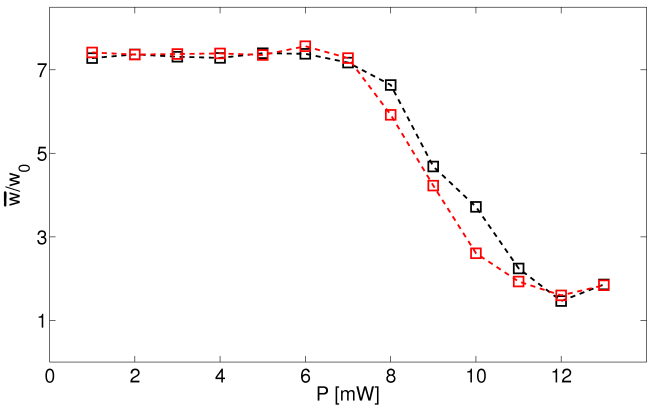

FIG. 8: Hysteresis cycle for an applied bias of 1V. Black and red lines are the measured beam widths (averaged over L_z) for increasing and decreasing input powers, respectively, at a temperature of 18° C.

5. DIFFRACTIONLESS GAUSSIAN EQUIVALENT OF THE LINEAR INPUT BEAM

Hereby we aim to find the effective width w_{eff} of a size-invariant beam of Gaussian transverse profile such that the OFT threshold power matches that of the input beam actually used in the experiments, a Gaussian of input waist 2μm. A diffracting Gaussian beam yields

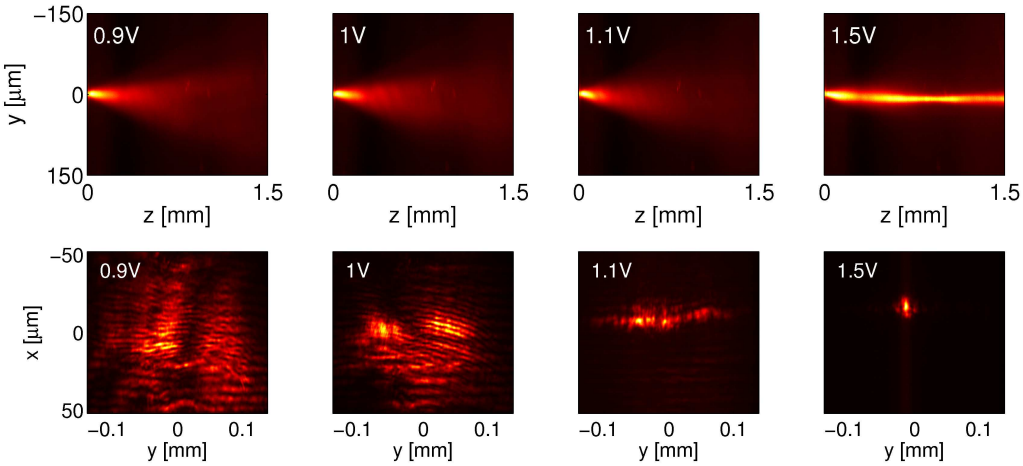

FIG. 9: Measured beam evolution in the plane yz (top) and beam profile at the cell output in xy (bottom). The applied voltage is 0.9, 1, 1.1 and 1.5 V from left to right, respectively. The input beam power was 2mW.

an exponentially decreasing reorientation along the propagation coordinate, owing to both optical losses (mainly due to Rayleigh scattering) and transverse spreading (associated to the Green function of the system). Since the latter contribution is the dominant one in our medium, we will assume that the director reorientation is maximum on the beam axis wherever its profile is narrower. In doing so, we will also account for the fact that $z = 0$ cannot be the position of maximum reorientation due to the imposed boundary conditions.

We study the OFT threshold using the equation

$$\nabla^2\theta + \gamma \sin(2\theta) I(x, y, z) = 0, \tag{4}$$

where $\gamma = \frac{\epsilon_0 \epsilon_a}{4K}$, I is a diffracting radially symmetric Gaussian beam in the form $I \propto e^{-2\frac{x^2+y^2}{w^2(z)}}$ with $w(z) = w_{\text{in}}\sqrt{1 + \left(\frac{z}{L_R}\right)^2}$, being $L_R = \pi w_{\text{in}}^2 n_\perp/\lambda$ the Rayleigh distance.
We are interested in the maximum reorientation angle $\theta_M(z)$, defined as the maximum in each plane $z = \text{const}$, considering a cell with input and output facets placed in $z = 0$ and $z = L_z$, respectively. After defining $I_M(z) = I(x = 0, y = 0, z)$, Eq. (4) projected on the z axis $(x = 0, y = 0)$ provides $\frac{d^2\theta_M}{dz^2} + \gamma \sin(2\theta_M) I_M(z) = 0$; then, integration between $z = 0$ and $z = L_z$ yields $\frac{d\theta_M}{dz}\big|_{z=L_z} - \frac{d\theta_M}{dz}\big|_{z=0} = -\gamma \int_0^{L_z} I_M(z) \sin(2\theta_M) dz$.
To estimate the threshold optical power, we linearize the sine factor by setting $\sin(2\theta_M) \approx$

$2\theta_M$; in addition, for a rapidly diverging beam $\frac{d\theta_M}{dz}\Big|_{z=L_z} \ll \frac{d\theta_M}{dz}\Big|_{z=0}$. Then we get

$$\frac{d\theta_M}{dz}\bigg|_{z=0} = 2\gamma \int_0^{L_z} I_M(z)\theta_M(z)dz = \frac{4\gamma P}{\pi}\int_0^{L_z} \frac{\theta_M(z)}{w^2(z)}dz. \tag{5}$$

Defining an effective intensity $I_{\text{eff}} = 2P_{\text{eff}}/(\pi w_{\text{eff}}^2)e^{-2r^2/w_{\text{eff}}^2}$, with the effective waist w_{eff} independent of z. For symmetry reason it is $\frac{d\theta_M^{\text{eff}}}{dz}\Big|_{z=L_z} = -\frac{d\theta_M^{\text{eff}}}{dz}\Big|_{z=0}$, thus the derivative of θ_M at the cell input is

$$\frac{d\theta_M^{\text{eff}}}{dz}\bigg|_{z=0} = \frac{2\gamma P_{\text{eff}}}{\pi w_{\text{eff}}^2}\int_0^{L_z} \theta_M^{\text{eff}}(z)dz. \tag{6}$$

The effective waist w_{eff} has to be chosen such that, for $P = P_{\text{eff}}$, the maximum θ_M and θ_M^{eff} have the same value. Hence, $\frac{d\theta_M}{dz}\Big|_{z=0} = \frac{d\theta_M^{\text{eff}}}{dz}\Big|_{z=0}$ and, in turn,

$$\frac{1}{w_{\text{eff}}^2}\int_0^{L_z} \theta_M^{\text{eff}}(z)dz = 2\int_0^{L_z} \frac{\theta_M(z)}{w^2(z)}dz. \tag{7}$$

We can distinguish three different regions along z: two transition layers of thickness L_x next to input and output facets and a bulk region comprised between L_x and $L_z - L_x$. Since in our case $L_z = 1.5$mm and $L_x \approx 100\mu$m, we can limit the integration to the bulk region. We start wth the LHS of Eq. (7): in the bulk we take $\theta_M^{\text{eff}}(z) = \theta_{max}^{\text{eff}} e^{-\alpha(z-L_x)}$ (i.e., we assume that the maximum orientation occurs at $z \approx L_x$ owing to the vanishing θ in $z = 0$), with α the scattering losses (from measurements $\alpha \approx 5\text{cm}^{-1}$). Thus

$$\frac{1}{w_{\text{eff}}^2}\int_0^{L_z} \theta_M^{\text{eff}}(z)dz \approx \frac{e^{-\alpha L_x} - e^{-\alpha(L_z-L_x)}}{\alpha w_{\text{eff}}^2}\theta_{max}^{\text{eff}} \tag{8}$$

We now focus on the RHS of Eq. (7). For narrow beams the dominant component of α is given by the exponential decay of the Green function: the intensity can be roughly approximated by a Dirac delta function placed in $z = L_x$ (hence, with peak value reduced by $e^{-\alpha L_x}$). We can therefore assume $\theta_M(z) \approx \theta_{max} e^{-\alpha_{3D}(z-L_x)}$, with $\alpha_{3D} = \pi/L_x$ due to the 3D Green function of our sample [12].

We find

$$2\int_0^{L_z} \frac{\theta_M(z)}{w^2(z)}dz \approx 2\theta_{max}e^{-\alpha L_x}\int_{L_x}^{L_z-L_x} \frac{e^{-\alpha_{3D}(z-L_x)}}{w^2(z)}dz = \frac{2\theta_{max}e^{-\alpha L_x}}{w_{\text{in}}^2}\int_{L_x}^{L_z-L_x} \frac{e^{-\alpha_{3D}(z-L_x)}}{1+\left(\frac{z}{L_R}\right)^2}dz. \tag{9}$$

We obtain the same OFT threshold when $\theta_{max} = \theta_{max}^{\text{eff}}$: solving Eq. (7) for w_{eff} provides

$$w_{\text{eff}} = w_{\text{in}} \sqrt{\frac{1 - e^{-\alpha(L_z - 2L_x)}}{2\alpha L_{\text{eff}}}}, \tag{10}$$

where we defined

$$L_{\text{eff}} = \int_{L_x}^{L_z - L_x} \frac{e^{-\alpha_{3D}(z - L_x)}}{1 + \left(\frac{z}{L_R}\right)^2} dz. \tag{11}$$

In our experiments $w_{\text{in}} = 2\mu$m and $L_x = 100\mu$m. A direct computation of w_{eff} from Eq. (10) provides $w_{\text{eff}} \approx 11\mu$m.

[1] A. Alberucci and G. Assanto, J. Opt. Soc. Am. B **24**, 2314 (2007).

[2] A. Alberucci and G. Assanto, Mol. Cryst. Liq. Cryst. **572**, 2 (2013).

[3] C. Conti, M. Peccianti, and G. Assanto, Phys. Rev. E **72**, 066614 (2005).

[4] Y. S. Kivshar and G. P. Agrawal, *Optical Solitons* (Academic, San Diego, CA, 2003).

[5] H. L. Ong, Phys. Rev. A **28**, 2393 (1983).

[6] E. Braun, L. P. Faucheux, and A. Libchaber, Phys. Rev. A **48**, 611 (1993).

[7] M. Peccianti, C. Conti, G. Assanto, A. DeLuca, and C. Umeton, Nature **432**, 733 (2004).

[8] I. C. Khoo, *Liquid Crystals: Physical Properties and Nonlinear Optical Phenomena* (Wiley, New York, 1995).

[9] E. P. Raynes, R. J. A. Tough, and K. A. Davies, Mol. Cryst. Liq. Cryst. **56**, 63 (1979).

[10] J. Li, C.-H. Wen, S. Gauza, R. Lu, and S.-T. Wu, J. Display Technol. **1**, 51 (2005).

[11] M. Peccianti, A. Fratalocchi, and G. Assanto, Opt. Express **12**, 6524 (2004).

[12] A. Alberucci, A. Piccardi, M. Peccianti, M. Kaczmarek, and G. Assanto, Phys. Rev. A **82**, 023806 (2010).

Nematicons in planar cells subject to the optical Fréedericksz threshold

Alessandro Alberucci,[1,*] Nina Kravets,[1] Armando Piccardi,[1] Oleksandr Buchnev,[2] Malgosia Kaczmarek,[2] and Gaetano Assanto[1,3]

[1] ***NooEL*** *- Nonlinear Optics and OptoElectronics Lab, University "Roma Tre", 00146 Rome - Italy*

[2] *Zepler Institute, University of Southampton, Southampton SO17 1BJ - United Kingdom*

[3] *Department of Physics, Tampere University of Technology, PO Box 692, FI-33101 Tampere - Finland*

[*] *alessandro.alberucci@gmail.com*

Abstract: We investigate, both theoretically and experimentally, self-trapping of light beams in nematic liquid crystals arranged so as to exhibit the optical Fréedericksz transition in planar cells. The resulting threshold in the nonlinear reorientational response supports a bistable behavior between diffracting and self-localized beam states, leading to the appearance of a hysteretic loop versus input excitation. Our results confirm the role of nematic liquid crystals in the study of non-perturbative nonlinear photonics.

OCIS codes: (190.1450) Bistability; (190.6135) Spatial solitons; (190.5940) Self-action effects; (190.4400) Nonlinear optics, materials.

References and links

1. R. Y. Chiao, E. Garmire, and C. H. Townes, "Self-trapping of optical beams," Phys. Rev. Lett. **13**, 479–482 (1964).
2. R. W. Boyd, S. G. Lukishova, and Y. R. Shen, eds., *Self-focusing: Past and Present* (Springer, 2009).
3. B. Shim, S. E. Schrauth, A. L. Gaeta, M. Klein, and G. Fibich, "Loss of phase of collapsing beams," Phys. Rev. Lett. **108**, 043902 (2012).
4. A. Barthelemy, S. Maneuf, and C. Froehly, "Propagation soliton et auto-confinement de faisceaux laser par non linearite optique de Kerr," Opt. Commun. **55**, 201 – 206 (1985).
5. E. L. Falcão Filho, C. B. de Araújo, G. Boudebs, H. Leblond, and V. Skarka, "Robust two-dimensional spatial solitons in liquid carbon disulfide," Phys. Rev. Lett. **110**, 013901 (2013).
6. J. E. Bjorkholm and A. A. Ashkin, "CW self-focusing and self-trapping of light in sodium vapor," Phys. Rev. Lett. **32**, 129–132 (1974).
7. W. E. Torruellas, Z. Wang, D. J. Hagan, E. W. VanStryland, G. I. Stegeman, L. Torner, and C. R. Menyuk, "Observation of two-dimensional spatial solitary waves in a quadratic medium," Phys. Rev. Lett. **74**, 5036–5039 (1995).
8. D. Suter and T. Blasberg, "Stabilization of transverse solitary waves by a nonlocal response of the nonlinear medium," Phys. Rev. A **48**, 4583–4587 (1993).
9. C. Conti, M. Peccianti, and G. Assanto, "Route to nonlocality and observation of accessible solitons," Phys. Rev. Lett. **91**, 073901 (2003).
10. A. E. Kaplan, "Bistable solitons," Phys. Rev. Lett. **55**, 1291–1294 (1985).
11. J. M. Christian, G. S. McDonald, and P. Chamorro-Posada, "Bistable Helmholtz solitons in cubic-quintic materials," Phys. Rev. A **76**, 033833 (2007).
12. M. Matuszewski, W. Krolikowski, and Y. S. Kivshar, "Spatial solitons and light-induced instabilities in colloidal media," Opt. Express **16**, 1371–1376 (2008).
13. M. Matuszewski, "Engineering optical soliton bistability in colloidal media," Phys. Rev. A **81**, 013820 (2010).
14. I. C. Khoo, "Nonlinear optics of liquid crystalline materials," Phys. Rep. **471**, 221–267 (2009).
15. G. Assanto, ed., *Nematicons: Spatial Optical Solitons in Nematic Liquid Crystals* (Wiley, 2012).
16. M. Peccianti and G. Assanto, "Nematicons," Phys. Rep. **516**, 147 – 208 (2012).

#224128 - $15.00 USD Received 30 Sep 2014; revised 6 Nov 2014; accepted 6 Nov 2014; published 3 Dec 2014

17. S. D. Durbin, S. M. Arakelian, and Y. R. Shen, "Optical-field-induced birefringence and Fréedericksz transition in a nematic liquid crystal," Phys. Rev. Lett. **47**, 1411–1414 (1981).
18. H. L. Ong, "Optically induced Fréedericksz transition and bistability in a nematic liquid crystal," Phys. Rev. A **28**, 2393–2407 (1983).
19. I. C. Khoo, "Optical bistability in nematic films utilizing self-focusing of light," Appl. Phys. Lett. **41**, 909–911 (1982).
20. E. Braun, L. P. Faucheux, and A. Libchaber, "Strong self-focusing in nematic liquid crystals," Phys. Rev. A **48**, 611–622 (1993).
21. A. Alberucci, A. Piccardi, N. Kravets, and G. Assanto, "Beam hysteresis via reorientational self-focusing," Opt. Lett. **39**, 5830–5833 (2014).
22. N. Kravets, A. Piccardi, A. Alberucci, O. Buchnev, M. Kaczmarek, and G. Assanto, "Bistability with optical beams propagating in a reorientational medium," Phys. Rev. Lett. **113**, 023901 (2014).
23. A. V. Zakharov and R. Y. Dong, "Giant optical nonlinearity in the mesophase of a nematic liquid crystals (ncl)," Phys. Rev. E **64**, 031701 (2001).

1. Introduction

The generation of spatial solitary waves (in the following simply *solitons*) stemming from the balance of diffractive beam spreading and self-focusing was one of the first topics studied in nonlinear optics [1]. In the simplest medium case, i.e. a Kerr medium with a local response, the so-called "Townes solitons" are intrinsically unstable in two transverse dimensions and subject to beam filamentation and collapse [2, 3]. Several approaches have been investigated to avoid collapse, such as 1D geometries [4], higher order [5] and saturating nonlinearities [6], parametric interactions [7], nonlocality [8, 9]. Due to the inherent nonlinear nature of self-localized beams, a natural question is whether solitons can be bistable versus beam excitation. In his pioneering theoretical work, Kaplan stated that two stable solitons can coexist for the same input power when the optical nonlinear response exhibits a threshold in the relationship between refractive index and beam intensity [10]. Since then, bistability of bright solitons has been theoretically investigated in cubic-quintic systems [11] and in colloidal media [12, 13].

Thanks to the high nonlinear response typical of nematic liquid crystals (NLCs) [14], self-trapping of light beams in this class of materials has been extensively investigated in the last years. Stable (2+1)D spatial solitons, named nematicons, have been demonstrated in several configurations, including voltage biased and unbiased cells (see Refs. [15, 16] for an exhaustive review) and exploiting the reorientational molecular response [14]. The latter is subject to a threshold when the electric field of the incident beam and the NLC molecules are orthogonal, the so called Optical Fréedericskz Transition (OFT) [17]. In this Paper we demonstrate that in NLCs subject to OFT, i.e. exhibiting a second-order transition when excited by plane wave-like beams [18], a finite size beam (appreciably diffracting as it propagates in the medium) can undergo a first order transition when self-trapping is accounted for, eventually leading to the formation of reorientational solitons. Self-focusing was shown to yield hysteretic effects with an external mirror in previous demonstrations with NLCs [19]. Hereby we demonstrate that, beyond a threshold input power, the free energy of the system has two local minima versus maximum reorientation. Thus, the equilibrium point becomes dependent on the previous evolution history, leading to a hysteresis loop versus excitation. Finally, while Braun *et al.* used a similar configuration in NLC-filled capillaries for light self-trapping [20], our system benefits from an external voltage bias in order to minimize the optical power for OFT, and our planar geometry permits to avoid the instabilities deriving from spontaneous symmetry breaking.

2. Self-trapping of light in the presence of OFT

The basic principle behind the reorientational nonlinearity of (undoped) NLCs is simple: the (electric component of the) impinging optical field induces dipoles in the elongated organic NLC molecules along a preferential direction, as dictated by their anisotropy; these dipoles in

turn tend to align to the field vector or polarization direction. The molecules tend to locally align with the same orientation due to strong intermolecular links; the macroscopic (average) alignment direction pointwise is called molecular director and usually indicated by $\hat{n}$ [14]. Hence, light in ordered NLCs propagates in an uniaxial crystal with the optic axis corresponding to $\hat{n}$ and refractive indices equal to $n_\perp$ and $n_\parallel$ for polarizations normal and parallel to $\hat{n}$, respectively. The net effect of an (intense) electric field distribution, such as a light beam, on the NLC molecules is to reorient the director $\hat{n}$ according to its intensity profile, thereby changing the local extraordinary refractive index n_e [15]. Let us consider a planar cell of thickness $L_x = 100\mu$m along x filled with the standard nematic liquid crystal E7, infinitely wide along y and extending from $z = 0$ to infinity (Figs. 1(a)-1(b)). We take the director $\hat{n}$ to be parallel to z everywhere in the absence of excitations. The director distribution is given pointwise by the angle θ formed with $\hat{z}$, with θ_m the maximum θ in each section normal to $\hat{z}$. A linearly polarized Gaussian (TEM_{00}) beam of wavelength of $\lambda = 1064$nm propagates paraxially along z and impinges on the sample; thus, its electric field $\boldsymbol{E}$ can be written as $\boldsymbol{E} = A\exp\left[ik_0 n_e(\theta_m)z\right]\hat{x}$ ($k_0 = 2\pi/\lambda$). To help the optical reorientation, a bias voltage V can be applied to the cell across x, providing a quasi-static electric field $E_{\mathrm{LF}} \approx V/L_x$. In the hypotheses above, the director can rotate in the plane xz and θ unambiguously determines the director as well as the extraordinary refractive index distributions. If spatial walk-off is ignored, the beam evolves according to

$$2ik_0 n_e(\theta_m)\frac{\partial A}{\partial z} + D_x(\theta_m)\frac{\partial^2 A}{\partial x^2} + \frac{\partial^2 A}{\partial y^2} + k_0^2 \Delta n_e^2(\theta)A = 0, \tag{1}$$

$$\nabla^2\theta + \frac{\varepsilon_0}{2K}\left(\frac{\varepsilon_a |A|^2}{2} + \Delta\varepsilon_{\mathrm{LF}} E_{\mathrm{LF}}^2\right)\sin(2\theta) = 0. \tag{2}$$

Equation (1) is the nonlinear Schrödinger equation (NLSE) modified to account for the medium anisotropy and the strong perturbation regime; $D_x = n_e^2(\theta_m)\Big/\left(n_\perp^2\sin^2\theta_m + n_\parallel^2\cos^2\theta_m\right)$ is the diffraction coefficient along x, whereas $\Delta n_e^2 = n_e^2(\theta) - n_e^2(\theta_m)$ is the nonlinear index well associated with the induced director rotation. Eq. (2) is cast in the single elastic constant K approximation [14, 15] and describes the director distribution affected by the external stimuli A and E_{LF}, weighted by the corresponding anisotropies $\varepsilon_a = n_\parallel^2 - n_\perp^2$ and $\Delta\varepsilon_{\mathrm{LF}}$, respectively. Thus, the nonlinear response is highly nonlocal owing to the Poisson-like form of the equation, and saturable owing to the sine term of the torque acting on the molecules [15]. Eqs. (1) and (2) model the propagation of self-confined waves in highly nonlocal NLC, namely nematicons [15].

In standard configurations, the nonlinear response governed by Eq. (2) is thresholdless because the angle θ is finite in the absence of external excitations [15], and Eq. (2) transforms into a Poisson equation for weak nonlinear perturbations. Conversely, when the (electric field) polarization of the input beam and the director are initially perpendicular to one another, θ_m is non-zero only above the OFT: in this case Eq. (2) cannot be linearized near threshold, with the breakdown of the analytical methods usually employed in nematicon-related models [15, 16]. In order to understand the transition in the presence of self-trapping (given by Eq. (1)), we need to compute the free energy of the system versus the maximum perturbation θ_m. The simplest approach is to find the equilibrium states studying the soliton case, i.e., with the ansatz $A(x,y,z) = \phi(x,y)\exp\left[ik_0(n_{\mathrm{S}} - n_e(\theta_m))z\right]$, assuming θ invariant across z as well. For the sake of simplicity, we calculate the free energy in the unbiased case $V = 0$: the application of a bias below the electric Fréedericksz threshold reduces the threshold optical power, without affecting the qualitative trend of the free energy [18].

The overall free energy of the system consisting of NLCs and the electromagnetic field is given by the combination of elastic energy $\mathscr{F}_{\mathrm{K}}$, given by $\frac{K}{2}(\nabla\theta\cdot\nabla\theta)$ in the limit of a single

#224128 - $15.00 USD Received 30 Sep 2014; revised 6 Nov 2014; accepted 6 Nov 2014; published 3 Dec 2014

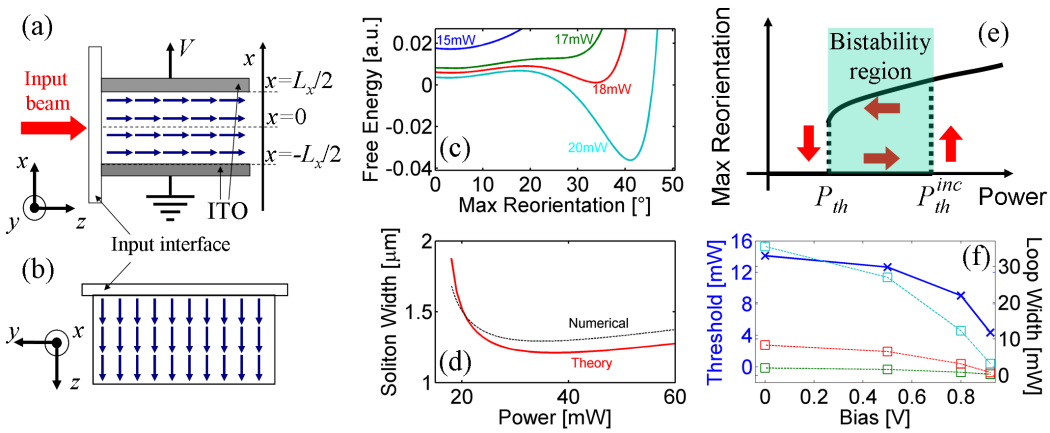

Fig. 1. (a) Side and (b) top view of NLC planar cell; the blue arrows indicate the director distribution at rest. (c) Free energy F versus θ_m when $K = 12\times10^{-12}$N and the temperature is $18^\circ C$. (d) Soliton width versus input power P corresponding to (c). (e) Sketch of the hysteresis loop in the plane (P,θ_m). (f) Power threshold for a fixed Gaussian beam of waist 3.5μm versus applied bias V (blue line with crosses, left axis); the dotted lines with squares graph the loop width versus V between $w_{\rm in} = 5,\ 11,\ 35\mu$m (from bottom to top, right axis) and a soliton with an average width of 3.5μm.

elastic constant, and Lagrangian of the light field $L_{\rm opt}$, given by $\frac{1}{2}\varepsilon_0 n_\perp^2 \boldsymbol{E}^2 + \frac{1}{2}\varepsilon_0\varepsilon_a(\hat{n}\cdot\boldsymbol{E})^2 - \frac{1}{2\mu_0}\boldsymbol{B}^2$. Note that the light-matter interaction, responsible for torque and reorientation, is contained in the term $L_{\rm opt}$. Due to the highly nonlocal character of the NLC reorientational response, ϕ can be taken Gaussian, i.e., $\phi = \sqrt{4Z_0P/[\pi n_e(\theta_m)w^2]}\exp[-(x^2+y^2)/w^2]$ [9], with P and w the soliton power and waist, respectively; hence, the optical reorientation is $\theta = 0.5\gamma Z_0 P\sin(2\theta_m)\sum_{l=1}^{\infty}V_l(y)\sin\left[\frac{\pi l(x-L_x/2)}{L_x}\right]/n_e(\theta_m)$, with $\gamma = \varepsilon_0\varepsilon_a/(4K)$ and $V_l(y) = \mathrm{sinc}(\pi l/2)[F(y)+F(-y)]$ with $F(y)\equiv \mathrm{erfc}[\sqrt{2}y/w + \pi l w/(2\sqrt{2}L_x)]e^{\pi l y/L_x}$ [21]. The overall free energy $F = \int_{-\infty}^{\infty}\int_{-L_x/2}^{L_x/2}(\mathscr{F}_{\rm K}+L_{\rm opt})\mathrm{d}x\mathrm{d}y$ is [21]

$$F \approx \frac{\alpha\kappa^2\theta_m^2}{2} + \frac{2\gamma Z_0 P}{\pi n_{\rm S} w^2}\int_{-\frac{L_x}{2}}^{\frac{L_x}{2}}\mathrm{d}x\int_{-\infty}^{\infty}\cos(2\theta)e^{-2\frac{x^2+y^2}{w^2}}\mathrm{d}y + \left\{\frac{\varepsilon_0 Z_0}{n_{\rm S}k_0^2K}\frac{1}{w^2} + \frac{\varepsilon_0 Z_0 n_{\rm S}}{K} - \frac{\gamma Z_0\cos(2\theta_m)}{n_{\rm S}}\right\}P, \tag{3}$$

where $\kappa(w) = -1/[\sum_{l=1}^{\infty}V_l(0)\sin(\pi l/2)]$ and $\alpha = 0.5\sum_{p=0}^{\infty}\int_{-\infty}^{\infty}\left[\pi^2V_{2p+1}^2/L_x + L_x\left(V_{2p+1}'\right)^2\right]\mathrm{d}y$, with $V_l'(y) = \mathrm{d}V_l(y)/\mathrm{d}y$.

Figure 1(c) shows that, below a threshold power $P_{\rm th}$, F monotonically increases with θ_m, thus reorientation does not occur and only the linear regime is stable (in the plot $P_{\rm th}\approx 18$mW). When the power overcomes $P_{\rm th}$, a local minimum with $\theta_m \neq 0$ appears in F, yielding the formation of a shape-preserving nematicon with width dictated by the power P. Besides the minimum, a local maximum corresponds to an unstable nematicon. Fig. 1(d) compares the nematicon width calculated from Eq. (3) and from numerical simulation of Eqs. (1) and (2). Since for a fixed P every point in Fig. 1(c) corresponds to a different beam width [21], it is straightforward to describe the insurgence of hysteresis. We take a power larger than the threshold $P_{\rm th}$ and fix the input beam width to $w_{\rm in}$. If the beam is wider than the unstable soliton (i.e., the input state is on the left of the local maximum), the beam evolves towards the linear regime $\theta_m = 0$. Conversely, if the input beam is narrower than the unstable soliton (i.e., the initial state is placed on the right of the local maximum), the beam reaches the minimum and turns into a stable soliton. Thus,

#224128 - $15.00 USD Received 30 Sep 2014; revised 6 Nov 2014; accepted 6 Nov 2014; published 3 Dec 2014

Eq. (3) predicts the occurrence of a hysteretic loop versus power: for a given input waist $w_{\rm in}$ a power $P_{\rm th}^{\rm inc}$ exists such that $w_{\rm in}$ corresponds to the local maximum. As power increases from zero to $P_{\rm th}^{\rm inc}(w_{\rm in})$, reorientation and self-focusing do not take place, and light propagates in the linear regime. When $P = P_{\rm th}^{\rm inc}(w_{\rm in})$, OFT occurs and the beam starts to self-focus, eventually forming a nematicon with width depending on P according to the existence curve in Fig. 1(d). Now, when decreasing the input power, the beam width differs from $w_{\rm in}$. Since the OFT depends on beam width [22], the director remains reoriented at powers lower than $P_{\rm th}^{\rm inc}(w_{\rm in})$, as long as $P > P_{\rm th}$. The feedback required for memory effects is the nonlocal NLC response, which stores in the director distribution the information on previous optical excitations. Thus, a hysteretic loop for $P_{\rm th} < P < P_{\rm th}^{\rm inc}(w_{\rm in})$ is predicted (Fig. 1(e)): the two coexisting stable states of the system correspond to a diffracting beam (lower branch, increasing power) and a nematicon (upper branch, decreasing power). The application of a bias lowers $P_{\rm th}$ (Fig. 1(f)). Finally, since the larger the input width the larger $P_{\rm th}^{\rm inc}(w_{\rm in})$ is, the loop width widens as $w_{\rm in}$ increases (Fig. 1(f)).

3. Observation of bistability

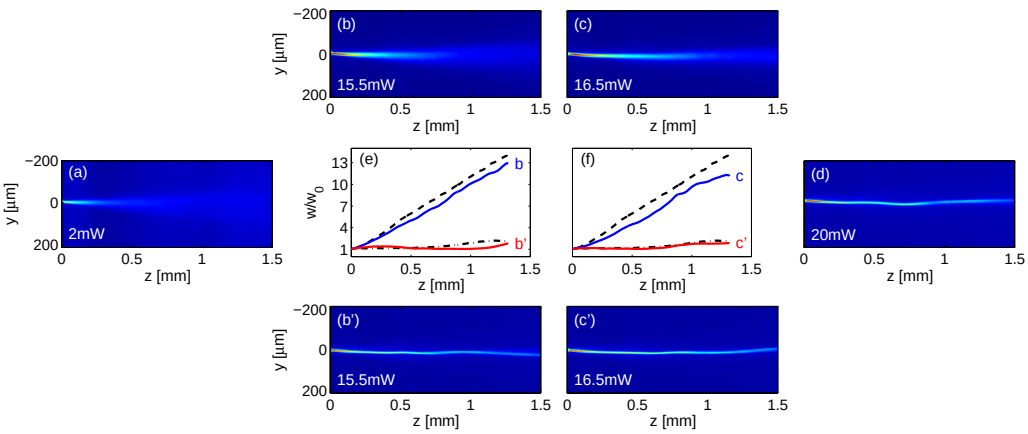

Fig. 2. Observation of the hysteresis loop by imaging beam propagation in the plane *yz*. (a) The input power is 2mW, corresponding to standard diffraction; the power is increased (b and c) until OFT occurs above 16.5mW; then (d) a stable nematicon is formed. Starting from a stable nematicon, the power is ramped down (b' and c'): the beam remains self-trapped for $P > 14.5$mW. Further decreases in power lead to linear diffraction (a) as in first half of the cycle. The beam width w normalized to the apparent input width w_0 [22] is plotted versus z for (e) $P = 15.5$mW and (f) $P = 16.5$mW; blue and red lines correspond to ramp-up (b-c) and ramp-down (b'-c') halves of the cycle. Dashed and dotted-dashed lines are the beam widths for $P = 2$mW and 20mW, respectively. The observed states were stable over time intervals of the order of 30 minutes.

The results shown in Sec. 2 assume (medium and beam) invariance along z, which is unrealistic in actual situations due to scattering losses, breathing and imperfections. Nonetheless, they provide a qualitative description of beam dynamics in actual experiments. First, the threshold power $P_{\rm th}^{\rm inc}$, monotonically increasing with $w_{\rm in}$ when z-invariance is invoked, shows a local minimum due to the interplay between the diffractive spreading -decreasing for larger $w_{\rm in}$- and the peak intensity -decreasing with $w_{\rm in}$-. Numerical simulations show that the power at OFT versus $w_{\rm in}$ initially diminishes, then has a local minimum when $w_{\rm in}$ is between 6 and 8μm and eventually grows indefinitely for further increases in $w_{\rm in}$. Hence, in actual experiments, the hysteresis is maximized when $w_{\rm in}$ is as small as possible. Second, when self-focusing occurs, the input

#224128 - $15.00 USD Received 30 Sep 2014; revised 6 Nov 2014; accepted 6 Nov 2014; published 3 Dec 2014

beam width does not change, as assumed in Sec. 2. Actually, the beam starts breathing (i.e. its size oscillates periodically) around the equilibrium state shown in Fig. 1(d) [16].

Experimentally, we launched a beam of waist $\approx 2\mu$m at the input. For $V = 0$V nematicons beyond OFT were subject to temporal instabilities [20]. To circumvent this limitation, we biased the cell with a voltage at 1kHz: such additional electric torque helps molecular reorientation, lowering P_{th} and avoiding instabilities. At the same time, the loop width reduces as V increases (Fig. 1(f)). We found a satisfactory tradeoff for $V = 0.92$V and used it in all measurements.

The measured beam evolution in the plane yz is shown in Fig. 2. As predicted, the beam underwent a bistable behavior: when power was ramped up from zero, self-localization did not occur below 16.5mW, the latter corresponding to $P_{\text{th}}^{\text{inc}}$ in experiments. Starting from the self-confined state and decreasing power, the system conserved memory of the former state through optical reorientation, and self-trapping was maintained down to 14.5mW, corresponding to P_{th}.

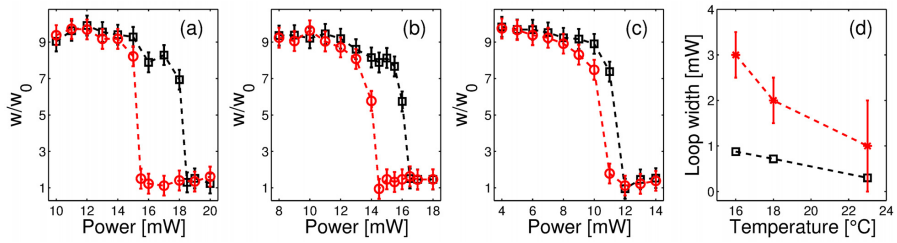

Fig. 3. Hysteresis of normalized beam width versus power in $z = 930\mu$m, at temperatures of (a) 16°, (b) 18° and (c) 23°C. Panel (b) corresponds to the experiment in Fig. 2. (d) Both the experimental (red stars) and the theoretical (black squares) data show that the loop shrinks at higher temperatures. The theoretical results are found with the z-invariant model [22] and effective widths 3.5 and 11μm for self-trapped and diffracting states, respectively.

The OFT is expected to depend on temperature [14]: Fig. 3 shows hysteresis loops versus temperature. The power threshold decreases as temperature increases, whereas the loop shrinks, nearly disappearing at room temperature. Such trend is confirmed by calculations accounting for the three different elastic constants and the temperature dependence of both refractive indices and elastic constants [22, 23]. Although the loop width is maximum at the lowest temperatures, side effects take place, including longer relaxation times reaching several minutes.

4. Conclusions

Using a Lagrangian approach for the theory and planar cells for the experiments with near-infrared light, we investigated the role of the optical Fréedericksz transition in the nonlinear propagation of finite-size optical beams. We predicted and observed a bistable behavior accompanied by hysteresis as power was ramped up and down, with stable states corresponding to diffracting and self-trapped beams. The role of power, bias voltage and temperature was addressed in detail and found consistent with simplified models. Our findings underline the role of nematic liquid crystals in the study of highly perturbed regimes in nonlinear optics and further illustrate the wealth of phenomena in nonlocal reorientational soft matter.

Acknowledgments

GA acknowledges the Academy of Finland for his Finnish Distinguished Professor project (282858).

Beam hysteresis via reorientational self-focusing

Alessandro Alberucci, Armando Piccardi, Nina Kravets, and Gaetano Assanto*

NooEL—Nonlinear Optics and OptoElectronics Lab, University "Roma Tre," Rome 00146, Italy

**Corresponding author: assanto@uniroma3.it*

Received August 1, 2014; revised September 5, 2014; accepted September 6, 2014;
posted September 10, 2014 (Doc. ID 219903); published October 7, 2014

We theoretically investigate light self-trapping in nonlinear dielectrics with a reorientational response subject to threshold, specifically nematic liquid crystals. Beyond a finite excitation, two solitary waves exist for any given power, with an hysteretic dynamics due to feedback between beam size, self-focusing and the nonlinear threshold. Soliton stability is discussed on the basis of the system free energy. © 2014 Optical Society of America

OCIS codes: (190.1450) Bistability; (190.6135) Spatial solitons; (190.5940) Self-action effects; (190.4400) Nonlinear optics, materials.

http://dx.doi.org/10.1364/OL.39.005830

Liquid crystals are key materials in modern optoelectronics, as they find application not only in displays [1], but also in optoelectronic devices [2–6], random lasers [7,8], tailorable metamaterials [9,10], angular momentum manipulators [11–13], etc. In the nematic phase the centers of mass of the liquid crystal molecules exhibit fluid-like positional disorder, but their orientational distribution peaks around a given direction (solid-like rotational symmetry), called director $\hat{n}$, are generally varying in space [1]. Standard nematic liquid crystals (NLCs) are positive uniaxials at optical frequencies, with the optic axis corresponding to $\hat{n}$ and refractive indices $n_\parallel$ and $n_\perp$ for electric fields parallel and normal to $\hat{n}$, respectively.

NLCs are well known for their nonlinear optical properties [14]. The dominant mechanism, the reorientational response, stems from the torque that the (extraordinarily polarized) electric field of a light beam exerts on the induced dipoles, which then tend to reorient and minimize the light–matter interaction energy [1,14]. For $n_\parallel > n_\perp$ optical reorientation provides an available index change up to $n_\parallel - n_\perp$, with the equilibrium distribution of $\hat{n}$ dictated by the interplay between optical torque and intermolecular forces [14]. The reorientational nonlinearity strongly depends on the initial angle between the field and the director [15]: when the two vectors are normal to each other, the torque is zero below the optical Fréedericksz threshold (OFT), i.e., $\hat{n}$ rotates only beyond a threshold beam power P_{th} [16,17]. In thermodynamical terms, the OFT can be a first- [18] or second-order [19] transition, according to dielectric and elastic properties of the NLC. The main requirement for a first-order, i.e., hysteretic, transition is a large optical anisotropy $\epsilon_a = n_\parallel^2 - n_\perp^2$ (e.g., $\epsilon_a > 0.5 n_\parallel^2$ when all the elastic constants assume the same value) [18], a condition which is not met by most (undoped) NLCs but could be circumvented in specific configurations [20–24]. In this Letter we investigate first-order transitions mediated by beam self-focusing and self-localization in planar NLC cells [25]. Optical bistability via self-focusing in NLCs was reported earlier with an external mirror [26]; more recently it was demonstrated with propagating nonlinear beams [27], with hysteresis between solitary and diffracting beams observed versus input power: here we model the latter effect, using the free energy associated to each state to address the dynamics.

We consider a planar cell of thickness L_x across x and infinitely extended across y, with propagation along z. Without loss of generality, we consider the NLC mixture E7 for a direct comparison with [27]: all the results presented hereby are computed for a wavelength $\lambda = 1.064\ \mu\text{m}$ and a single elastic constant $K = 12 \times 10^{-12}$ N [16,25]. The input beam is a single-humped Gaussian with the wavevector along z and field polarized along x. We name θ the angle of director $\hat{n}$ with z. In the absence of excitation $\hat{n}$ is uniformly aligned to z by anchoring at the cell boundaries, i.e., $\theta = 0$ everywhere. Since $\hat{n}$ and the light polarization are mutually orthogonal at low power, this geometry is subject to OFT [27], with a power threshold $P = P_{\text{th}}$, depending on the width of the beam itself [28]: when the director gets reoriented above OFT, the beam narrows via self-focusing [25], in turn lowering P_{th}. Therefore, the threshold P_{th} depends on the previous state of the system through the feedback provided by self-focusing between the nonlinear perturbation θ and the beam profile.

For an extraordinary polarized electric field $E = Ae^{ik_0 n_\perp z}$ ($k_0 = 2\pi/\lambda$) and neglecting walk-off, the scalar model for nonlinear beam propagation is

$$\frac{\partial^2 A}{\partial z^2} + 2ik_0 n_\perp \frac{\partial A}{\partial z} + D_x \frac{\partial^2 A}{\partial x^2} + \frac{\partial^2 A}{\partial y^2} + k_0^2 \Delta n_e^2(\theta) A = 0, \quad (1)$$

$$\nabla^2 \theta + \gamma |A|^2 \sin(2\theta) = 0, \quad (2)$$

with $\gamma = \epsilon_0 \epsilon_a/(4K)$ and $D_x = n_e^2(\theta)/\epsilon_{zz}$ the diffraction coefficient in the plane xz. The nonlinear photonic potential $\Delta n_e^2(\theta) = n_e^2(\theta) - n_\perp^2$ governs the beam width versus propagation, with $n_e(\theta) = [\cos^2\theta/n_\perp^2 + \sin^2\theta/n_\parallel^2]^{-1/2}$ [15]. At variance with previous work [29], the relationship Eq. (2) between θ and the light intensity $I \propto |A|^2$ is highly nonlinear: in particular, the threshold-like behavior due to the sine term permits the observation of hysteresis [18,27].

Let us start from the solution of Eq. (2) alone, i.e., assuming a solitary wave invariant along z, with a transverse profile $A = \sqrt{4Z_0 P/[\pi n_e(\theta_m) w^2]} \exp[-(x^2+y^2)/w^2] = u_m \exp[-(x^2+y^2)/w^2]$ (Z_0 is the vacuum impedance), the subscript m indicating maxima of the corresponding

quantities and $\theta_m = \theta(x = 0, y = 0)$ owing to symmetry. For narrow beams (with respect to L_x) Eq. (2) can be approximated by $\nabla^2_{xy}\theta + \gamma \sin(2\theta_m)|A|^2 = 0$. Using the Green function approach [30], for the nonlinear perturbation $\theta(x, y)$ we find

$$\theta = \frac{\gamma Z_0 P \sin(2\theta_m)}{2n_e(\theta_m)} \sum_{l=1}^{\infty} V_l(y) \sin\left[\frac{\pi l(x - L_x/2)}{L_x}\right], \quad (3)$$

where $V_l(y) = \mathrm{sinc}(\pi l/2)[F(y) + F(-y)]$ with $F(y) \equiv \mathrm{erfc}[\sqrt{2}y/w + \pi l w/(2\sqrt{2}L_x)]e^{\pi l(y/L_x)}$ and $\mathrm{sinc}(x) \equiv \sin(x)/x$. Otherwise stated, we perform a perturbative expansion of the nonlinear perturbation θ around θ_m. Thus, we get an implicit equation for the maximum θ_m

$$\frac{\theta_m n_e(\theta_m)}{\sin(2\theta_m)} = \frac{2\gamma Z_0 P}{\pi} \sum_{l=0}^{\infty} \frac{1}{2l+1} \mathrm{erfc}\left(\frac{\pi(2l+1)w}{2\sqrt{2}L_x}\right). \quad (4)$$

Equation (3) can be used to compute the OFT power for a fixed Gaussian beam. Similar to the OFT calculation for plane waves in (1 + 1)D [16], just above threshold the maximum reorientation is small: we name it $\theta_m^\star(P_{\mathrm{th}}, w)$, with P_{th} and w the beam power and waist, respectively. In this case, Eq. (3) is the exact solution of the reorientational Eq. (2) with $\sin(2\theta_m^\star) \approx 2\theta_m^\star$ and yields

$$P_{\mathrm{th}} = \frac{\pi n_\perp}{4\gamma Z_0} \left[\sum_{l=0}^{\infty} \frac{1}{2l+1} \mathrm{erfc}\left(\frac{\pi(2l+1)w}{2\sqrt{2}L_x}\right)\right]^{-1}. \quad (5)$$

The comparison between numerical and predicted [by Eq. (5)] results for the threshold power is visible in Fig. 1(a). As expected from the assumptions, the agreement improves as the waist becomes smaller. The theoretical curves are plotted down to a waist of 1 μm, consistently with the scalar approximation for the field; for $w = 0$, Eq. (5) is singular due to the divergence of the Green function, thus providing unphysical results. Figure 1(b) plots the maximum reorientation θ_m for fixed waist w: the model works better for small waists as the accuracy of solution (3) is higher for narrow beams [30]. The discrepancy between the two sets of curves is due to letting $\theta \approx \theta_m$ in the torque term.

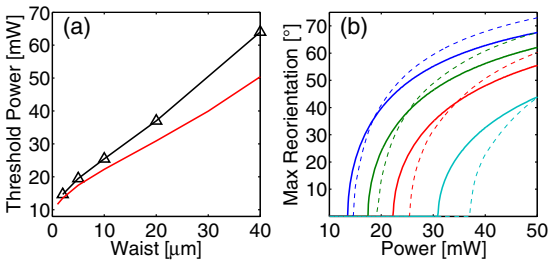

Fig. 1. (a) Threshold power versus beam waist computed numerically (black line with triangles) and predicted theoretically from Eq. (5) (solid red line). (b) Maximum reorientation θ_m versus beam power P as predicted by Eq. (4) (solid lines) and computed via an over-relaxed Gauss–Seidel algorithm (dashed lines). Beam waists are 2, 5, 10, and 20 μm, from left to right, respectively.

Next, we account for the field A dependence on the director profile $\theta(x, y)$ by solving Eq. (1) jointly with Eq. (2). We are interested in the shape-preserving solutions of Eqs. (1) (2) in the form $\theta = \theta_S(x, y)$ and $A = A_S(x, y)e^{ik_0(n_S - n_\perp)z}$, with n_S the effective refractive index of the soliton. Following the Snyder–Mitchell's (SM) approach [31] with $D_x = 1$, the corresponding nonlinear eigenvalue problem can be solved analytically in the limit of a high nonlocality [32]. We assume a cylindrically-symmetric parabolic shape for the perturbation θ [30,32], which, in the highly nonlocal limit, is well approximated by its Taylor's expansion around θ_m up to the quadratic term. Thus, setting $\theta_S = \theta_m(P) - \theta_2(P)(x^2 + y^2)$ and taking a Gaussian ansatz for the field, i.e., $u_S = u_m \exp[-(x^2 + y^2)/w_S^2]$ with $u_m = \sqrt{4Z_0P/[\pi n_e(\theta_m)w_S^2]}$, we find $\theta_2(P) = \gamma u_m^2/(4\eta)\sin(2\theta_m)$ [33]. The factor η accounts for discrepancies with respect to the SM model; the best-fit with the exact solution is found for $\eta = 2$ [32]. Since the extraordinary index varies slowly across the beam cross-section, we assume $\Delta n_e^2 \approx [n_e^2(\theta_m) - n_\perp^2] - 2n_e(\theta_m)n_e'(\theta_m)\theta_2(P)(x^2 + y^2)$ (we set $n_e' \equiv dn_e/d\theta$) for the soliton profile. Thus, the soliton width is

$$w_S(P, \theta_m) = \frac{1}{k_0}\left(\frac{2\pi\eta}{Z_0\gamma \sin(2\theta_m)n_e'(\theta_m)}\frac{1}{P}\right)^{1/2}. \quad (6)$$

Figure 2(a) plots w_S versus maximum reorientation θ_m at fixed powers: consistent with [34], solitons are narrower when $\theta_m \approx \pi/4$ and tend to plane waves for either $\theta_m \to 0$ or $\theta_m \to \pi/2$ due to a vanishing nonlinearity.

Figure 2(b) illustrates how to find the nonlinear modes using Eqs. (4) and (6). The solid lines are the soliton existence curves in Fig. 2(a), whereas the dashed curves plot—for fixed power—the waist of the Gaussian profiles corresponding to a given maximum reorientation θ_m, as calculated from Eq. (4). In agreement with Fig. 1(b) the width w of the Gaussian decreases monotonically as θ_m increases, while the beam radius required for a given θ_m increases with power P. The soliton solutions correspond to the crossing between the two sets of curves: for a given P, solitons do not exist when the two curves do not intersect (see $P = 12$ mW); a degenerate soliton solution exists when the two curves are tangent (see case $P = 16$ mW); two solitons exist when the two curves have two points in common (e.g., $P = 19$ mW).

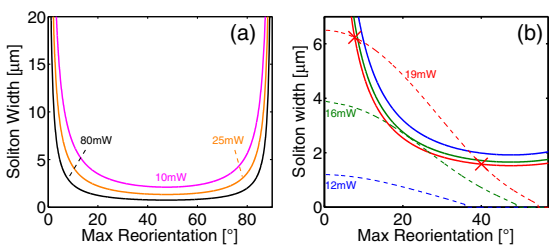

Fig. 2. (a) Soliton width w versus maximum reorientation θ_m for a fixed power, calculated from Eq. (6) for $\eta = 2$. (b) Graphic computation of the soliton width for a fixed power: solid and dashed lines are from Eqs. (4) and (6), respectively.

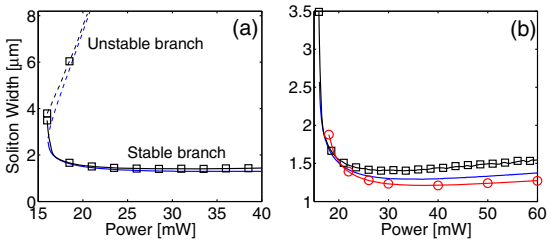

Fig. 3. (a) Width of stable (solid line) and unstable (dashed line) solitons versus power as computed from Eqs. (4) and (6) (no symbols), and from the free energy Eq. (8) (lines with squares). (b) Width of stable solitons versus power as predicted from Fig. 2(b) (blue solid line), from the free energy (black line with squares) and as calculated numerically from Eqs. (1), (2) (red line with circles).

Figure 3(a) summarizes the results: our simplified model predicts a threshold $P_{\rm th}^S$ for the existence of shape-preserving solitary waves, corresponding in our case to about 16 mW. For $P > P_{\rm th}^S$ two distinct solitons are found: one is highly localized and induces a large perturbation θ_m, the other is wider and induces a smaller reorientation, the latter decreasing as the power increases. We will show below that the family of narrower solitons is stable, whereas the other branch is unstable. Figure 3(b) compares exact solitons computed numerically from Eqs. (1), (2) and theoretical predictions. We note that our numerical algorithm, based on a Newton–Raphson method coupled with an overrelaxed Gauss–Seidel scheme to solve Eq. (2), can only find stable solutions. The soliton width is well approximated by our theory based on the SM model (blue line with no symbols), with an underestimation of the threshold $P_{\rm th}^S$ for self-localization (numerical simulations yield ≈18 mW).

Dynamical behavior is addressed computing the free energy associated with each Gaussian beam. Neglecting the contribution stemming from breathing along z [33], the free energy $\mathcal{F}$ (or equivalently, the Lagrangian) of the system is [16,35]

$$\mathcal{F} = \frac{1}{2}\left(\frac{\partial\theta}{\partial x}\right)^2 + \frac{1}{2}\left(\frac{\partial\theta}{\partial y}\right)^2 + \frac{\gamma Z_0\cos(2\theta)}{n_{\rm S}} I - \frac{\epsilon_0 Z_0\left(\epsilon_\perp + \frac{\epsilon_a}{2}\right)}{2n_{\rm S}K} I + \frac{\epsilon_0 Z_0}{2n_{\rm S}Kk_0^2}\left[\left|\frac{\partial\sqrt{I}}{\partial x}\right|^2 + \left|\frac{\partial\sqrt{I}}{\partial y}\right|^2 + k_0^2 n_{\rm S}^2 I\right], \quad (7)$$

with $I = I_0\exp[-2(x^2+y^2)/w^2]$ the beam intensity $[I_0 = 2P/(\pi w^2)]$. In agreement with Eq. (3), for θ we take the trial function $\theta = \kappa\theta_m\sum_{l=1}^{\infty} V_l(y)\sin[\pi l(x - L_x/2)/L_x]$, with $\kappa(w) = -1/[\sum_{l=1}^{\infty} V_l(0)\sin(\pi l/2)]$. If walk-off is neglected we find $n_e^2 = \epsilon_\perp + (\epsilon_a/2)[1-\cos(2\theta)]$; thus, the integrated free energy $F = \int_{-\infty}^{\infty}\int_{-L_x/2}^{L_x/2}\mathcal{F}\,{\rm d}x{\rm d}y$ can be approximated as

$$F \approx \frac{1}{2}\alpha\kappa^2\theta_m^2 + \frac{2\gamma Z_0 P}{\pi n_{\rm S} w^2}\int_{-\frac{L_x}{2}}^{\frac{L_x}{2}}{\rm d}x\int_{-\infty}^{\infty}\cos(2\theta)e^{-2\frac{x^2+y^2}{w^2}}{\rm d}y + \left\{\frac{\epsilon_0 Z_0}{n_{\rm S}k_0^2 K}\frac{1}{w^2} + \frac{\epsilon_0 Z_0 n_S}{K} - \frac{\gamma Z_0\cos(2\theta_m)}{n_{\rm S}}\right\}P, \quad (8)$$

where $\alpha = \frac{1}{2}\sum_{m=0}^{\infty}\int_{-\infty}^{\infty}[(\pi^2/L_x)V_{2m+1}^2 + L_x(V'_{2m+1})^2]{\rm d}y$, with $V'_l(y) = dV_l(y)/dy$. Due to the assumption of a Gaussian profile for the field, in Eq. (8) we can set $n_S = n_e(\theta_m) - \sqrt{n'_e\theta_2/[4k_0^2 n_e(\theta_m)]}$. On the RHS of Eq. (8) the three terms are the energy contributions stemming from elastic NLC distortion, transverse variation in light–matter coupling, and beam diffraction/confinement, respectively.

The *master equation* (8) allows for qualitatively investigating the system dynamics. We first check the *mechanic* portion of Eq. (8) by computing F for a fixed Gaussian, i.e., neglecting the last term on the RHS. Figure 4(a) graphs F versus θ_m: the actual orientation corresponds to the minimum of F, with the final results perfectly matching the numerical simulations for $\theta_m < 60°$ (not shown). The free energy always shows a single local extremum, thus inhibiting hysteresis [18]. The energy landscape completely changes as self-focusing is accounted for: Fig. 4(b) shows F versus θ_m for fixed P [consequently, each value of θ_m corresponds to a different beam width w according to Eq. (4)]. Below $P_{\rm th}^S$ (the latter now dictated by the joint action of OFT and self-focusing), F monotonically increases and solitons do not exist. Above the threshold both local maximum and minimum appear, the latter for a larger θ_m. Thus, out of the two equilibrium points for a given power, the minimum corresponds to the narrower (stable) soliton in Fig. 3(a), while the maximum represents the wider (unstable) soliton, given by the dashed lines in Figs. 3(a) and 4(b).

The free energy permits us to describe qualitatively the beam dynamics. For powers above $P_{\rm th}^S$, when the input beams are wider than the unstable soliton (in Fig. 4(b) on the left of the local maximum), waves collapse to linear diffracting beams corresponding to a vanishing reorientation $\theta_m = 0$ or, in other words, reorientation is inhibited; conversely, when the input beams are narrower than the unstable soliton (on the right of the local maximum), the beam evolves toward the minimum, with nonlinear reorientation and, in turn, self-focusing and self-trapping. Whatever the input waist, as the power of an input beam is ramped up, a (stable) soliton forms [33], breathing in width around the minimum in Fig. 4(b); then when the power is ramped down, the soliton state is maintained until $P = P_{\rm th}^S$, when the beam returns to linear diffraction, in perfect agreement with [27]. At

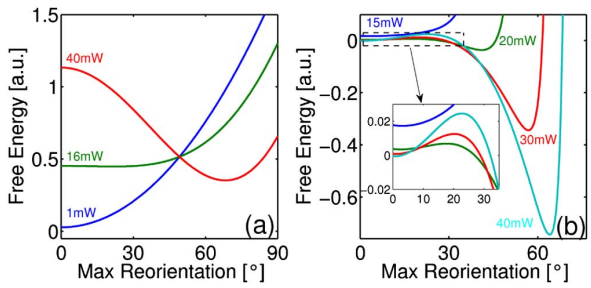

Fig. 4. (a) Free energy versus θ_m for $w = 2$ μm when self-focusing is neglected; 16 mW correspond to the OFT [see Fig. 1(b)]. (b) Free energy when self-focusing is considered; inset shows magnification around the local maxima.

variance with Kaplan's prediction of two stable soliton states [36], such dynamics is similar to what is expected in colloids [37]. The emerging hysteresis cycle versus power is a first-order transition encompassing solitary and diffracting states.

In conclusion, we investigated theoretically light self-trapping in NLCs subject to the Fréedericksz threshold, demonstrating that, beyond a threshold, two solitons exist but only the narrower is stable. Due to the interplay of self-focusing and molecular dynamics we predict hysteresis versus beam power between a self-trapped and a diffracting beam, as recently reported experimentally [27].

GA thanks Prof. Minzoni for enlightening discussions.

References

1. D.-K. Yang and S.-T. Wu, *Fundamentals of Liquid Crystals Devices* (Wiley, Chichester, 2006).
2. A. Fratalocchi and G. Assanto, Appl. Phys. Lett. **86**, 051109 (2005).
3. P. Valley, M. R. Dodge, J. Schwiegerling, G. Peyman, and N. Peyghambarian, Opt. Lett. **35**, 2582 (2010).
4. N. Tabiryan, S. Nersisyan, T. White, T. Bunning, D. Steeves, and B. Kimball, AIP Adv. **1**, 022153 (2011).
5. W. D. Cort, J. Beeckman, T. Claes, K. Neyts, and R. Baets, Opt. Lett. **36**, 3876 (2011).
6. J. Ptasinski, S. W. Kim, L. Pang, I.-C. Khoo, and Y. Fainman, Opt. Lett. **38**, 2008 (2013).
7. G. Strangi, S. Ferjani, V. Barna, A. DeLuca, C. Versace, N. Scaramuzza, and R. Bartolino, Opt. Express **14**, 7737 (2006).
8. H. Coles and S. Morris, Nat. Photonics **4**, 676 (2010).
9. A. Minovich, J. Farnell, D. Neshev, I. McKerracher, F. Karouta, J. Tian, D. A. Powell, I. V. Shadrivov, H. Hoe Tan, C. Jagadish, and Y. Kivshar, Appl. Phys. Lett. **100**, 121113 (2012).
10. O. Buchnev, J. Y. Ou, M. Kaczmarek, N. I. Zheludev, and V. A. Fedotov, Opt. Express **21**, 1633 (2013).
11. A. Fratalocchi, A. Piccardi, M. Peccianti, and G. Assanto, Opt. Lett. **32**, 1447 (2007).
12. S. Slussarenko, B. Piccirillo, V. Chigrinov, L. Marrucci, and E. Santamato, J. Opt. **15**, 025406 (2013).
13. R. Barboza, U. Bortolozzo, G. Assanto, E. Vidal, M. Clerc, and S. Residori, Phys. Rev. Lett. **111**, 093902 (2013).
14. I. C. Khoo, Phys. Rep. **471**, 221 (2009).
15. A. Alberucci, A. Piccardi, M. Peccianti, M. Kaczmarek, and G. Assanto, Phys. Rev. A **82**, 023806 (2010).
16. F. Simoni, *Nonlinear Optical Properties of Liquid Crystals* (World Scientific, 1997).
17. E. Braun, L. P. Faucheux, and A. Libchaber, Phys. Rev. A **48**, 611 (1993).
18. H. L. Ong, Phys. Rev. A **28**, 2393 (1983).
19. S. D. Durbin, S. M. Arakelian, and Y. R. Shen, Phys. Rev. Lett. **47**, 1411 (1981).
20. A. J. Karn, S. M. Arakelian, Y. R. Shen, and H. L. Ong, Phys. Rev. Lett. **57**, 448 (1986).
21. S.-H. Chen and J. J. Wu, Appl. Phys. Lett. **52**, 1998 (1988).
22. E. Babayan, I. Budagovsky, S. Shvetsov, M. Smayev, A. Zolot'ko, N. Boiko, and M. Barnik, Phys. Rev. E **82**, 061705 (2010).
23. I. Budagovsky, D. Pavlov, S. Shvetsov, M. Smayev, A. Zolot'ko, N. Boiko, and M. Barnik, Appl. Phys. Lett. **101**, 021112 (2012).
24. F. Simoni, D. E. Lucchetta, L. Lucchetti, H. L. Ong, S. V. Serak, and N. Tabiryan, Opt. Lett. **38**, 878 (2013).
25. M. Peccianti and G. Assanto, Phys. Rep. **516**, 147 (2012).
26. I. C. Khoo, Appl. Phys. Lett. **41**, 909 (1982).
27. N. Kravets, A. Piccardi, A. Alberucci, O. Buchnev, M. Kaczmarek, and G. Assanto, Phys. Rev. Lett. **113**, 023901 (2014).
28. I. C. Khoo, T. H. Liu, and P. Y. Yan, J. Opt. Soc. Am. B **4**, 115 (1987).
29. J. M. L. MacNeil, N. F. Smyth, and G. Assanto, Physica D **284**, 1 (2014).
30. A. Alberucci and G. Assanto, J. Opt. Soc. Am. B **24**, 2314 (2007).
31. A. Snyder and D. Mitchell, Science **276**, 1538 (1997).
32. A. Alberucci, C. P. Jisha, and G. Assanto, Opt. Lett. **39**, 4317 (2014).
33. C. Conti, M. Peccianti, and G. Assanto, Phys. Rev. Lett. **92**, 113902 (2004).
34. A. Alberucci and G. Assanto, Opt. Lett. **35**, 2520 (2010).
35. C. Dartora, G. Cabrera, K. Nobrega, V. Montagner, M. Matielli, F. de Campos, and H. Filho, Phys. Rev. A **83**, 012110 (2011).
36. A. E. Kaplan, Phys. Rev. Lett. **55**, 1291 (1985).
37. M. Matuszewski, W. Krolikowski, and Y. Kivshar, Opt. Express **16**, 1371 (2008).

nature COMMUNICATIONS

ARTICLE

Received 23 Jul 2014 | Accepted 10 Oct 2014 | Published 25 Nov 2014

DOI: 10.1038/ncomms6533

Power-controlled transition from standard to negative refraction in reorientational soft matter

Armando Piccardi[1], Alessandro Alberucci[1], Nina Kravets[1], Oleksandr Buchnev[2] & Gaetano Assanto[1]

Refraction at a dielectric interface can take an anomalous character in anisotropic crystals, when light is negatively refracted with incident and refracted beams emerging on the same side of the interface normal. In soft matter subject to reorientation, such as nematic liquid crystals, the nonlinear interaction with light allows tuning of the optical properties. We demonstrate that in such material a beam of light can experience either positive or negative refraction depending on input power, as it can alter the spatial distribution of the optic axis and, in turn, the direction of the energy flow when traveling across an interface. Moreover, the nonlinear optical response yields beam self-focusing and spatial localization into a self-confined solitary wave through the formation of a graded-index waveguide, linking the refractive transition to power-driven readdressing of copolarized guided-wave signals, with a number of output ports not limited by diffraction.

[1] NooEL—Nonlinear Optics and OptoElectronics Lab, University 'Roma Tre', 00146 Rome, Italy. [2] Zepler Institute, University of Southampton, Southampton SO17 1BJ, UK. Correspondence and requests for materials should be addressed to G.A. (email: assanto@uniroma3.it or optow.ele.uniroma3.it).

Light refraction at dielectric interfaces under the Snell–Descartes law is among the best known concepts in optics, its theoretical basis stemming from Maxwell's equations and momentum conservation[1]. Ray-tracing techniques and the design of several optical devices rely on refraction. In isotropic media and at frequencies well removed from absorption regions, incident and refracted rays at an interface always lie on opposite sides of the normal to it, that is, they undergo standard (positive) refraction or, simply, refraction. Some natural and man-made media can also exhibit negative refraction, when both impinging and refracted rays belong to the same half-plane[2]. Owing to the conservation of momentum across the interface, negative refraction requires a nonzero walk-off angle between the phase velocity v_p and the group velocity v_g in the medium hosting the refracted beam. Two main types of light–matter interactions can satisfy this requirement: with backward waves when $v_p \cdot v_g < 0$, or with forward waves when $v_p \cdot v_g > 0$, respectively[2]. The case of backward waves corresponds to the so-called negative refractive index, a counterintuitive phenomenon occurring in absorptive media or in metamaterials[3,4]. In the first decade of the twentieth century, Schuster (following W. Lamb's original idea in mechanical systems) studied negative refraction considering backward waves in the presence of a lossy medium at an interface, and predicted its unobservability due to the evanescent character of the involved waves[5]. Nearly one century later, negative refraction was revived by Pendry's seminal paper on the superlens effect based on amplified evanescent waves in a metamaterial[6]. Negative refraction in metamaterials has been recently demonstrated at microwave[7,8] as well as near-infrared[9], visible[10] and ultraviolet wavelengths[11]. Surfing this wake of interest, researchers have also investigated negative refraction with forward waves, devoting special attention to photonic crystals[12,13] and natural anisotropic media[14,15]. In the latter class of materials, where double refraction was first described by E. Bartholinus in the seventeenth century[16], negative refraction stems from birefringent walk-off when the Poynting vector (directed as the energy flux) lies on the opposite side of the refracted wavevector with respect to the normal at the interface[2].

The superlens effect in natural non-absorbing crystals is ruled out by the cutoff on transverse wavevectors (it might survive in photonic crystals when photons have a negative effective mass[12] and behave as in a hyperbolic material[17]); nonetheless, negative (or backward) refraction remains relevant as it can maximize the angular beam deflection associated with impedance matching at an interface[14]. In this scenario, anisotropic soft matter—such as liquid crystals—has been used in the pursuit of electrically-adjustable negative refraction with either diffracting[18,19] or self-confined beams[20].

In this article, we report on nonlinear refraction with forward wavepackets in uniaxial nematic liquid crystals (NLCs): we obtained standard and negative light refraction at an interface using a single extraordinary polarization and were able to nonlinearly control the transition from one (positive) to the other (negative) by exploiting the walk-off dependence on beam power. At variance with previous attempts based on wave mixing[15,21], in NLCs the optic axis can undergo reorientation by light self-action with continuous-waves at mW powers, achieving self-tunability of the beam direction, that is, self-steering: as the incident power increases, nonlinear walk-off modifies the light path and steers the refracted beam to the opposite side of the interface normal, achieving negative refraction with overall angular deflections as large as 7°. Moreover, reorientation is accompanied by self-focusing with beam self-localization into spatial solitary waves[22]: these are self-induced waveguides that permit to balance out the diffractive spreading, enhance the all-optical response, guide copolarized signals of different wavelengths and maximize the transverse resolution on steering, that is, the number of resolvable output spots or signal exit ports.

Results

Self-steering and negative refraction in NLCs. NLCs are states of matter sharing the properties of both solid-state crystals and liquids: they exhibit orientational order with the constituent elongated molecules randomly distributed in position[23]. The molecular orientation is macroscopically described by a space/time-dependent vector field, the molecular director $\hat{\mathbf{n}}$, collinear with the average alignment of the main (long) molecular axes. At optical frequencies, most NLCs are positive uniaxials with their optic axis along $\hat{\mathbf{n}}$, extraordinary refractive index $n_{\|}$ for electric fields oscillating parallel to $\hat{\mathbf{n}}$ and ordinary index $n_{\perp}$ for fields normal to $\hat{\mathbf{n}}$, respectively. NLCs exhibit a giant all-optical response observable with low-power continuous-wave excitations[24], the reorientational optical nonlinearity: a suitably (extraordinarily) polarized electric field can induce molecular dipoles and make them reorient within the principal plane in order to minimize the system energy in the presence of elastic (intermolecular) interactions[23,24]. Such reorientational response is at the basis of a number of observed phenomena, ranging from bistability[25] to pattern formation[26], generation of complex topological structures[27–29] or light-controlling-light; in particular, the latter has been exploited—at mW and sub-mW power levels—for generating, controlling and routing 'nematicons', that is, spatially self-localized beams stemming from the balance between transverse spatial dispersion (diffraction) and self-focusing[22].

NLCs are ideal candidates for the observation of nonlinear negative refraction: they are highly birefringent (typically $\Delta n = n_{\|} - n_{\perp} \approx 0.2$ in the visible spectrum), with walk-off (angular departure of Poynting vector from wavevector) as large as $\approx 7°$, thus enhancing the role of anisotropy at dielectric interfaces[30,31]; moreover, they are transparent from infrared to ultraviolet, with losses mainly due to Rayleigh scattering[23,24]; finally, their response is such that a non-perturbative nonlinear regime can be experimentally accessed in the context of classical optics[32].

The basic configuration for studying nonlinear tunable refraction from standard to negative in NLCs is sketched in Fig. 1. A thick NLC layer is homogeneously aligned in a planar cell with director $\hat{\mathbf{n}}$ along the axis z normal to the input interface in $z=0$. A light beam is launched across the air-(glass)-NLC interface with input wavevector $\mathbf{k}_{in}$ at an angle β_{in} with respect to z; its electric field $\mathbf{E}$ oscillates in the principal plane yz of the uniaxial NLC and excites extraordinary waves. The system has mirror symmetry with respect to z, thus the light evolution is unaffected by the transformation $\beta_{in} \rightarrow -\beta_{in}$. Fig. 1 illustrates the case $\beta_{in} < 0$: the Snell–Descartes law provides the implicit equation $\beta = \arcsin\,[\sin\beta_{in}/n_e(-\beta)]$ for the refraction angle β, where $n_e(\theta) = \left(\cos^2\theta/n_{\perp}^2 + \sin^2\theta/n_{\|}^2\right)^{-1/2}$ depends on the angle θ between $\hat{\mathbf{n}}$ and $\mathbf{k}$; in the linear regime θ corresponds to $-\beta$.

Common NLCs are positive uniaxials with $\Delta n > 0$; hence, the Poynting vector is always coplanar with the wavevector $\mathbf{k}$ and the optic axis $\hat{\mathbf{n}}$, and lies between them. The walk-off angle is $\delta = \arctan\{\epsilon_a \sin(2\theta)/[\epsilon_a + 2n_{\perp}^2 + \epsilon_a\cos(2\theta)]\}$, with $\epsilon_a = n_{\|}^2 - n_{\perp}^2$ the optical anisotropy; therefore, δ and θ have the same sign. Defining γ the angle of the Poynting vector with z, in the linear regime it is $\gamma\beta > 0$, that is, light rays undergo positive refraction for every incidence angle β_{in}. In the nonlinear regime, conversely, the reorientation of the optic axis can affect the beam (ray) direction. With reference to Fig. 1, an extraordinarily

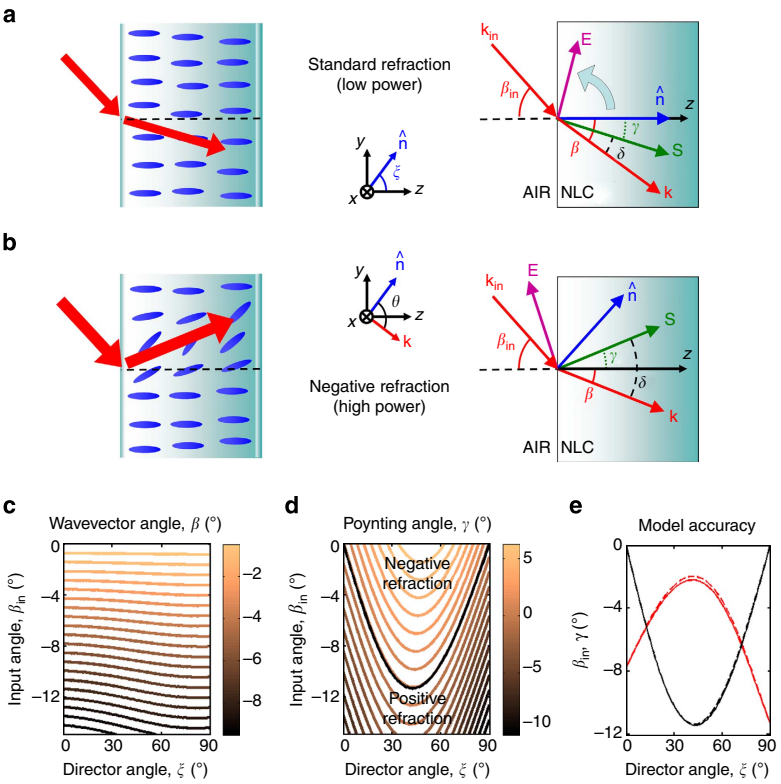

Figure 1 | Basic configuration and initial assessment of the phenomenon. An extraordinarily polarized light beam impinges on the air-(glass)-NLC interface defining the input to the planar cell. (**a**) At low powers, the molecular director is parallel to z and positive refraction occurs for any incidence angle β_{in} of wavevector $\mathbf{k}_{in}$. (**b**) As the input beam power increases, the reorientational torque rotates the director $\hat{\mathbf{n}}$ towards the **E**-field vector (as indicated by the curved arrow in **a**), reducing the angle of refraction $|\beta|$ and increasing the walk-off δ, eventually resulting in negative refraction when $|\beta_{in}|$ gets small enough. All angles are defined positive when taken clockwise with respect to the x axis: β remains negative regardless of the type of refraction, whereas γ changes sign in the transition from positive (Poynting vector **S** in the $y<0$ half-plane) to negative (**S** in the $y>0$ half-plane) refraction. Insets: definitions of (lower inset) angle θ between **k** and $\hat{\mathbf{n}}$ (positive in the example) and (upper inset) angle ξ between $\hat{\mathbf{n}}$ and z. (**c**) Contour plot of wavevector angle β and (**d**) contour plot of Poynting vector angle γ versus director orientation ξ and incidence angle β_{in}; the black solid line in (**d**) corresponds to a Poynting vector along z (that is, $\gamma=0$). (**e**) Graph of the largest β_{in} versus ξ (black lines) corresponding to $\gamma=0$ (that is, maximum angle of incidence to support negative refraction, black line in **d**) and γ versus ξ for $\beta_{in}=-15°$ (red lines), respectively; solid and dashed lines are exact and approximate solutions, respectively. Here $n_{||}=1.7$ and $n_{\perp}=1.5$; the wavelength of light is $\lambda=1.064\,\mu$m.

polarized light beam can induce a rotation of the molecular director $\hat{\mathbf{n}}$ away from the wavevector, in turn increasing the size of the walk-off $|\delta|$. Even if β remains negative for every angle ξ between $\hat{\mathbf{n}}$ and z, since $\theta=\xi-\beta$ the Poynting vector can change side with respect to z, giving rise to negative refraction when $|\delta|>|\beta|$.

From Fig. 1 and the Snell–Descartes law, it is straightforward to obtain the refraction angle for light rays as

$$\gamma(\beta_{in},\xi)=\delta(\xi-\beta)+\arcsin\left[\frac{\sin\beta_{in}}{n_e(\xi-\beta)}\right]. \quad (1)$$

In the limit of small incidence angles β_{in}, equation (1) gives

$$\gamma(\beta_{in},\xi)=\delta(\xi)+\left[1-\frac{2\epsilon_a\cos(2\xi)}{\Theta(\xi)}-\frac{2\epsilon_a^2\sin^2(2\xi)}{\Theta^2(\xi)}\right]\frac{\beta_{in}}{n_e(\xi)}, \quad (2)$$

where we set $\Theta(\xi)=\epsilon_a+2n_{\perp}^2+\epsilon_a\cos(2\xi)$. Neglecting the terms containing powers of ϵ_a larger than 2, it stems from equation (2) that negative refraction can only occur if

$$|\beta_{in}|<\frac{\epsilon_a}{2n_{\perp}}\left(1-\frac{\epsilon_a}{4n_{\perp}^2}\right). \quad (3)$$

Figure 1c,d graph wavevector and Poynting vector angular directions in the NLC versus the two free parameters, that is, director orientation ξ and angle of incidence β_{in} (in the interval $[-15°\ 0°]$); we set $n_{||}=1.7$ and $n_{\perp}=1.5$ as in the E7 mixture at 1064 nm (ref. 33). When $|\beta_{in}|<5°$, the refraction angle β slightly changes with ξ, never exceeding variations of 1°; negative refraction occurs for small β_{in}, with smaller β_{in} corresponding to larger negative refraction. Figure 1e compares approximate (from equation (2)) and exact solutions (from equation (1)) for γ in the (worst) case $\beta_{in}=-15°$; in the same figure (red lines) the validity of equation (3) is apparent in calculating the maximum input beam tilt, which permits the observation of negative refraction. Exact and approximate results are mutually consistent to a good accuracy.

Experimental verification. To validate our prediction with experiments, we prepared a planar glass cell of thickness $L=100\,\mu$m across x, filled it with the E7 mixture ($\Delta n\approx0.2$) and sealed the input to ensure a homogeneous director distribution

and the absence of a meniscus[22]. The molecular director was aligned along the normal z to the input interface, as in Fig. 1a. Due to the cell shape, the sample was subject to one-dimensional boundary effects versus x but could be considered infinitely extended across y (ref. 34). A TEM_{00} laser beam of wavelength $\lambda = 1.064\,\mu m$ was gently focused into the sample, slightly past the input glass/NLC interface to avoid spurious interactions with the molecules anchored at the boundary; the input waist was set to $w_0 \approx 8\,\mu m$ by using two lenses in a telescopic arrangement and a microscope objective. Two mirrors (M_1 and M_2 in Fig. 2) ensured accurate control of the input conditions, particularly the incidence angle β_{in}.

The beam-to-cell alignment was monitored by acquiring the trajectories of extraordinary and ordinary rays propagating in the linear regime (Fig. 2b), using a CCD (charge-coupled device) camera to collect the out-of-plane (yz) scattered light; the acquired beam paths could then be compared with the calculated ones (Fig. 1c,d; ref. 35). A second CCD camera was used to acquire the output profile through the exit facet of the sample. Fig. 2c shows the measured beam width, defined as $w = 2\sqrt{\int r^2|A|^2 dr / \int |A|^2 dr}$, versus z in the linear regime and normalized with respect to w_0; A is the amplitude of the light wavepacket. In the described conditions (cell configuration, beam waist, small β_{in} and low power), beam propagation was ruled by diffraction, with a Rayleigh distance of $\approx 280\,\mu m$.

When the optical excitation is larger (in the highly nonlinear regime), nonlinear refraction can take place: the director orientation ξ depends on the input power through optical reorientation, providing in turn a change in walk-off[36]; in addition, a (smaller) nonlinear correction of β is caused by the increase of the extraordinary refractive index $n_e(\beta)$ (see Eq.(1) and Fig. 1c). Therefore, for high-enough excitations the light beam can adjust the direction of its own Poynting vector by altering the walk-off.

Figure 3a displays the acquired images of beam evolution and output profile for $\beta_{in} = -4.9°$. As expected, the beam moves sideways versus input power. At variance with the predictions of equation (2), however, it does not propagate straight when steered by way of nonlinear walk-off: the observed bending is due to scattering losses, which cause a reduction in beam power versus z, hence a reduced nonlinear response with progressively vanishing reorientation[36]. In particular, for $P \approx 30$ mW the beam positions at sample input and output nearly coincide, with an apparent $\gamma = 0$ resulting at the exit. Further increases in input power allow for negative refraction, that is, the outgoing beam can be seen to emerge in the same half-plane $y > 0$ of the incident beam (rightmost panels of Fig. 3a for $P > 30$ mW).

For a better assessment of the phenomenon, Fig. 3b,c plot the beam trajectories and normalized widths versus z, corresponding to Fig. 3a. The paths change non-monotonically with power due to the δ dependence on θ, with a maximum δ for $\theta \approx 45°$ (Fig. 1d). The combined effect of (scattering) losses and nonlinear walk-off is responsible for the change (in both amplitude and sign) of the initial slope of the trajectories. As stated above, a stronger reorientation corresponds to a larger walk-off up to its maximum, with the opposite trend for further (nonlinear) increases in θ: the analysis of the trajectories (Fig. 3b) and their slope (inset Fig. 3b) allows estimating an angle $\theta \approx 45°$ near the input interface for powers slightly above $P = 40$ mW. For $P = 30$ mW the angle γ results positive up to $z \approx 600\,\mu m$, then retrieves its linear value owing to vanishing reorientation, as losses reduce the local beam power. For $P \approx 40$ mW the maximum orientation is $\approx 45°$: γ monotonically decreases along z, going from positive to negative values after a propagation distance z which lengthens with power. For $P > 70$ mW the initial γ reduces as power increases, conserving its sign along z. Eventually, for $P \approx 100$ mW, the Poynting vector angle γ monotonically increases versus z up to a maximum, with $\theta \approx 45°$ at the output.

Furthermore, the measured beam width confirms the occurrence of light self-trapping, more and more effective as power increases (Fig. 3c). For $P = 30$ mW and $P = 40$ mW, when the beam profile gets narrower (that is, self-confinement is stronger, inset in Fig. 3c), the outgoing beam results wider due to the stronger diffraction after losses prevail on self-focusing. In particular, the minimum waist is obtained for $P = 40$ mW, confirming the value of $\theta \approx 45°$ inferred from Fig. 3b when the nonlinearity is maximized. For $P = 100$ mW, in the early stages of propagation the beam is wider than at lower powers due to saturation of the nonlinear response ($\theta > 45°$ (ref. 32)).

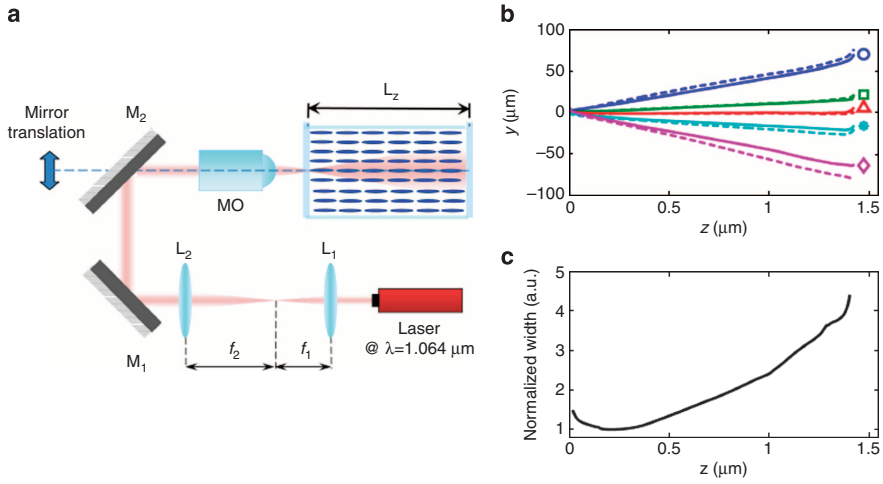

Figure 2 | Setup and linear characterization. (**a**) Sketch of the experimental set-up: lenses L_1 and L_2 form a telescope; mirror M_1 is fixed, mirror M_2 can be translated to adjust the beam path and the incidence angle. (**b**) Beam trajectories in the linear limit (2 mW input power) for $\beta_{in} = 0°$ (red line with triangle), $\pm 1.5°$ (green line with square and cyan line with star) and $\pm 5°$ (blue line with circle and magenta line with diamond); solid and dashed lines correspond to extraordinary and ordinary waves, respectively. (**c**) Normalized beam width w/w_0 versus z at normal incidence for $\beta_{in} = 0°$ and 2 mW input power. Here $w_0 = 8\,\mu m$.

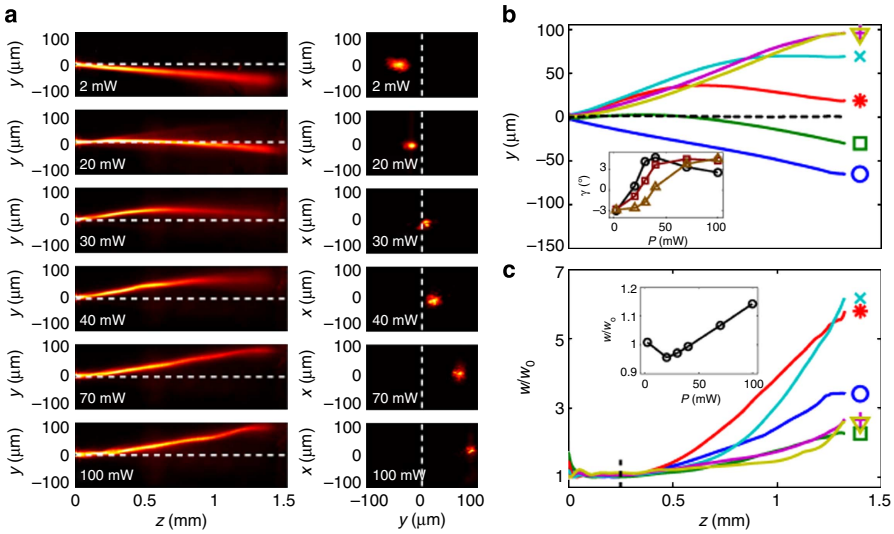

Figure 3 | Demonstration of nonlinear negative refraction. (**a**) Beam evolution in the observation plane *yz* (left) and output profiles in the transverse plane *xy* (right) when $\beta_{in} = -4.9°$. The dashed line indicates the cell mid-section $y = 0$. (**b**) Corresponding trajectories and (**c**) normalized beam width versus *z* for an input power of 2 mW (blue line with circle), 20 mW (green line with square), 30 mW (red line with star), 40 mW (cyan line with cross), 70 mW (magenta line with plus) and 100 mW (yellow line with inverted triangle). The black dashed line in **b** indicates the trajectory in the linear regime when $|\beta_{in}| \approx 0°$ within the experimental accuracy. Inset in **b**: angle γ versus input power, measured in $z = 150$ μm (black line with circle), $z = 500$ μm (clay line with square) and $z = 1$ mm (mustard line with triangle). Inset in **c**: normalized beam width versus power measured in $z = 250$ μm.

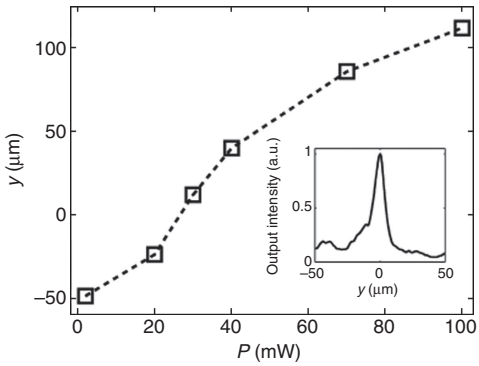

Figure 4 | Power-dependent beam refraction and steering. Output beam position on the *y* axis versus input power, for an angle of incidence $\beta_{in} = -4.9°$. The self-confined beam and the associated graded-index waveguide undergo angular steering and transverse displacement versus excitation. The resulting power-controlled router has a number of output ports (and outgoing guided-wave signals) defined by the overall angular span and the width of the self-trapped beam. The inset shows a typical self-guided (solitary) beam profile ($P = 30$ mW).

The power-controlled steering action is shown in Fig. 4, for the case $\beta_{in} = -4.9°$. Clearly, in the solitary regime the beam size is of the order of the input width (see inset), permitting to resolve a large number of output positions versus *y*, that is, a number of output ports for signals guided by solitons. Careful engineering (reducing input waist and scattering losses, increasing wavelength and propagation distance) could easily result in spatial read-dressing to >30 output channels with negligible crosstalk.

The experimental results on nonlinear beam refraction are summarized in Fig. 5: the output beam position in *y* changes with input power for various incidence angles β_{in}. Nonlinear negative refraction is largest for small β_{in}, consistently with Fig. 1d. The maximum nonlinear deflection of the beam was obtained for a finite β_{in}, rather than the predicted $\beta_{in} = 0$, because powers above an upper value caused the beam to wiggle strongly due to temporal instabilities in the medium[37,38]. Figure 5a is not perfectly symmetric due to the unavoidable sample imperfections and the finite experimental accuracy. For an input power of 100 mW, the graph shows a maximum nonlinear deflection of about 150 μm, the largest self-steering obtained to date (significantly larger than in ref. 36) via power-dependent walk-off. Finally, we checked the mirror symmetry of our sample by comparing the experimental data for positive and negative β_{in}: the plots in Fig. 5b,c confirm that, within measurement errors, the system is specularly symmetric.

Discussion

We reported on the first experimental observation of nonlinear refraction—from positive to negative — by beam self-action in reorientational NLCs, supported by walk-off dependence on beam power when the nonlinear response becomes comparable with the linear one. While both light self-deflection and nonlinear negative refraction could be observed in other anisotropic media with a reorientational nonlinearity[39], our geometry in NLCs optimizes their observation and characterization in highly nonlinear and highly anisotropic soft matter. This work may impact in the study of light-matter interactions towards the design and realization of novel light-controlling-light devices and systems. Here nonlinear refraction is obtained through self-confinement and solitary wave propagation at relatively low powers; hence, self-trapped optical wavepackets in space enhance the nonlinear response and make this configuration appealing towards power-steerable waveguides or reconfigurable interconnects, where the same optical element realizes both signal guidance and control. Accessing the negative refraction regime enables to maximize the total angular span of such waveguide steering, permitting to resolve a large number of

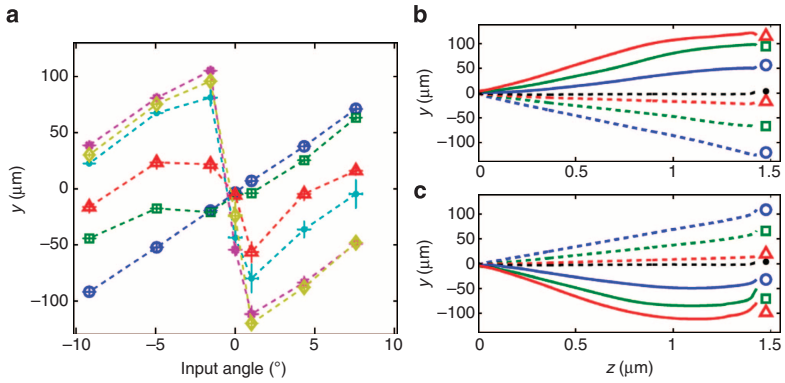

Figure 5 | Nonlinear refraction and its mirror symmetry versus incidence angle. (**a**) Output beam position in y versus β_{in}, measured in $z=1.1$ mm for an input power of 2 mW (blue with circle), 20 mW (green with square), 30 mW (red with triangle), 40 mW (cyan with dot), 70 mW (magenta with star) and 100 mW (yellow with diamond). (**b**) Beam paths for $\beta_{in}<0$ and (**c**) beam paths for $\beta_{in}>0$: input powers are 2 mW (linear case, dashed lines) and 70 mW (solitary wave propagation, solid lines). The incidence angles for $\beta_{in}<0$ ($\beta_{in}>0$) are $-9.2°$ (7.6°) (blue with circle), $-4.9°$ (4.3°) (green with square), $-1.6°$ (1.0°) (red with triangle). The dashed black lines with dot are the paths corresponding to $\beta_{in}\approx 0°$.

output ports (channels) and increase the system capacity. As further developments, we envisage the generalization of the phenomena here shown to, for example, optomechanical meta-atoms[39,40], soft matter with metallic nanoparticles[41], solutions of graphene-oxide flakes[42]. We also foresee fascinating new phenomena stemming from the combined effects of artificial magnetoelectric coupling in metamaterials and natural dielectric anisotropy, for example, exploring the tunability of liquid crystals-based metamaterials[43], where the interplay of nonlinear refraction (discussed hereby) and a negative refractive index or negative diffraction could be exploited towards novel exotic phenomena.

Methods

Modeling light propagation in the nonlinear regime. In the nonlinear regime, in the absence of losses and under the single elastic constant (K) approximation[24], an extraordinarily polarized electromagnetic wave in the harmonic regime at pulsation ω propagates in reorientational uniaxial NLC according to

$$\frac{\partial H}{\partial z}+\frac{\epsilon_{yz}}{\epsilon_{zz}}\frac{\partial H}{\partial y}-i\omega\epsilon_0 n_e^2(\theta)E_y-\frac{i}{\omega\mu_0}\frac{\partial^2 E_y}{\partial x^2}=0, \quad (4)$$

$$\frac{\partial E_y}{\partial z}+\frac{\epsilon_{yz}}{\epsilon_{zz}}\frac{\partial E_y}{\partial y}-i\omega\mu_0 H-\frac{i}{\omega\epsilon_{zz}}\frac{\partial^2 H}{\partial y^2}=0, \quad (5)$$

$$\nabla^2\xi+\frac{\epsilon_0\epsilon_a}{4K}\sin[2(\xi-\gamma)]\ |E_t|^2=0, \quad (6)$$

where ϵ_{ij} are Cartesian components of the dielectric tensor, μ_0 is the magnetic permeability of vacuum, H and E are the magnetic (linearly polarized along x) and electric (polarized in yz) fields, respectively; the subscript t in equation (6) refers to the local polarization of the electric field, in turn determined by γ. Owing to the highly nonlocal response of NLC[22,24], all the dielectric parameters in equations (4–6) can be evaluated on the beam axis, except for $n_e^2(\theta)$, which is responsible of self-focusing[32]. Thus, the walk-off angle is $\delta(\xi_{max}-\beta)$, with $\xi_{max}(z)$ the maximum reorientation at the field peak on each z.

Sample preparation. The planar cells used in the experiments consist of two parallel glass slides placed normal to the x axis, measuring 1.5 and 40 mm along z and y, respectively: the length along z allows observing the output profiles despite scattering losses; the width along y allows preventing boundary effects. The cell thickness across x, $L_x=100$ μm determined by Mylar spacers, ensures both bulk-like beam propagation and operation in the highly nonlocal regime[32]. Both slides were covered by a polymer (polyvinyl carbazole doped with C60) thin film and mechanically rubbed along z in order to ensure the planar alignment of the molecular director along the z axis, with a pretilt angle $\approx 0°$, as measured by the crystal rotation method[44]. The cell was uniformly filled with the commercial nematic mixture E7 by capillarity. To maximize the coupling of the input laser beam to the extraordinary wave component in the NLC layer, two additional glasses of thickness 100 μm were attached to the edges of the cell (perpendicular to z in $z=0$ and $z=1.5$ mm) using ultraviolet curable glue after depositing a thin polyimide layer; these two glasses were treated to induce homeotropic alignment, thus ensuring a homogeneous director distribution in absence of external stimuli. Such input and output glass facets prevented the formation of NLC menisca and undesired beam depolarization at the input, as well as degradation of the sample in time.

Experimental set-up. Accurate measurements of beam incidence were carried out by calibrating the angular deflection of the beam after the microscope objective (MO) against the lateral shift of the mirror (M_2, Fig. 2a), mechanically controlled with a resolution of 1 μm. The sample was placed as close as possible to MO in order to minimize changes in the impact point, the latter changes being detrimental when trying to avoid artifacts associated with possible inhomogeneities in director distribution at the input facet. The input beam direction corresponding to the optimum parallelism between the input wavevector and the z axis (normal to the input facet) was achieved by maximizing the overlap of the trajectories of ordinary (input polarization along x) and extraordinary (input polarization along y) components in the sample at low powers (linear regime): ordinary- and extraordinary-wave Poynting vectors are collinear when the initial wavevector is parallel to the optic axis. The evolution (plane yz) and output profiles (plane xy) of the beams were imaged by single-shot acquisitions of the out-of-plane scattered light and intensity distribution at the exit facet, respectively. The measured trajectories and beam widths were averaged over several acquisitions to reduce the impact of noise.

References

1. Born, M. & Wolf, E. *Principles of Optics* (Pergamon Press, 1975).
2. Boardman, A. D., King, N. & Velasco, L. Negative refraction in perspective. *Electromagnetics* **25,** 365–389 (2005).
3. Veselago, V. G. The Electrodynamics of Substances with Simultaneously Negative Values of ε and μ. *Sov. Phys. Usp.* **10,** 509 (1968).
4. Zheludev, N. I. The road ahead for metamaterials. *Science* **328,** 582–583 (2010).
5. Schuster, A. *An Introduction to the Theory of Optics* (Edward Arnold, 1904).
6. Pendry, J. B. Negative refraction makes a perfect lens. *Phys. Rev. Lett.* **85,** 3966–3969 (2000).
7. Smith, D. R., Padilla, W. J., Vier, D. C., Nemat-Nasser, S. C. & Schultz, S. Composite medium with simultaneously negative permeability and permittivity. *Phys. Rev. Lett.* **84,** 4184–4187 (2000).
8. Parazzoli, C. G., Greegor, R. B., Li, K., Koltenbah, B. E. C. & Tanielian, M. Experimental verification and simulation of negative index of refraction using Snell's law. *Phys. Rev. Lett.* **90,** 107401 (2003).
9. Shalaev, V. M. *et al.* Negative index of refraction in optical metamaterials. *Opt. Lett.* **30,** 3356–3358 (2005).
10. Yao, J. *et al.* Optical negative refraction in bulk metamaterials of nanowires. *Science* **321,** 930 (2008).
11. Xu, T., Agrawal, A., Abashin, M., Chau, K. J. & Lezec, H. J. All-angle negative refraction and active flat lensing of ultraviolet light. *Nature* **497,** 470–474 (2013).
12. Luo, C., Johnson, S. G., Joannopoulos, J. D. & Pendry, J. B. All-angle negative refraction without negative effective index. *Phys. Rev. B* **65,** 201104 (2002).
13. Cubukcu, E., Aydin, K., Ozbay, E., Foteinopoulou, S. & Soukoulis, C. Negative refraction by photonic crystals. *Nature* **423,** 604–605 (2003).

14. Zhang, Y., Fluegel, B. & Mascarenhas, A. Total negative refraction in real crystals for ballistic electrons and light. *Phys. Rev. Lett.* **91,** 157404 (2003).
15. Harutyunyan, H., Beams, R. & Novotny, L. Controllable optical negative refraction and phase conjugation in graphene. *Nat. Phys.* **9,** 423 (2013).
16. Bartholinus, E. *Experimenta Crystalli Islandici Disdiaclastici Quibus Mira Et Insolita Refractio Detegitur* (Hafniae, 1669).
17. Jacob, Z., Alekseyev, L. V. & Narimanov, E. Optical hyperlens: Far-field imaging beyond the diffraction limit. *Opt. Express* **14,** 8247–8256 (2006).
18. Pishnyak, O. P. & Lavrentovich, O. D. Electrically controlled negative refraction in a nematic liquid crystal. *Appl. Phys. Lett.* **89,** 251103 (2006).
19. Kang, L., Zhao, Q., Li, B., Zhou, J. & Zhu, H. Experimental verification of a tunable optical negative refraction in nematic liquid crystals. *Appl. Phys. Lett.* **90,** 181391 (2007).
20. Peccianti, M. & Assanto, G. Nematicons across interfaces: anomalous refraction and reflection of solitons in liquid crystals. *Opt. Express* **15,** 8021–8028 (2007).
21. Katko, A. R. *et al.* Phase conjugation and negative refraction using nonlinear active metamaterials. *Phys. Rev. Lett.* **105,** 123905 (2010).
22. Peccianti, M. & Assanto, G. Nematicons. *Phys. Rep.* **516,** 147–208 (2012).
23. Simoni, F. *Nonlinear Optical Properties of Liquid Crystals* (World Scientific, 1997).
24. Khoo, I. C. Nonlinear optics of liquid crystalline materials. *Phys. Rep.* **471,** 221–267 (2009).
25. Khoo, I. C. Optical bistability in nematic films utilizing selffocusing of light. *Appl. Phys. Lett.* **41,** 909–911 (1982).
26. Residori, S. Patterns, fronts and structures in a liquid-crystal-light-valve with optical feedback. *Phys. Rep.* **416,** 201–272 (2005).
27. Chen, B. G.-g., Ackerman, P. J., Alexander, G. P., Kamien, R. D. & Smalyukh, I. I. Generating the hopf fibration experimentally in nematic liquid crystals. *Phys. Rev. Lett.* **110,** 237801 (2013).
28. Ketara, M. E. & Brasselet, E. Observation of self-induced optical vortex precession. *Phys. Rev. Lett.* **110,** 233603 (2013).
29. Barboza, R. *et al.* Harnessing optical vortex lattices in nematic liquid crystals. *Phys. Rev. Lett.* **111,** 093902 (2013).
30. Peccianti, M., Assanto, G., Dyadyusha, A. & Kaczmarek, M. Non-specular total internal reflection of spatial solitons at the interface between highly birefringent media. *Phys. Rev. Lett.* **98,** 113902 (2007).
31. Alberucci, A. *et al.* Interactions of accessible solitons with interfaces in anisotropic media: the case of uniaxial nematic liquid crystals. *New J. Phys.* **15,** 043011 (2013).
32. Alberucci, A. & Assanto, G. Nematicons beyond the perturbative regime. *Opt. Lett.* **35,** 2520–2522 (2010).
33. Li, J., Wu, S.-T., Brugioni, S., Meucci, R. & Faetti, S. Infrared refractive indices of liquid crystals. *J. Appl. Phys.* **97,** 073501–073505 (2005).
34. Alberucci, A., Peccianti, M. & Assanto, G. Nonlinear bouncing of nonlocal spatial solitons at the boundaries. *Opt. Lett.* **32,** 2795–2797 (2007).
35. Kwasny, M. *et al.* Self-guided beams in low-birefringence nematic liquid crystals. *Phys. Rev. A* **86,** 013824 (2012).
36. Piccardi, A., Alberucci, A. & Assanto, G. Soliton self-deflection via power-dependent walk-off. *Appl. Phys. Lett.* **96,** 061105 (2010).
37. Beeckman, J., Neyts, K., Hutsebaut, X., Cambournac, C. & Haelterman, M. Time dependence of soliton formation in planar cells of nematic liquid crystals. *IEEE J. Quantum Electron.* **41,** 735–740 (2005).
38. Peccianti, M., Dyadyusha, A., Kaczmarek, M. & Assanto, G. Escaping solitons from a trapping potential. *Phys. Rev. Lett.* **101,** 153902 (2008).
39. Zharov, A. A., Zharov, A. A. & Zharova, N. A. Spontaneous reorientations of meta-atoms and electromagnetic spatial solitons in a liquid metacrystal. *Phys. Rev. E* **90,** 023207 (2014).
40. Liu, M. *et al.* Nonlinear response via intrinsic rotation in metamaterials. *Phys. Rev. B* **87,** 235126 (2013).
41. Dintinger, J. *et al.* A self-organized anisotropic liquid-crystal plasmonic metamaterial. *Adv. Mater.* **25,** 1999–2004 (2013).
42. Shen, T.-Z., Song, S.-H. & Song, J.-K. Electro-optical switching of graphene oxide liquid crystals with an extremely large kerr coefficient. *Nat. Mater.* **13,** 394–399 (2014).
43. Buchnev, O., Ou, J. Y., Kaczmarek, M., Zheludev, N. I. & Fedotov, V. A. Electro-optical control in a plasmonic metamaterial hybridised with a liquid-crystal cell. *Opt. Express* **21,** 1633–1638 (2013).
44. Han, K., Miyashita, T. & Uchida, T. Accurate determination and measurement error of pretilt angle in liquid crystal cell. *Jpn J. Appl. Phys.* **32,** 277–279 (1993).

Acknowledgements

We are grateful to Professor M. Kaczmarek (University of Southampton, UK) for useful discussions.

Author contributions

All co-authors contributed equally to this work. A.P. and N.K. performed the experimental measurements and analysed the data, A.A. developed the concept, dealt with model and numerical simulations. O.B. realized the sample. G.A. gave conceptual advice and supervised the work. All authors discussed the results and implications and commented on the manuscript.

Additional information

Competing financial interests: The authors declare no competing financial interests.

Reprints and permission information is available online at http://npg.nature.com/reprintsandpermissions/

How to cite this article: Piccardi, A. *et al.* Power-controlled transition from standard to negative refraction in reorientational soft matter. *Nat. Commun.* 5:5533 doi: 10.1038/ncomms6533 (2014).